TRIBOLOGICAL PROPERTIES OF NANOPARTICE-BASED LUBRICATION SYSTEMS

A Dissertation

by

BASSEM ALI KHEIREDDIN

Submitted to the Office of Graduate Studies of
Texas A&M University
in partial fulfillment of the requirements for the degree of

DOCTOR OF PHILOSOPHY

Chair of Committee,	Mustafa Akbulut
Committee Members,	Zhengdong Cheng
	Dara Childs
	Sreeram Vaddiraju
Head of Department,	Nazmul Karim

August 2013

Major Subject: Chemical Engineering

ABSTRACT

New nanomaterials and nanoparticles are currently under investigation as lubricants or lubricant additives due to their unusual properties compared to traditional materials. One of the objectives of this work is to investigate the tribological properties of these materials in relation to surface topography. Chemical etching and metal evaporation methods were employed to prepare surfaces with various topographies. Surfaces were sheared with the use of a nanotribometer and characterized with an atomic force and scanning electron microscopes. For a system consisting of ZnS nanowires dispersed in dodecane sheared across ductile surfaces, it was found that the geometry of the nanowire relative to the surface topography plays a significant role. Moreover, for brittle surfaces, it was found that beyond a certain roughness the frictional properties remain unchanged.

In addition, this work is also intended to explore novel lubricants with nanoparticle additives in efforts to control friction and wear. A system consisting of silica nanoparticles dispersed in ionic liquids was examined at various concentrations. It was found that an optimum concentration of nanoparticles exists and yields the best tribological properties.

Such work represents an important step in understanding the tribological properties of nanoparticle lubricant additives in general; one that may ultimately provide the guidelines necessary for designing novel, low-friction, and wear-controlling nanoparticle-based lubrication systems that minimize energy and material losses due to friction.

DEDICATION

This dissertation is dedicated to my parents, Ali and Hana, for their unconditional love and support throughout the course of my academic career. To my aunt, Baria, whose endless support helped shape the person I have become.

ACKNOWLEDGEMENTS

I would like to acknowledge the contribution and extensive knowledge of Dr. Mustafa Akbulut, whose patience and guidance were invaluable. Many thanks also go to Dr. Sreeram Vaddiraju and Dr. Zhengdong Cheng whose insights and creative ideas were extremely helpful. I would also like to extend my thanks to the staff of the material and characterization facility at Texas A&M University for their support and training on state-of-the-art equipment. Finally, I would like to thank Randy Marek for his help in providing the tools and machining of parts necessary for the success of this work.

TABLE OF CONTENTS

Page

LIST OF FIGURES

Page

LIST OF TABLES

Page

CHAPTER I

INTRODUCTION

1.1 Description

The first chapter of this dissertation aims to provide a brief overview of tribology and its related fields including friction, wear, and lubrication. Definitions, theories as well as examples of each phenomenon are given to help understand the discussions provided in later chapters.

1.2 Tribology

The word tribology is deduced from the greek word “tribos”, which means rubbing, hence tribology is essentially the science of rubbing. A more preferred definition of tribology is “the science and technology of interacting surfaces in relative motion and the practices relating thereto”. Tribology is mainly concerned with phenomena related to friction, wear and lubrication and dates back to the days of the Pharaohs in Egypt.

One of the first tribology centers was built in the United Kingdom as a response from the British government to the infamous “Jost Report”. In this report, Lord Peter Jost was able to convince the British government that approximately 515 million pounds sterling per year in wasteful resources occurred due to the lack of understanding and knowledge of tribological phenomena [1]. It is also estimated that the costs of tribological deficiencies are expected to be in excess of 1% of the gross national product (GNP) of industrialized nations. A more recent analysis reveals that supplying all worn

gear drives in the United States with a lubricant allows a relative increase of 5% in mechanical efficiency compared to conventional mineral oil and would result in savings of approximately $1 billion per annum [2]. Therefore, for economic reasons and long-term reliability of machinery, the significance of understanding tribological phenomena in terms of friction reduction and wear control cannot be overemphasized. This is especially true, because oil reserves continue to dwindle and energy costs are rising relentlessly. Addressing such critical lubrication demand is one of the grand challenges for efficient and durable operation of advanced engineered mechanical systems.

1.3 Friction

Friction is one of the most ancient problems in physics/mechanical engineering with major implications on our everyday lives. The friction force, F_f, is defined as the interfacial force that opposes the relative motion of two bodies in contact as shown in Figure 1. That said, it is important to distinguish between two equally important frictional phenomena [3]: the static friction force, F_s, and the kinetic friction force, F_k. F_s is defined as the minimal force required to initiate sliding, while F_k is the force required to maintain the sliding process. Depending on the application friction can be desirable or undesirable. For example, the ability of humans to walk and vehicles to move would not be possible without friction. High friction is also desired in the tightening of screws and bolts as well as in clutch systems. In contrast, friction is undesirable in car engines, moving components of machinery, human joints, turbines, and microelectromechanical systems (MEMS).

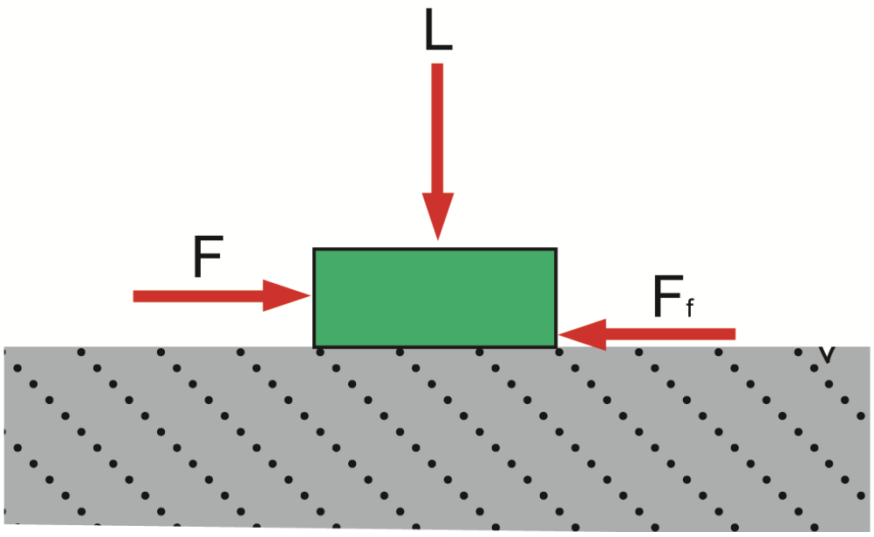

Figure 1. Schematic illustration of a block subject to a lateral force F and a normal force L and an opposing friction force F_f.

Leonardo Da Vinci (1452-1519) is considered as the first to have conducted a systematic study on sliding friction. In his experiment, Da Vinci measured the friction force required to move a solid object against a solid surface, reportedly wood on wood and wood on iron. Following his experiments, he made the following observations [4, 5]:

1. The friction force is directly proportional to the applied load.
2. The friction force is independent of the apparent area of contact.

The aforementioned observations were later confirmed by the Frenchman Guillaume Amontons (1699) and became known as Amontons' first and second law, respectively. A third observation was noted a few years later by another Frenchman Charles Augustin Coulomb in which he stipulated that the friction force is independent of the sliding velocity.

These observations have been formulated into a mathematical expression as shown in Equation 1:

$$\mu = \frac{F}{L} \tag{1}$$

Where μ is known as the friction coefficient (arguably the most common and important parameter that characterizes the frictional characteristics of surfaces), F is the friction force and L is the normal load.

Over the years, researchers and scientists have debated and placed the origins of Amontons' law under intense scrutiny. Bowdon and Tabor's attempt to give a physical explanation concluded that the real contact area is directly proportional to the normal load [6]. Since the lateral force required to shear an asperity is proportional to the area of the asperity, Amontons' law can be readily recovered. However, this theory does not agree well with Hertz theory [7] of a sphere in non-adhering contact with a flat surface ($A \sim (RL)^{2/3}$). Greenwood and Willamson in what came to be known as GW theory proposed that the contact area is indeed proportional to the normal load for elastically deformed asperities [8]. Many models have proven useful in understanding the elastic behavior of non-adhesive and adhesive surfaces and their asperities when these are modeled by the continuum of Hertz and Johnson-Kendall-Roberts (JKR) theories, respectively [9-11]. However, these theories are usually highly model-dependent, e.g., assuming only elastic deformations and roughness on a single-length scale [12]. Some investigators have refined the continuum models to include more realistic surfaces that can have arbitrary roughness and deform plastically [13, 14]. Continuum models are assumed to be independent of the size or scale of the roughness. MD simulations have

shown, as expected, that they break down on the nano and atomic scales [15-17]. However, MD simulations have suggested that Amontons' law remains valid on the nanoscale [8, 18, 19] . Moreover, it was found to be valid for dry and lubricated sliding across rough and smooth surfaces. However, there are situations where Amontons' law completely fails namely in adhesive contact and high velocity and load ranges. In this case, the friction force will have an adhesion term added to the load term as shown in Equation 2:

$$F = S_c A + \mu L \quad (2)$$

Where S_c is the adhesion-critical shear stress, A is the real contact area. When the first term of the above equation dominates, friction is considered adhesion-controlled and load-controlled if the second term is dominant.

1.4 Wear

Wear is defined as the removal of material from solid surfaces caused by the mechanical action of one surface moving relative to another. Modern research suggests that there are four wear mechanisms [5, 20]:

a. Adhesive wear
b. Abrasive wear
c. Fatigue wear
d. Chemical wear

Adhesive wear is the most common mechanism and occurs when the asperities of one surface are strongly adhered to the asperities of another surface resulting in the formation of a junction. When these surfaces are sheared against each other, the softer

asperities are separated and material is removed [21]. Abrasive wear occurs when a hard surface is sheared against a significantly softer one; hence the hard asperities are able to penetrate the softer ones. When these surfaces move relative to one another, grooves and scratches are formed owing to the ploughing action resulting in the removal of material from the softer surface in the form of loose particles [20]. Fatigue wear occurs when the same volume of asperities are repeatedly sheared against each other. With time, this repetitive sliding will eventually result in the formation voids surface cracks that continue to propagate under the shearing action [22]. This type of wear generally occurs in brittle materials [1] and results in the breakup and removal of materials from the surface. Chemical wear occurs when the shearing action takes place in destructive and corrosive environments where a chemical reaction takes place and may result in the removal of material [23]. The chemical reaction may make the surfaces softer and therefore more prone to material removal.

It is clear from the definitions above that wear is a complex phenomenon that depends on the materials in contact as well as environmental conditions. Therefore, it is not surprising that no universal equation of wear exists. However, Archard observed that the wear rate is directly proportional to the worn volume and indirectly proportional to the normal load and hardness of the material. With this in mind, he formulated an equation for the wear rate [24]:

$$K = \frac{V}{ws} \tag{3}$$

Where K is the wear rate (wear coefficient normalized by the hardness of the material) V is the worn volume, w is the normal load, s is the distance of movement, and H is the

hardness of the material. While this equation has been commonly and successfully used in the field of tribology, there are several tribological situations where it is invalid.

1.5 Lubrication

The tremendous losses incurred by friction and wear can be a huge burden on any national economy. The most traditional route to control these losses has been through lubrication. Lubrication is an ancient technology that dates back to the days of the Egyptian Pharaohs who used animal fats and water in their building of the pyramids [25]. The idea is to simply reduce the intimate contact between surfaces through the introduction of a lubricant between them. There are two common types of lubrication: a) fluid lubrication where a fluid is introduced between the mating surfaces and b) surface film lubrication where a film is physically or chemically bonded to the surface. While solids, liquids, and gases can be used as lubricants, the main focus of this dissertation will be on lubrication through liquid films.

The well-known Stribeck curve [26], illustrated in Figure 2, has been widely employed in determining the lubrication regime. It describes the variation of the friction coefficient, μ, as a function of the quantity ($\eta V/P$), where η is the dynamic viscosity of the lubricant, V is the sliding velocity and P is the applied load. From Figure 2, one can clearly distinguish between three lubrication regimes: Hydrodynamic Lubrication (HL), Elastohydrodynamic Lubrication (EHL), and Boundary Lubrication (BL). Note that the main difference in the three lubrication regimes is the thickness of the lubricating film. Each of these three regimes will be discussed in the following sections.

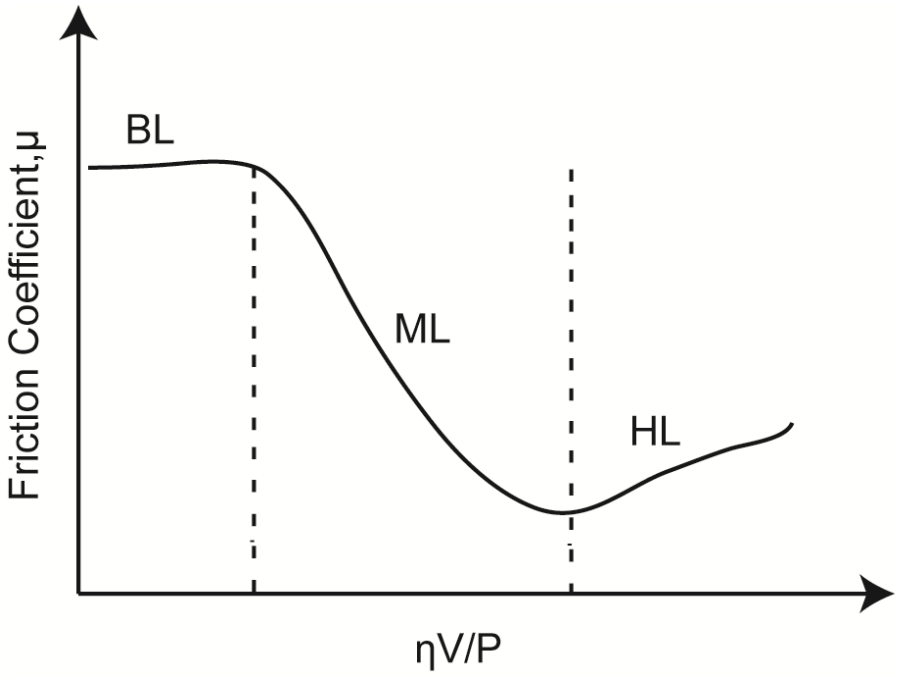

Figure 2. Stribeck curve illustrating the different lubrication regimes.

1.5.1 Hydrodynamic lubrication

In hydrodynamic lubrication, also referred to as “full-film” lubrication, the moving surfaces are separated by a viscous and thick lubricant film. Generally speaking, the film thickness is usually 10 to 100 times thicker than the height of asperity of the moving surfaces (Figure 3).

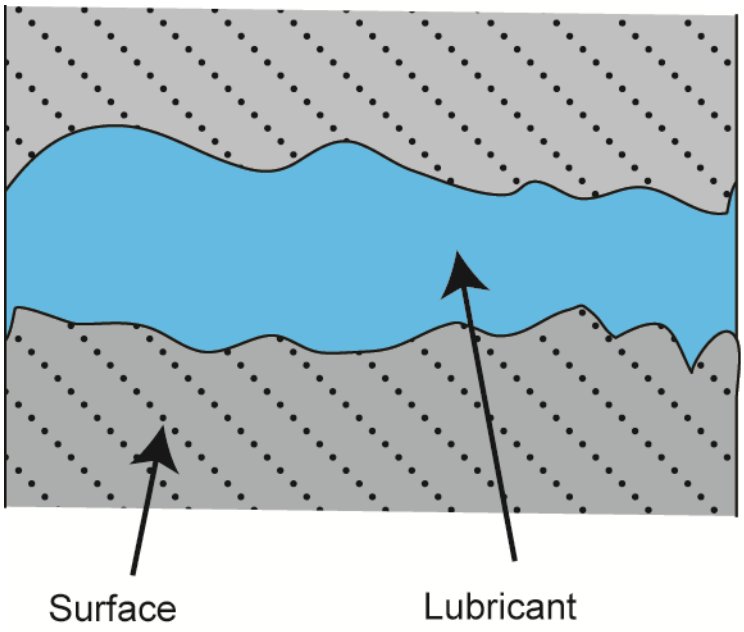

Figure 3. Hydrodynamic lubrication.

This will result in friction coefficients on the order of 0.001-0.01 [5, 20]. Moreover, hydrodynamic lubrication requires that one of the surfaces be tilted forward in the direction of the motion. This converging configuration will result in the dragging of the fluid to the narrowing gap while at the same time developing a positive pressure that will support the load in the gap, and keep the surfaces apart [27]. It is clear from the quantity $\eta V/P$, that this type of lubrication is governed by the viscosity of the fluid and the speed of moving surfaces. Therefore, a relatively viscous fluid and high speed conditions will prevent asperity-asperity contact and result in low friction coefficients.

1.5.2 Elastohydrodynamic lubrication (EHL)

This type of lubrication occurs when a lubricant is introduced between two surfaces that are in a rolling, non-conformal contact such as those found in gears, rolling

bearings etc [28]. The thickness of the lubricating film is typically much lower than that found in hydrodynamic lubrication (Figure 4).

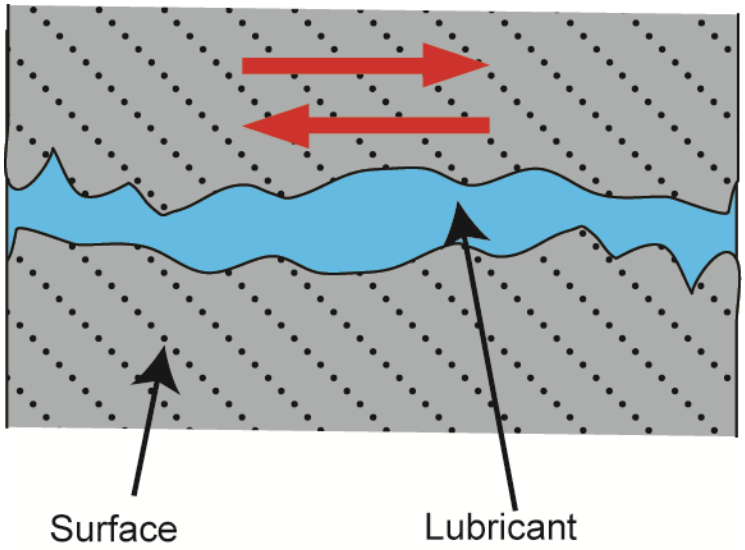

Figure 4. Elastohydrodynamic lubrication.

While pressure is still generated to force the surfaces apart, elastic deformation of the surfaces can occur when this pressure is sufficiently great. This usually occurs in the deformed region that is often referred to as the Hertzian region due to the resemblance of the pressure distribution to that of a Hertzian pressure distribution. However, the contact pressure may give rise to plastic deformation of the surfaces should their elastic limit be exceeded [5]. Besides the deformation of the surfaces, the contact pressure has an effect of the viscosity of the lubricant. In fact, for non-conformal contacts, the viscosity of the lubricant, η, increases exponentially with increasing pressure according to equation 4 [29]:

$$\eta = \eta_0 e^{\alpha P} \tag{4}$$

Where η_0 is the viscosity of the lubricant at ambient pressure and constant temperature, P is the contact pressure, and α is the viscosity-pressure coefficient defined as:

$$\alpha = \frac{1}{\eta}\frac{\partial \eta}{\partial P}|_{P=0}$$

The EHL derives its name from the effect it has on the properties of the surface and rheological properties of the lubricant. Therefore, multiple combinations of these effects exist. Esfahanian and Dowson [30-32] identified 4 different regimes that describe these combinations:

a) Rigid-isoviscous: the contact pressure is not sufficiently great to cause an elastic deformation or a significant change in the viscosity of the lubricant.
b) Rigid-viscous: the contact pressure is not sufficiently great to cause an elastic deformation but is great enough to cause a viscosity increase.
c) Elastic-isoviscous: the contact pressure is large enough to cause an elastic deformation but has a negligible effect on viscosity.
d) Elastic-viscous: the contact pressure is sufficiently great to cause an elastic deformation as well as a viscosity increase.

The most important parameter researchers seek when dealing with EHL is the minimum film thickness, h_{min}. The film thickness is on the order of 0.1 to 1 μm but still manages to separate the surfaces resulting in friction and wear reduction [33]. However, the calculation of h_{min} is not straightforward and depends on the geometry of the contact. For elliptical contacts, (For other contact geometries and more film thickness

calculations, see ref [34]), for example, Hamrock and Dowson presented the following expression [5] :

$$h_{min} = 3.63R_x \frac{U^{0.68}G^{0.49}}{W^{0.073}}(1 - e^{-0.68k}) \quad (5)$$

Where,

R_x: the contact radius in the direction of motion.

G = αE, is a material parameter

E: combined elastic modulus

$U = \frac{\mu_0(u_1 - u_2)}{2ER}$, is a speed parameter, u_1 and u_2 are surface velocities in contact region.

$W = \frac{w}{ERL}$, is a load parameter, *w* and *L* are length and total load on the cylinder.

k: elliptical parameter related to the contact dimensions.

The above equation and many other equations for various contact geometries have been commonly employed and found to be valid for smooth surfaces and uniform lubricant properties. However, in solutions where the properties of the lubricant vary (i.e. polymer additives), these equations are invalid. Furthermore, departure from these equations has been encountered with rough surfaces. In order to account for the roughness effect, researchers have resorted to the use of the so-called Λ ratio, which is a non-dimensional parameter given by:

$$\Lambda = \frac{h_{min}}{\sigma} \quad (6)$$

Where σ is a combined roughness parameter of the two surfaces (top and bottom) given by:

$$\sigma = \sqrt{{\sigma_1}^2 + {\sigma_2}^2} \quad (7)$$

This ratio has been found to be useful in determining the type of lubrication regime. For EHL, $3 < \Lambda < 10$, and it's significantly smaller than unity for the boundary lubrication regime which is discussed next [5].

1.5.3 Boundary lubrication

There are many practical situations where the lubricant film thickness is not large enough to prevent direct contact between asperities, resulting in high friction and wear rates. This mode of lubrication is commonly referred to in the literature as boundary lubrication often abbreviated as BL (Figure 5).

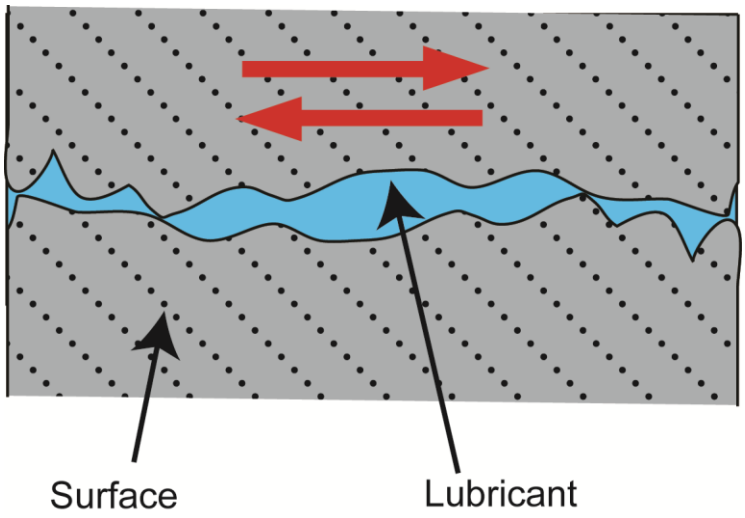

Figure 5. Boundary lubrication.

This phenomenon typically occurs under high loads where it becomes difficult to maintain a thin film between the contacting surfaces i.e. the film is squeezed out of the contact area. The rhetorical question then becomes: How does the lubrication

mechanism take place under these extreme circumstances? The answer lies in the presence of additives in the base lubricant commonly referred to as boundary lubricants. The idea is that molecules that adsorb on the contacting surfaces are able to provide a protective layer which prevents direct contact between the asperities. This protective layer is characterized by low shear strength and results in significant reduction in the friction coefficient. To better understand this effect, consider an alternative expression for the friction coefficient given by [33]:

$$\mu = \frac{\tau}{\sigma_y} \tag{8}$$

where τ is the effective shear stress and σ_y is the plastic flow stress of the material. From equation 8 it can easily be seen that with low shear stress and high plastic flow stress (i.e. high hardness), low friction coefficients can be obtained.

Research suggests that there are two ways molecules can adsorb on surfaces: a) physisorption and b) chemisorption. Physisorption, or physical adsorption, occurs when molecules are attached to the surface via bonds resulting from van der Waals forces [35]. Therefore, these molecules are weakly bounded to the surface and very sensitive to temperature, and can desorb if the temperature is sufficiently high. However, so long as they remain bonded to the surface, they can provide a protective layer. On the other hand, chemisorption, or chemical adsorption, occurs when molecules of the adsorbate (i.e. lubricant) and those of the substrate are held together via chemical bonds. A chemically attached protective layer is effective under moderate loads and temperatures and typically contains reactive elements such as sulfur, chlorine and phosphorus [20].

Whether the protective layer is formed via physisorption or chemisorption, the molecular structure of the lubricant plays a significant role in the effectiveness of lubrication. For instance, studies suggest that lubricants composed of straight (linear) chains perform more effectively than those composed of non-linear or crooked chains [36]. Moreover, a minimum chain length (i.e. n=9) is required for effective lubrication and that lubrication is improved with increasing chain length. These requirements can be better understood by considering the surface coverage and the cohesion strength between adsorbing molecules [37, 38]. In boundary lubrication, the typical film thickness ranges from 0.005 to 0.1 μm resulting in friction coefficients on the order of 0.03-0.2.

CHAPTER II

NANOPARTICLE-BASED LUBRICATION SYSTEMS: CHALLENGES AND OPPORTUNITIES[*]

2.1 Overview

This chapter is intended to serve as a resource for researchers and scientists wishing to design nanoparticle-based lubrication systems. The chapter will review previous studies of nanoparticle-based lubrication systems and discuss in detail the important considerations that must be taken into account when designing such systems for tribological applications. Considerations are classified as: a) physicochemical b) mechanical or c) geometrical). Each of these categories encompasses a wide variety of parameters which have been examined. Overall, the aim of this article is to provide the insight necessary for the accurate design of a NBLS for a particular target application. I hope that this review will advance knowledge in the field of nanoparticle lubricant additives, and ultimately have a positive impact by prolonging the lifetime of machinery and leading to a significant reduction in energy losses.

[*] Reprinted with permission from *Polymer adhesion, friction, and lubrication*, by Hongbo Zeng, 2013, Wiley, New York. Copyright 2013 by Wiley.

2.2 Introduction

All process industries that convert raw materials into useable goods require a large amount of energy in the form of electricity or fuel to power machinery and equipment. For any machine to move, energy must be provided to overcome friction. Minimizing the amount of energy lost to friction increases the efficiency of machines. In addition, wear caused by friction is one of the major reasons for failure of vital engineering components in systems such as pin-joints, engines, power generators, gears in wind turbines, parts used in aerospace systems, bearings, camshafts, pumps, etc. Energy and material losses due to tribological deficiencies occur on virtually every mechanical device in operation, and comprise a significant portion of the cost in any national economy [39]. For instance, a few decades ago the Jost Report convinced the British government that approximately 515 million pounds sterling per year in wasteful resources occurred due to the lack of understanding and knowledge of tribological phenomena [1]. A more recent analysis reveals that supplying all worn gear drives in the United States with improved lubricants would allow a relative increase of 5% in mechanical efficiency compared to conventional mineral oil and would result in savings of approximately $1 billion per annum [2]. The significance of friction reduction and wear control cannot be overemphasized, especially as oil reserves dwindle and energy costs rise relentlessly.

In addition to improving existing machinery, it is desirable to develop lubrication systems that are able to meet the needs of advanced machinery currently being developed in the manufacturing, energy, and defense industries. Addressing demand for

novel lubrication systems is one of the grand challenges for efficient and durable operation of advanced engineered mechanical systems. Tribological deficiencies have been shown to be the critical factors hindering the transition from prototype to product in many high-tech applications [40-43]. Therefore, as existing lubricants reach their performance limits, one of the major scientific tasks in the 21st century is to develop new lubricants that fulfill unique requirements across a multitude of fields, ranging from computer storage media to energy or manufacturing industries, for use under increasingly stringent conditions.

Recent research has shown that Nanoparticle-Based Lubrication Systems (NBLS) demonstrate improved lubrication properties compared to traditional lubricants for some tribological systems [44-50]. Because of these promising results, NBLS have received increasing attention in various lubrication applications such as MEMS [51], engines [52-54], turbines [55], and gears [54-56] with a hope of achieving better tribological efficiency and durability. These applications involve a variety of surface topographies ranging from molecularly smooth to macroscopically rough surfaces. That said, there is a little doubt that designing a NBLS is a complex phenomenon and requires careful considerations. This article will review previous studies on nanoparticle-based lubrication systems and detail the important considerations that must be taken into account when designing such systems for tribological applications. These considerations are divided into three different categories: 1) Physicochemical, 2) Mechanical, and 3) Geometrical. These categories were selected in light of the current literature that found size, shape, nanostructure, colloidal stability, surface functionalization, and

concentration of nanoparticles as well as surface properties and environmental conditions to be the most critical parameters influencing the tribological behavior of nanoparticle-based lubrication systems. Each category will be discussed in detail in the following sections.

2.3 Mechanism of lubrication

Nanoparticle additives have been successfully dispersed in various solvents and proven to be efficient in lowering the friction coefficients and reducing wear compared to stand-alone lubricants under similar circumstances. The reason behind this improved lubricity is the increase in the load carrying capacity of the base lubricant and the prevention of asperities from coming into intimate contact. Over the past few decades, researchers have identified various mechanisms that explain the reasons behind the improved lubricity. In this article, we divided these mechanisms into three main categories: a) ball-bearing effect b) smoothing out process and c) tribofilm formation.

The ball bearing effect is commonly found in nanoparticles that are spherical or quasi-spherical in shape. When surfaces are sheared against each other, these nanoparticles can roll between the surfaces provided their size exceeds the surface roughness (Figure 6). Otherwise, they can be trapped between the asperities and lose their lubricity. Therefore, the friction mechanism changes from sliding to a combination of rolling/sliding which results in friction and wear reductions. One of the requirements for this mechanism to occur is that low-load conditions be maintained between the rubbing surfaces so that the shape and rigidity of the nanoparticles are preserved [57].

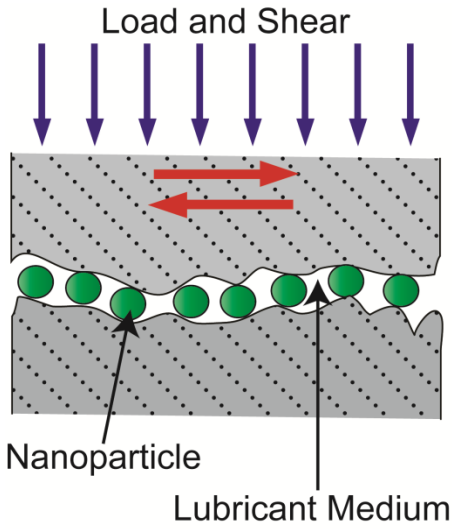

Figure 6. Illustration of the ball-bearing mechanism.

In addition to the ball-bearing effect, it was hypothesized and proven experimentally, that nanoparticles can fill out the valleys between the asperities, in a process we refer to as the smoothing out process as shown in Figure 7. This "*artificial smoothing*" mechanism will lead to improved tribological properties primarily due to the reduction in surface roughness.

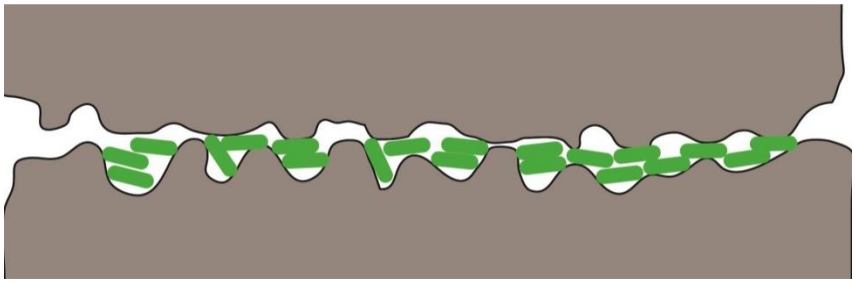
Figure 7. Schematic illustration of the artificial smoothing mechanism.

In boundary lubrication conditions, nanoparticles dispersed in oil can form a protective film and deposit on the rubbing surfaces. Under these circumstances, the nanoparticles carry part of the load and prevent asperities from contacting each other thereby exhibiting better friction and antiwear properties. This tribofilm, which acts to decrease the shearing stress, is the result of a physical or chemical interaction between the nanoparticles and the surfaces. The formation of such films is a complex phenomenon and much work has been done to understand its mechanism and composition [58-60]. Rapoport et al. reported improved tribological properties by dispersing IF-WS_2 nanoparticles in lubricating oil due to formation of a physical protective film consisting of deformed nanoparticles depositing on the interfaces [61]. Liu et al. also reported the formation of a tribochemical film via the deposition of chemical reaction products formed under the shearing action on the rubbed surfaces [62, 63]. These aforementioned studies are examples of tribofilms that exhibit both friction and wear reduction. However, this is not always the case as studies using CeF_3 nanoparticles yielded poor anti-wear due to corrosion resulting from F^- surface atoms [64].

2.4 Tribological studies on nanoparticle-based lubrication systems

Tribological studies seek to determine which nanoparticle characteristics provide superior lubricant performance, and to elucidate the physical processes promoting performance improvements. Studies observing nanoparticles made of metals, alloys, chalcogenides, and both organic and inorganic fullerene-like structures are reviewed here. Numerous nanoparticle synthesis methods [65, 66] and surface characterization

techniques [Experimental Section] are employed in this body of research. Tribometers are used to measure the wear rates, load carrying capacities, and friction coefficients that determine the performance of a lubricant additive.

2.4.1 Metal nanoparticles

Soft metals have been employed as surface coatings on tribological materials, however these systems fail to provide adequate lubrication under high loads, and are limited by difficulties in the application and repair of the surface film [67]. Metal nanoparticles are viable alternatives to surface coating because the size of the particles allows them to be suspended in media such as oil and carried directly to sites of asperities on the tribosurface. Performance of various metal nanoparticles is shown in Table 1.

Table 1. Performance of metal nanolubricants.

Metal	D (nm)	Surfactant	Concentration	Solvent	μ	Ref.
Ag	7	Carboxylates	2%	MACs	0.1	[68]
Bi	40	-	0.1%	LP	0.06	[67]
Cu	8	DDP	4 wt%	LP	0.05	[69]
Cu	20	Resin	0.2wt%	50CC Engine Oil	0.09	[70]
In	40	-	0.1%	LP	0.065	[19]
Pd	2	TBA Acetate	5 wt%	LP	0.077	[71]
Sn	40	-	0.25%	LP	0.065	[19]

Cu nanoparticles capped with DDP increased the maximum non-seizure load of lubricating oil by 218%, and reduced wear scar diameter by 51%, however the study

found that results were very sensitive to parameters such as concentration, particle size, and the nature of interparticle forces (i.e. whether or not surfactants were employed) [69]. Friction and wear reduction of copper nanoparticles was found to improve at higher temperatures and pressures [67, 70]. In addition to improving lubricant performance, noble metals such as Pd resist oxidation and lower the electrical contact resistance between surfaces [71]. Sun and Zhang observed that DDP coated Ag nanoparticles increased the load-carrying capacity of liquid paraffin from 300 to 800 N [72]. These materials are more expensive than metals such as copper, but are still feasible for MEMS applications. A series of studies performed by Zhao and Chen examined the performance of In-Sn, Bi-In, Pb-Bi, Sn-Bi and Sn-Cd alloy nanoparticles. At optimal concentrations, these alloys exhibited better wear reduction than either single component [19]. In particular, bismuth has good potential for use as a lubricant additive because it is environmentally friendly, and its chemical similarity to lead allows it to easily be incorporated into lubrication systems that have already been developed [73].

2.4.2 Inorganic nanoparticles

The performance of a wide variety of inorganic nanoparticle shapes have been observed: rods [44, 74], wires[75], sheets[76], and multi-walled fullerene-like structures [45, 77]. Metal borides, oxides, and chalcogenides possess crystalline structures which lead to interesting lubricative behavior [78, 79]. Compounds such as $CaCO_3$ and silica are distinct as environmentally friendly lubricant additives. Table 2 reports the friction coefficients obtained by testing various inorganic nanoparticle based lubrication systems.

Table 2. Performance of inorganic nanolubricants.

Inorganic Compound	**Size (nm)**	**Surfactant**	**Concentration**	**Solvent**	**μ**	**Ref.**
Magnesium Borate	10	Sorbitol monostearate	0.757 wt%	500 SN Oil	0.035	[80]
Titanium Borate	10 - 70	Sorbitol monostearate	0.375 wt%	500 SN Oil	0.03	[81]
Zinc Borate	20 - 50	Sorbitol monostearate	0.757 wt%	500 SN Oil	0.03	[82]
$CaCO_3$	40	TEA Mono-oleate	1 wt %	PAO	0.095	[83]
$CaCO_3$	40	Polysorbate / Polyether	0.6 wt%	40CD Oil	0.0865	[84]
CeO_2	11	Polysorbate / Polyether	0.6 wt%	40CD Oil	0.1008	[84]
CeO_2 / $CaCO_3$ (1:1)	11 & 40	Polysorbate / Polyether	0.6 wt%	40CD Oil	0.0798	[84]
LaF_3	6	DDP	1 wt%	LP	0.088	[85]
$Ni(NO_3)_2$	10	SDS	0.50%	500SN Oil	0.068	[86]
$La(OH)_3$	30	Amines	1 wt %	LP	0.08	[87]
CuO	30-50	-	1%	PAO6	0.017	[88]
Fe_2O_3	20-50	Sorbitol monostearate	0.38 wt%	500 SN Oil	0.037	[89]
SiO_2	15-20	Silanes	0.3 wt%	ST5W/30 Oil	0.027	[90]
SiO_2	20	-	0.05 wt%	Ionic Liquid	0.2	
TiO_2	20	Sorbitol monostearate	0.92 wt%	500 SN Oil	0.037	[89]
TiO_2	5	2-ethyl hexoic acid	2%	LP	0.09	[91]
TiO_2	30	*cis*-9-octadecenoic acid	1 wt%	Water	0.08	[92]
ZnO	20	-	0.50%	PAO6	0.016	[88]
ZrO	20-30	-	0.50%	PAO6	0.016	[88]
CuS	20	Oleic Acid	0.4wt%	LP	0.064	[93]

In addition to particle concentration, the mole ratio of surfactant to nanoparticle was found to affect both friction and wear reduction. A study of CuS nanoparticles

indicates that the optimal mole ratios for friction and wear reduction can be different. Investigation of metal borates found that titanium and magnesium borate systems exhibited the highest load carrying capacity and greatest wear scar reduction. Titanium and zinc borate systems exhibited the lowest friction coefficients [80]. A study performed by Gu indicated that a 1:1 ratio of CeO_2 and $CaCO_3$nanoparticles outperformed either single compound. Hernandez systematically studied metal Cu, Zn, and Zr oxides and found that CuO effected the greatest wear reduction, while Zn and Zr provided superior friction reduction.

2.4.3 Fullerenes and inorganic fullerene-like nanoparticles

In addition to functioning as a solid lubricant, graphite is capable of enhancing the effectiveness of liquid lubricants. However, graphite is outperformed by shapes such as multi-layered onions and nanotubes. Fullerenes provide friction and wear reduction, and are more resistant to oxidation than graphite, but are limited by their ability to disperse in oil. The friction coefficients obtained with various carbon based nanolubricants are recorded in Table 3.

Table 3. Performance of carbon nanolubricants.

Organic						
Compound	**Shape**	**D (nm)**	**Concentration**	**Solvent**	**μ**	**Ref.**
Graphite	Sheet	50	0.1 wt%	PAO	0.08	[94]
C60	Sphere	1	0.1 wt%	PAO	0.07	[94]
Onion	Sphere	50	0.1 wt%	PAO	0.06	[94]
Onion (Diamond Core)	Sphere	50	0.1 wt%	PAO	0.06	[94]
Diamond	Sphere	5	1 wt%	LP	0.08	[95]
SWCNTs	Tube	10	1 wt%	PAO	0.07	[94]
MWCNTs	Tube	10-20	0.1 wt%	Water	0.08	[96]

Interestingly, concentration was not found to have significant effect on the friction coefficient obtained by these additives. Wear reduction was affected by both concentration and particle size. Carbon onions outperform graphite when the particle diameter is larger than the surface roughness. The length of carbon nanotubes severely limits successful dispersion of nanotubes in oil.

Molybdenum disulfide and Tungsten disulfide form fullerene-like structures and have been studied extensively as lubricant additives. These compounds exhibit excellent friction and wear reduction.Nanolub, a WS_2nanoparticle based lubrication system, is currently manufactured and sold by ApNano. Table 4 summarizes the performance of inorganic fullerene-like compounds used as lubricant additives.

Table 4. Performance of inorganic fullerene-like nanolubricants.

IF						
Compound	**Shape**	**Diameter (nm)**	**Concentration**	**Solvent**	**μ**	**Ref.**
MoS_2	Onion	15 - 60	2 wt%	150 SN Oil	0.036	[77]
MoS_2	Onion	15 - 60	1 wt%	PAO	0.045	[36]
MoS_2	Spherical	8 - 20	0.2 wt%	LP	0.059	[97]
WS_2	Rod	15	2 wt%	Oil	0.06	[74]
MoS_2	Onion	70	1 wt%	PAO	0.05	[98]
WS_2	Onion	100	1 wt%	PAO	0.05	[98]
NbS_2	Onion	60	1 wt%	PAO	0.06	[78]
TaS_2	Onion	50	1 wt%	PAO	0.09	[78]
WS_2	Tube	30 x 500	1 wt%	PAO	0.06	[78]

The friction reduction effected by MoS_2 lubricant additives is most pronounced at high contact pressures. WS_2 systems do not show the same relationship between contact pressure and friction coefficient. MoS_2 systems initially show slightly lower friction coefficient than WS_2 systems, however WS_2 outperforms MoS_2 by the end of tests lasting over 1000 cycles [98]. This is attributed to the lower chemical stability of MoS_2 as compared to WS_2. Particles made of NbS_2 and TaS_2 did not exhibit as much friction reduction as MoS_2 or WS_2, and TaS_2 actually caused an increase in WSD compared to pure PAO. Dispersion of IF nanoparticles in oil, especially long nanotubes, are again the biggest challenge to successful implementation. Improved dispersion of MoS_2clusters by surface modification with DDP has been reported by Zhang [97].

2.4.4 Polymeric nanoparticles

Banquy et al. [99] investigated the correlation between surface roughness and the friction coefficient of polymeric nanoparticles as elastoplastic asperities. The polymeric NP'S were made of N,N-diethyl acrylamide and 2-hydroxyethyl methacrylate using the method reported in [100] and had an average diameter of 660 nm. The NP were grafted on mica sheets by using different grafting densities (0.41-2.63 NP/μm^2) in order to obtain different surface topographies. An AFM was used to quantitatively determine the *rms* roughness of the surfaces, which was found to increase with increasing grafting density. The frictional forces between the opposing NP monolayers were measured using a surface force apparatus (SFA), by compelling the upper surface to slide past the stationary lower surface for 3 cycles under 30% relative humidity and at 25 C environmental conditions. For all surfaces, it was found that the frictional force increased linearly with increasing normal force, in accordance with Amontons' law which states that the friction coefficient is independent of the normal load. This result was expected due to the absence of adhesion. Moreover, it was found that the friction coefficient increased quasi exponentially with increasing surface roughness. This increase in friction was related to an increase in plasticity of NP's and was explained using a ratchet mechanism developed by Tabor.

Another class of polymeric nanoparticles is that which consists of inorganic or organic nanoparticles functionalized with polymers. This type of NP's has been featured as nanofillers of in polymer matrices due their improvement of tribological properties like friction and wear. For instance, Rong et al. [101] used alumina, silicon carbide and

silicon nitride nanoparticles and functionalized them with polyacrylamide (PAAM) via a grafting polymerization technique. Briefly, the bare nanoparticles were treated with a KH570 (γ-methacryloxypropyl tri-methoxy silane) coupling agent and subsequently dried. The nanoparticles were then dispersed in water and grafting polymerization of acryalamide was performed under a nitrogen environment. The resulting PAAM-grafted nanoparticles had a percent grafting value of 10% and were used as fillers in an epoxy composite. The effect of polymer grafting onto the surfaces was investigated by dispersing the untreated and treated Al_2O_3 and SiC nanoparticle in acetone and THF, respectively. The results indicated that the untreated nanoparticles exhibited unstable dispersion and precipitated whereas the treated ones displayed good dispersibility. Moreover, the frictional properties of the untreated and treated nanoparticles in the epoxy matrix were evaluated by performing sliding wear tests using a block-on-ring apparatus under dry conditions. The results show that in both cases (i.e. AL_2O_3 and SiC), the treated particles possessed a lower friction coefficient and wear rates than their untreated counterparts. These improvements in the tribological properties were attributed to the increase in interfacial adhesion between the treated nanoparticles and the epoxy matrix and the increase of the shear strength of the matrix due to the presence of the fillers.

Pei et al. [102] conducted a study involving the use of poly (ionic liquids) (PILs) grafted on multiwalled carbon nanotubes (MWCNTs), MWCNTs-g-PILs as lubricant additives and investigated their tribological behavior. Using an oscillating friction tester, friction tests were performed on MWCNTs-g-PBIM-PF_6 and ungrafted MWCNTs after

dispersion in a conventional ionic liquid (LP104). These tests were achieved by varying the concentrations of MWCNT's-g-PILs from 0% (ungrafted) to 0.05% under loads ranging from 100 to 500 N. The results indicate that the addition of MWCNTs-g-PIls to the base lubricant acted to decrease the friction coefficients. Moreover, an optimal concentration of 0.01 % was observed for all loads applied. Furthermore, the friction coefficient also decreased with increasing loads. This reduction in friction was attributed by the load carrying capacity of the nanotubes and the good dispersibility of the MWCNTs-g-PILs.

2.5 Considerations in designing nanoparticle-based lubrication systems

2.5.1 Physicochemical considerations

The physicochemical considerations encompass different parameters such as colloidal stability, melting point, adsorption and adhesion of nanoparticles, and the strength of interactions of nanoparticles and the shearing surfaces. Each of these parameters plays an important tribological role and will be discussed in detail in the following subsections.

2.5.2 Colloidal stability

The homogeneity of a liquid lubricant in which nanoparticles have been dispersed controls its ability to perform reliably and smoothly and is ultimately influenced by the colloidal stability. The rate at which nanoparticles settle out of dispersions is an important parameter determining colloidal stability and can be calculated using Stokes' law [103].

$$v_z = \frac{2(\rho_{NP} - \rho_F) g r^2}{9\mu} \quad (9)$$

Where v_z is the settling or terminal velocity, ρ is density (the subscripts NP and F indicate nanoparticle and fluid, respectively), g is gravity, r is the radius of the nanoparticle, and μ is the dynamic viscosity of the fluid. This equation indicates that for a given base-oil fluid, when the size of the nanoparticle additives decreases, say 10-fold, the settling time will increase 100-fold. This simple calculation reveals that potential improvement in the stability of nanoparticle dispersion can be achieved through decreasing the particle size.

The colloidal stability and homogeneous distribution of nanoparticles in a base-fluid depend ultimately on the interactions among the particles. The main source of these inter-particle interactions is the ubiquitous van der Waals force which stems from induced dipole-induced dipole interactions. Van der Waals forces are attractive in nature (could be repulsive for dissimilar materials) and generally favor the aggregation or flocculation of the particles. To better illustrate this, let us consider two spherical nanoparticles of equal radius, R, separated by a distance, D, and interacting across a medium as depicted in Figure 8.

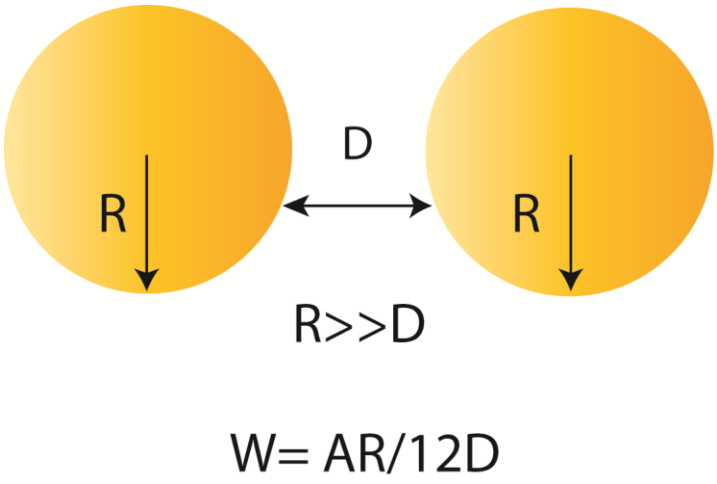

Figure 8. Schematic illustration of the interaction between two bare nanoparticles.

For short separation distances (i.e. D << R), the energy of interaction, W, is given by equation 10.

$$W = -\frac{AR}{12D} \tag{10}$$

where A is the Hamaker constant which is typically in the order of 10^{-19} and and 10^{-21} J and is a function of the properties of the material and suspending medium:

$$A = \frac{3}{4}kT\left(\frac{\varepsilon_1-\varepsilon_3}{\varepsilon_1+\varepsilon_3}\right)^2 + \frac{3h\vartheta_e}{16\sqrt{2}}\frac{(n_1^2-n_1^2)^2}{(n_1^2+n_1^2)^{\frac{3}{2}}} \tag{11}$$

where k is Boltzmann's constant, T is the absolute temperature, ε is the dielectric constant (a measure of polarizability), h is Planck's constant, ϑ_e is the maximum electronic absorbance frequency, and n is the refractive index. The subscripts 1 and 3 refer to the particle and medium, respectively.

The Hamaker constant is an important parameter because its sign determines whether the interaction is repulsive or attractive, while its magnitude determines the strength of the interaction. From Equation 11, it can be seen that, for the case of bare

nanoparticles, will always take on a positive sign, indicating the interaction is always attractive. Therefore, bare nanoparticles of metals, metal oxides, ceramic materials, and chalcogenides, dispersed in inert non-polar liquids (such as hydrocarbons) will aggregate and form clusters resulting in an unstable dispersion. This will ultimately lead to the precipitation of nanoparticles in oil and will not improve the tribological performance of the base oil. The reason is that bare nanoparticles experience material transfer when they come into direct contact with shearing surfaces although they do prevent their cold-welding (Figure 9).

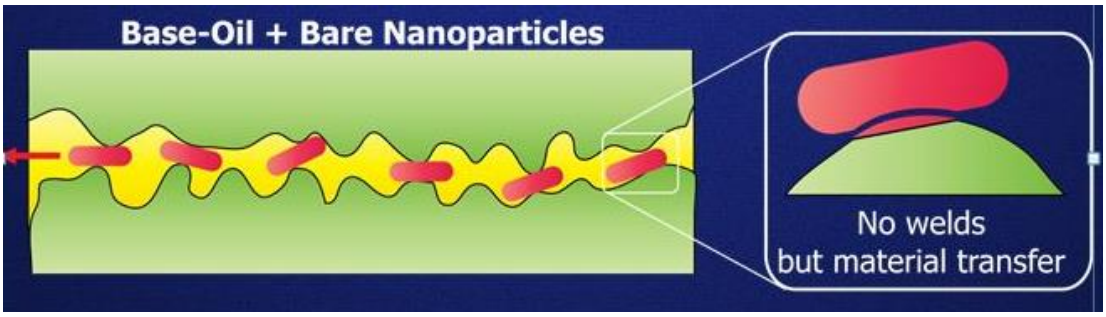

Figure 9. Schematic illustration of material transfer by bare nanoparticles.

To circumvent the nanoparticle aggregation problem, researchers have developed two methods to improve the stability of nanoparticle dispersion: a) electrostatic repulsion b) steric repulsion. Electrostatic repulsion is typically done via the adsorption of ionic surfactants on the nanoparticle surface. The theory behind this type of interaction is based on the fact that like-charged particles repel each other in accordance with Coulomb's law. Moreover, the choice of solvent (i.e. dielectric constant), concentration

and chemical nature of the surrounding ions have emerged as critical parameters that affect the magnitude and scale of electrostatic forces.

Steric repulsion is achieved by functionalizing the nanoparticle surface with a tightly bound polymer or a surfactant monolayer [104]. The general requirement is that the surfactant layer must have an affinity to the solvent so that easy dissolution is enabled. That is, it should be hydrophilic in an aqueous medium and hydrophobic in a low polar organic medium [105]. The organic surfactant typically consists of a polar group which chemisorbs onto the nanoparticle surface and long alkyl chain which enables its dissolutions in the lubricating oil. The theory behind employing polymer brushes has been treated thoroughly in the literature and is based on the repulsive forces developed upon compression of neighboring polymer "brushes". From a mathematical point of view, the equilibrium thickness, h_0, as well as the free energy per unit area , f, of the polymer brush can be approximated by [106]:

$$h_0 = N\left(\frac{12\Gamma b^5\omega}{\pi^2}\right)^{\frac{1}{3}} \tag{12}$$

$$f(h) = \frac{\pi^2 kT\Gamma {h_0}^2}{6Nb^2}\left[\frac{1}{2}\left(\frac{h_0}{h}\right) + \frac{1}{2}\left(\frac{h}{h_0}\right)^2 - \frac{1}{2}\left(\frac{h}{h_0}\right)^5\right] \tag{13}$$

Where N is the degree of polymerization, Γ is the surface density, b is the characteristic length of each monomer, and ω is the excluded volume parameter. It can be concluded from Equation 13 that the free energy increases with increasing osmotic pressure difference between the brush and the solvent. The counteracting force to this increase in osmotic pressure comes in the form of compression of the polymer brushes which leads to the repulsive nature of this interaction.

To summarize, surface functionalization is a prerequisite when the enhanced colloidal stability and homogenous distribution in base-oil are required. The resulting core-shell structures are usually referred to as “oil-soluble” additives owing to their high stability and solubility in lubricating oil which make them attractive in terms of enhancing tribological properties. The reason behind this enhancement is that surfactant-coated nanoparticles have a hybrid structure, with a hard interior and a soft exterior. This synergistic combination eliminates the possibility of cold-welding and provides nanoparticles with a rigid shape and a slippery fluid-like surface. This allows for a high load carrying capacity without trading off any lubricity.

2.5.3 Interaction between nanoparticles and surfaces

Apart from the inter-particle interaction, it is of vital importance to take into account the interaction between the nanoparticles and shearing surfaces. The main role of the nanoparticle additives in lubricating oil is to be present in the contact zone at the time they are required. This phenomenon requires a fundamental understanding of the particle-substrate interaction which can be physical, chemical or both. Consider, for example, a scenario in which a spherical nanoparticle of radius, R, is interacting with a substrate, a distance D away from the nanoparticle as shown in Figure 10.

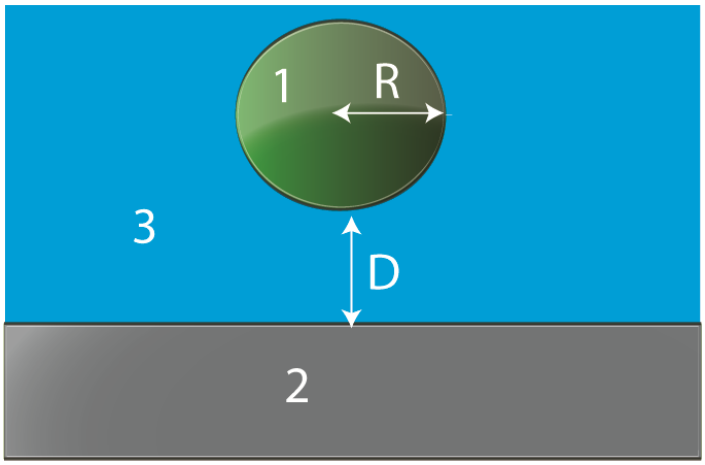

Figure 10.Interaction between a nanoparticle and a surface.

The energy of interaction is given by Equation 14:

$$W = -\frac{AR}{6D} \tag{14}$$

Where $A = \frac{3}{4}kT\left(\frac{\varepsilon_1-\varepsilon_3}{\varepsilon_1+\varepsilon_3}\right)\left(\frac{\varepsilon_2-\varepsilon_3}{\varepsilon_2+\varepsilon_3}\right) + \frac{3h\vartheta_e}{8\sqrt{2}}\frac{(n_1^2-n_3^2)(n_2^2-n_3^2)}{(n_1^2+n_3^2)^{\frac{1}{2}}(n_2^2+n_3^2)^{\frac{1}{2}}\left\{(n_1^2+n_3^2)^{\frac{1}{2}}+(n_2^2+n_3^2)^{\frac{1}{2}}\right\}}$ (15)

and the subscripts 1, 2, and 3 refer to the particle, substrate and medium, respectively. Note that when $\varepsilon_1>\varepsilon_2>\varepsilon_3$ or $\varepsilon_3>\varepsilon_2>\varepsilon_1$ or $\varepsilon_3>\varepsilon_1>\varepsilon_2$ or $\varepsilon_2>\varepsilon_1>\varepsilon_3$, A will always take on a positive sign resulting in an attractive interaction. However, when $\varepsilon_1>\varepsilon_3>\varepsilon_2$ or $\varepsilon_2>\varepsilon_3>\varepsilon_1$ (i.e when the medium has an intermediate dielectric constant), A will always take on a negative sign resulting in a repulsive interaction. As a result, by simply considering the magnitude of the dielectric constants of the materials and media involved, one can manipulate the sign of A and consequently the type of interaction. For instance, if it is desired to adsorb nanoparticles onto the surfaces, then these nanoparticles should be made out of materials with high dielectric constants (i.e. metals). Moreover, the van der Waals interaction of nanoparticles with the substrate can result in their deformation and

have direct implications on their tribological properties. This behavior was found in the study of carbon nanotubes which deformed axially and radially due to strong van der Waals interaction with the substrate [107]. This strong binding energy leads to an increase in the contact area between the tube and the substrate and results in the increase of shearing forces.

2.5.4 Melting point

Usually below 50 nm, the melting temperature of a nanoparticle sharply decreases with decreasing size [108-111]. For example, while the melting point of bulk CdS is about 1600 ºC, 2-nm CdS nanoparticles melt at 400 ºC [111]. Such size-dependent melting depression of nanomaterials needs to be considered during the design of nanoparticle-based lubricants to ensure that the nanoparticles intended for lubrication of engines and machines do not melt at the typical operation temperature ranges of the engines and machines. However, in some cases melting of nanoparticles can result in the formation of a protective film which leads to enhanced tribological properties. Consider the case of copper nanoparticles whose melting point is 490 ºC compared to 1073 °C, the melting point of their bulk counterparts. When these nanoparticles undergo high shearing forces and pressure across steel surfaces, their coating is no longer retained and uncouples from the core. The now bare nanoparticles are in direct contact with the steel surfaces whose flash temperature under the shearing process exceeds the melting point of the Cu nanoparticles. As a result liquid copper is formed and spreads across the steel surfaces under the shearing action, leading to the formation of a protective film [112].

Consequently, the friction coefficients as well as the abrasive wear are significantly reduced.

2.5.5 Concentration

Previous studies have indicated that the concentration of nanoparticles within base oil strongly influences the tribological properties of such lubrication systems [44]. In general, there is an optimum concentration at which the coefficient of friction is at a minimum. The principle behind this reasoning lies in the extent of nanoparticle coverage on the shearing surfaces. That is, when the nanoparticle concentration is too low, the nanoparticle coverage may not be enough to prevent the surfaces from engaging in intimate contact. However, when the nanoparticle concentration is too high, then the possibility of aggregation increases, thereby forming large clusters that can act as abrasive bodies which can damage the surfaces leading to a drastic increase in their wear and friction behavior [113]. Therefore, an optimum concentration is one which presumably provides enough nanoparticle coverage to protect the shearing surfaces without agglomeration. However, the optimum concentration for a specific tribosystem cannot be predicted. In other words, the optimum concentration is strongly system dependent, in that the lubricant formulation needs to be tuned for each operation condition.

2.5.6 Humidity

Humidity and other environmental conditions can have deep consequences on the surface properties and thus on the tribological behavior of nanoparticle-based lubrication systems. Studies have shown that even when the humidity is low, a water film will be

present on hydrophilic surfaces, and therefore the effect of humidity should never be neglected [114] . Moreover, friction and adhesion forces can be significantly influenced by the adsorption of such a thin water film due to the additional effect of capillary forces [115]. With respect to the nanoparticle-water interaction, it has been found that the presence of water is enough to disturb the structure of a surfactant-coated nanoparticle. That is, water is able to penetrate the region between the surfactant and the nanoparticle core, which in turn diminishes the stabilizing function of the surfactant and ultimately leads to nanoparticle aggregation via van der Waals forces. The surfactant layer is thus replaced by a water layer which can contribute to the bridging of the shearing surfaces through capillary action (or attractive Laplace pressure) generated by condensation leading to increased adhesion between the surfaces. To better understand the consequences of adhesion on the frictional properties, it is important to consider the adhesion-dependent contribution, $S_c A$, to the total friction force, F, as shown in Equation 16:

$$F = S_c A + \mu L \tag{16}$$

where S_c is the adhesion-critical shear stress, A is the real contact area, μ is the friction coefficient and L is the applied normal load. It can clearly be seen from the above equation that the increase in adhesion will result in an increase in the frictional forces. This effect was demonstrated in hexadecylamine-coated ZnS nanoparticles dispersed in dodecane, where an increase in the friction coefficient was observed with increasing relative humidity and exposure time [116]. This behavior was attributed to the increase in normal forces due to the capillary action. The aforementioned example illustrates the

negative role played by humidity in a nanoparticle based lubrication system. However, in some instances humidity can impart enhanced tribological properties in the case of graphite nanoparticles as it weakens the interlayer forces leading to lower shearing strength [57, 117]. The opposite effect is observed in the case MoS_2 nanoparticles where humidity can be detrimental to their structures and lead to poor tribological properties [118].

2.5.7 Tribochemistry

In a contact between tribo-pairs, local heating may be generated due to the shearing process. It is well known that many nanoparticle additives contain tribo-active elements such as sulfur, phosphorus, chlorine that can strongly adsorb on the shearing surfaces. The local heating effect combined with tribo-active elements is the ideal setting for a chemical reaction to take place, resulting in the formation of a tribochemical film which may provide good friction and anti-wear properties. For instance, it is well known that fullerene-like structures such as MoS_2 and WS_2 exhibit excellent friction and antiwear properties due to their exfoliation into nanosheets and subsequent deposition on the asperities of shearing surfaces [119, 120]. However, only recently has there been an investigation on the possibility of a chemical interaction occurring between MoS_2 nanosheets and the interacting surfaces [121]. Obviously, the chemical reaction is dependent on the type of interacting surfaces as well as the environmental conditions. For instance, tribochemical film was observed on the steel surfaces due to the chemical reaction that took place between MoS_2 nanosheets and the iron/iron oxide atoms of the shearing surfaces. This tribochemical film was absent when the nanosheets were sheared

across non-reactive species such as DLC and Alumina [121]. Similar tribochemical films were observed with Lanthanum borate and Magnesium borate nanoparticles in a steel/steel tribopair [122]. Moreover, some researchers have shown that deliberate incorporation of materials into non-reactive substrates can enhance the reactivity of the surface. This will lead to the formation of a lubricious film owing to the chemical reaction between the nanoparticle additives and the incorporated materials [20]. Studies also show that tuning the surface morphology can influence its chemical reactivity and therefore the formation of a tribochemical film or lack thereof [123]. Akbulut and co-workers later confirmed that the surfaces with lower roughness are less reactive that their high roughness counterparts [124].

Tribochemical reactions could also occur between the nanoparticles, wear debris as well as the surrounding air. Oxidized products resulting from the reaction between the particles and surrounding air can act as a lubricating film. However, one of the main reasons layered MoS_2 nanoparticles have been avoided as lubricant additives is because their lubrication structure is destroyed when exposed to oxidizing environments. That said, some researchers have found that low oxidation environment may lead to enhanced tribological properties while extreme oxidation can have deleterious consequences due to increase in interparticle cohesion.

2.6 Mechanical properties

2.6.1 Nanoparticle hardness

The variables influencing the mechanical properties of nanoparticles are expected to influence their tribological properties. For instance, the hardness of materials

increases with decreasing grain size due to increased number of dislocation pileups for crystals in the range of 100 nm or higher (Hall-Petch regime) [125-127]. In this regime, the hardness increases with the inverse square root of solid size. At the critical grain size, typically below 10 nm, nanomaterials become softer with decreasing size (Inverse Hall-Petch) regime [127-129].

Knowledge of the relative hardness of the nanoparticles in comparison with that of a coating on a substrate is also an important consideration when designing a nanoparticle based lubrication system. Therefore, different combinations of soft and hard nanoparticles interacting with a soft or hard coating can result in a distinct tribological performance. Consider the case where the nanoparticle is harder than the coating as shown in Figure 11. If the size of the nanoparticle is considerably smaller than the thickness of the coating, under loading and shearing, the nanoparticles are embedded in the soft coating and no improvement in the frictional properties is observed. However, when the size of the nanoparticle is comparable or larger than the thickness of the coating, the nanoparticles can penetrate and scratch the coating, and become anchored on the substrate causing its degradation by abrasion and plowing actions. This behavior is followed by a considerable increase in friction due to an increase in wear. On the other hand, if the nanoparticles are softer than the substrates, particle disintegration can occur under normal loading resulting in frictional increase [20]. However, if the nanoparticles are spherical or near-spherical in shape, then the particles may act as roller-bearings which results in a decreased friction.

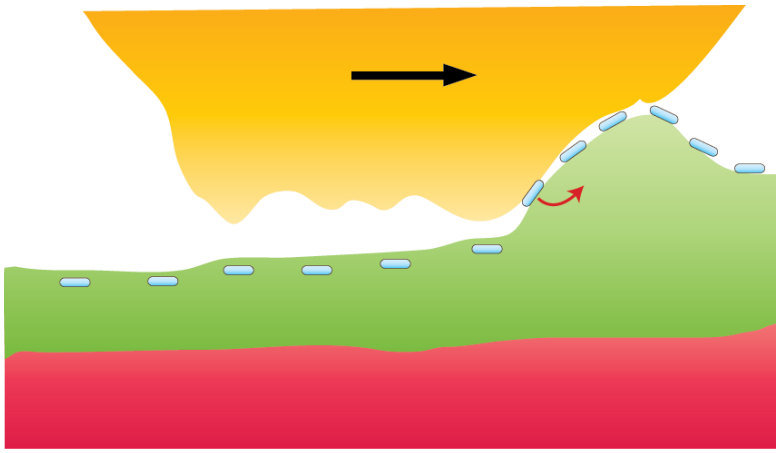

Figure 11. Schematic illustration of the embedding of hard nanoparticles into a soft coating.

2.6.2 Internal structure

The internal nanostructure of nanoparticles can influence their mechanical properties and therefore their tribological properties. For instance, vacancies within nanomaterials act as pinning centers inhibiting dislocation motion, thereby enhancing the mechanical strength within a certain concentration [130, 131]. Thus, the presence of a limited amount of atomic vacancies can enhance the mechanical strength of the nanomaterials and could be desirable from a tribological perspective. However, excessive amounts of cavities are disadvantageous for the mechanical strength of the nanomaterials. For example, the Young's modulus of a defected nanotube is gradually reduced with each atomic defect, and the plastic strength of the nanotubes is dramatically influenced by the existence of just a few atomic defects [132, 133].

That said, consider a nanoparticle with a lamellar internal structure, in which the internal layers are held together by weak van der Waals forces. These weak forces allow for the easy shearing of the planes thereby resulting in friction reduction. In addition, when a

normal force is applied, a strong resistance is encountered which confers a high yield strength to the nanoparticle. This high yield strength will help carry part of the normal load applied, thereby increasing the load carrying capacity of the lubricant. This combination of high yield strength and weak inter-layer forces forms the basis of excellent tribological performance displayed by nanoparticles such as MoS_2, WS_2, and graphite.

2.7 Geometrical considerations

2.7.1 Effect of nanoparticles size

One of the main reasons nanoparticles have gained popularity as lubricants or lubricant additives is their ability to penetrate the contact area owing to their nanometer size. It is well known that when nanoparticles are squeezed out of the contact region upon loading and shearing, the shearing surfaces do not gain any tribological benefits. In other words, for nanoparticles to perform as effective lubricants, they must remain in the contact region during loading and shearing in order to prevent direct contact between the surfaces. That said, at a given concentration, smaller nanoparticles are able to penetrate the contact zones more easily than larger ones, and form a better protective film because there are more nanoparticles available. Larger particles tend to collect and accumulate in front of the leading edge of the base body and counterbody leading to the starvation of the contact zones from the flow of lubricant [134].

Some researchers have found that this mechanism depends on the lubrication regime and ultimately the film thickness and type of contact. For example, in the elastohydrodynamic regime of a rolling contact, if the nanoparticle diameter is larger

than the film thickness, then the nanoparticles are mechanically entrapped and adhere to the surfaces thereby contributing to the film thickness. However, if the EHD film thickness is larger than the particle diameter, the particles can pass through the contact and be ejected from the contact zone without any contribution to the film thickness [135]. In mixed lubrication, when the film thickness is comparable to the size of nanoparticle, sliding/rolling mechanism takes place and the nanoparticle shape is preserved [61]. On the other hand, when the nanoparticle size exceeds the film thickness, distortion and destruction of nanoparticle occurs, which leads to the formation of a transfer film onto the substrate.

The nanoparticle size effect can play a significant role in the so called "rolling friction", a mechanism that results in reduced friction. Previous work with original fullerene C_{60} has shown that they function and roll as miniature ball bearing. However, when the surface topography is considered, they failed to provide a similar effect since they become trapped between asperities. The reason for this trapping is that the size of C_{60} is comparable to the lattice atoms or to the characteristic roughness scale of the surface asperities [115]. A similar phenomenon was observed when using different size gold nanoparticles. On the other hand, when the nanoparticle size exceeds the roughness of the shearing surfaces, the rolling mechanism is retained and improved tribological properties are observed, as in the case of SiO_2 nanoparticles [136]. However, when the size of the nanoparticles is significantly larger than the relative surface roughness, the particles can agglomerate and act as abrasive bodies and become damaging to the

surfaces. Additionally, they can hinder the flow of lubricant by accumulating at the inlet.

2.7.2 Nanostructure and shape

The shape of nanoparticles used in lubricant additives is another important parameter to consider in the context of designing nanoparticle-based lubricants. The shape of the nanoparticles directly determines the pressures experienced by the nanoparticles upon loading. For instance, for a given load, nanospheres experience the largest pressure and nanosheets the smallest, because while nanospheres make a point contact with a counter surface, nanoplatelets make a planar contact (Figure 12). Thus, for a given load, nanosheets have the least probability of indenting and deforming the asperities of shearing surfaces. Moreover, the nanoparticle shape plays a significant role in the initiation and strength of adhesion under different shearing circumstances. For instance, a comparison between the adhesion dynamics of a nanosphere and a nanorod shows that under a medium shear rate, the nanoparticle is in the standing position (i.e. makes a point contact with the wall) and maybe removed from the contact area easier than a nanosphere. However, under high shear rates the opposite effect is observed due to the larger contact area (i.e. nanorod lays parallel to the wall) which results in a higher shear resistance.

Figure 12. Illustration of effect of nanoparticle shape on the contact pressures.

Previous studies have also shown that the shape and structure of nanoparticle films have a great influence on their adhesion and frictional properties. Perhaps the most famous example of nanoparticle additives is the inorganic fullerenes of metal dichalcogenide such as MoS_2 and WS_2 which have shown excellent tribological properties. The platelet kind consists of lamellar structure that is characterized by weak van der Waals forces between the lamellae which allows for their ease of shearing. However, their hollow nearly-spherical counterparts have been found to provide a superior performance because they can roll and act as miniature bearings (provided their size exceeds that of the surface roughness) and depending on the load used, they are susceptible to deformation and subsequent exfoliation and deposition on the asperities, thereby providing an extra cushion to better protect the surfaces.

The structure of nanoparticles has a significant effect on the ordering and organization of the nanoparticles under confinement. These phenomena have tremendous ramifications on the normal and shear forces. For example, consider two systems of nanowires having different structures (i.e. curved and straight). Under confinement, the normal forces exhibit a different behavior with a hard-wall separation for curved nanowires equal to 4 times that of the straight nanowires, a behavior

attributed to the elasticity of the curved nanowires [137]. However, the frictional forces can be higher for the curved nanowires due to their higher probability of entanglement. Another example that sheds the light on the structural effect of nanoparticles is that which involves the comparison between a perfectly crystalline versus amorphous structure in the case of inorganic-fullerenes. It was found that the latter outperforms the former owing to the presence of defects which facilitates their exfoliation and deposition on the surfaces, thereby forming a tribofilm with enhanced tribological properties. On the other hand, the lubrication functionality decreases with decreasing crystallinity in the case of graphite. A hexagonal crystal configuration is preferred over a cubic configuration in the case of BN for lubrication purposes [57].

2.7.3 Surface structure

To the authors' knowledge, it was not until a mere two years ago that a systematic study on the effect of surface structure on nanoparticle-based lubrication systems has been investigated. The motive for this type of investigation was to answer two fundamental questions: a) Does a nanoparticle-based lubrication system having a superior tribological properties across a given surface, also possess these properties on another type of surface? b) If the answer is no, then what are the most important parameters of shearing surfaces and nanoparticles influencing tribological properties of nanoparticle films?

It was hypothesized that roughness and surface structure can strongly influence the friction behavior of nanoparticle-based lubrication systems based on the fact that 1-2 nm roughness can significantly affect the friction and adhesion of unlubricated surfaces.

As stated earlier, nanoparticles must remain in the contact zone for effective lubrication to take place. Therefore, the asperities of shearing surfaces can act as physical barrier to help keep the nanoparticles within the contact zones. To better illustrate this effect, let us consider two different conceptual cases. The first case is that when the characteristic roughness length scale of shearing surfaces is smaller than the nanoparticle radius, the ratio of the *rms* roughness to the radius of nanoparticle is an indicator of how much lateral force is required to dislodge a nanoparticle out an asperity barrier. This means that if the nanoparticles are too large and non-adhering, they can easily escape from the contact zone and lead to poor lubrication. In the second case, when the characteristic roughness length scales are much larger than the nanoparticle radius, the valleys between the asperities of shearing surfaces can be filled with nanoparticles, i.e. nanoparticles artificially smooth out the shearing surfaces, and, hence can improve the tribological properties.

2.8 Outlook

The effectiveness of surface functionalized nanoparticles as lubricant additives has been well established, and the parameters which determine the performance of such systems have been thoroughly examined; the next step is to identify the challenges that must be overcome for practical application of these systems. If the energy saved by implementation of nanoparticle-based lubrication systems is not enough to offset the cost of manufacturing, then it is unreasonable to pursue their application. In this section we discuss current advances in the scale-up of nanoparticle synthesis, anticipate

environmental consequences of NBLS use, and suggest directions in which further investigation might prove useful.

2.8.1 Scale-up of NBLS production

A report from the DuPont R&D Experimental Station identified four aspects to the commercial application of nanotechnology that must be addressed in order to manufacture nanotechnology products at a reasonable cost: initial nanosynthesis, nanofabrication/processing, incorporation into bulk products, and characterization of final product properties [138].

With regards to NBLS, nanosynthesis will entail the large scale production of nanoparticles with uniform size, shape, and crystalline structure. Hyeon et. al have developed procedures for the liquid-phase synthesis of highly monodisperse metal, metal oxide, and metal chalcogenide nanoparticles using relatively inexpensive and environmentally friendly starting materials such, as iron chloride and sodium oleate for synthesis of iron oxide particles. The highest yield reported with these methods is 40 g per single batch. Parallel reactors could be set up for the production of kilogram amounts of nanoparticles, and the high degree of monodispersity achieved eliminates the need for product separation by particle size [139]. Flow reactors such as impinging jet mixers and diffusion flame reactors can be used to produce larger quantities of nanoparticles, generally at the cost of higher polydispersity [140]. With diffusion flame reactors, Wegner reports 25g/hr production of SiO_2 particles with size ranging from 50 to 80 nm, and Jang reports 20g/hr production of TiO_2 particles with size ranging from 10 to 30 nm [141, 142]. These production scales will not generate the amount of nanoparticles

needed for widespread adoption in commercial machinery lubricants, so advances the scale-up of nanoparticle production are needed before they become commercially viable. Nanofabrication/processing and nanoincorporation entail the surface functionalization and uniform dispersion of nanoparticles in lubricants. Surface functionalization of nanoparticles is essential for colloidal stability. While the liquid phase synthesis methods reviewed in tribological studies typically generate nanoparticles with surface coatings, flow reactors produce bare nanoparticles. Tsutsumi et. al report the use of impinging-jet reactors to coat the surfaces of SiO_2 and TiO_2 particles with paraffin. Silica particles with average diameter of 1 μm were successfully coated, however the 20 nm diameter titanium dioxide particles tended to agglomerate before the surface layer formed. The distance between impinging jets was found to be the most important factor influencing the coating rate [143]. Nanoparticle lubricant additives could be easily incorporated into bulk products with existing technology. Nanocharacterization entails the systematic organization of products tailored for specific tribological applications. Ideal combinations of anti-wear and friction reducing additives will be unique to individual systems and may change over time. For example, the optimal particle size for friction reduction, which is proven to be a function of relative surface roughness, will change over time as wear changes the surface roughness of machinery. This implies that the optimal NBLS for a machine will depend on the age of the machinery.

2.8.2 Environmental implications

Increasingly stringent emission standards for machinery necessitate the development of environmentally friendly lubricants. In order to accurately anticipate the

ecological consequences of NBLS use, it is necessary to understand the mobility, reactivity, toxicity, and persistency of nanoparticles in the environment [144]. Nanoparticles such as silica, CaCO3, and CNTs are chemically inert and environmentally friendly; the primary environmental concern is with nanoparticles containing toxic metals, or surface coatings containing reactive elements such as sulfur and phosphorous.

Current models for the quantitative risk assessment of nanoparticles in the environment are limited by reliability of data regarding the worldwide production of nanosized materials, and by the scarcity of data regarding measured concentrations of nanoparticles in the environment. There simply does not exist a comprehensive list of all products containing nanoparticles, or all types of nanoparticles used as ingredients [145]. Furthermore, existing techniques to quantitatively monitor the presence of engineered nanomaterials in the environment are lacking [146]. Current literature suggests that TiO_2 and ZnO nanoparticles may already be present in aquatic environments at concentrations that pose a threat to living organisms, while CNTs and Ag nanoparticles do not seem pose an imminent hazard [147]. These studies are of course restricted by the reliability and availability of data. In addition to accurate data and measurements, fundamental studies of the behavior of nanoparticles in the environment are needed. Evaluation of the entire life-cycles of NBLS will entail particle release during manufacturing, use, and disposal of products, as well as movement of released nanoparticles throughout the environment and ecosystem.

2.8.3 Current opportunities

Until further advances are made in the scale-up of nanoparticle production, it is unlikely to see adoption of NBLS in industrial settings. However, as the fields of MEMS and NBLS are simultaneously maturing, it is likely that new electromechanical systems will continue to utilize the latest in lubricant technology. Many of the tribological studies reviewed in this article are fundamental in nature, seeking to observe and understand the improvements effected by nanoparticle lubricant additives. The next logical step towards large-scale implementation of these systems is to study combinations of anti-wear, friction reducing, and corrosion inhibiting additives with regards to specific applications. The variety of machinery in industry will certainly demand numerous unique lubrication systems. A methodical development of NBLS for industrial applications will enable efficient use of these systems as soon as production capacities are sufficient, so it is worthwhile to pursue such studies even while production capacities are still limiting. It is also important to note that many lubricant additives exhibiting superior performance are potentially hazardous, therefore development of environmentally friendly additives with similar performance is particularly desirable. As indicated in the previous section, research into the lifecycles of engineered nanomaterials will enable a more complete understanding of the environmental effects associated with NBLS use.

2.9 Conclusion

The motivation for development of novel lubrication systems ranges from improving the performance of existing industrial machinery to enabling the use of advanced engineered systems currently being developed. Nanoparticle based lubrication

systems are capable of significantly reducing energy losses and material wear due to friction. Enhanced lubrication is achieved by the ball-bearing effect of nanoparticles between shearing surfaces, and by tribochemical reactions leading to the formation of protective films. Fundamental studies of nanoparticle lubricant additives made of a numerous materials, with various sizes, shapes, and surface modifications have established their effectiveness and clarified the importance of the physiochemical, mechanical, and geometrical parameters which control the performance of these lubrication systems.

The most important physiochemical consideration in the design of a NBLS is the colloidal stability of the nanoparticles in base oil. The particle size and nature of interparticle forces determine whether particles will agglomerate and settle or stay uniformly dispersed. Surface modification is frequently employed to improve the colloidal stability of nanoparticle lubricant additives. The nature of interaction between nanoparticles and shearing surfaces controls the ability of particles to stay in the contact zone while shearing occurs. Optimal concentrations of nanoparticle additives are unique to individual tribosystems, and the presence of humidity can dramatically alter the performances of these systems. Tribochemical reactions can take place at temperatures above the melting point of nanoparticles and form protective films over shearing surfaces. The hardness and melting point of nanoparticles are dependent on size and crystalline structure, and it is also important to consider the size of particles relative to the roughness of the shearing surface.

Currently, the greatest challenge to overcome for industrial application of NBLS is the scale-up of processes for the synthesis of monodisperse nanoparticles. However, this should not preclude the systematic development of NBLS for various commercial uses. Moving from fundamental studies to determination of optimal additive combinations for particular applications will spawn a new body of research, where all of the aforementioned parameters must be considered simultaneously. As accurate studies of the environmental effects of nanoparticles in the environment emerge, it is also important to pursue the development of ecologically safe additives which achieve the same performance as potentially hazardous additives.

CHAPTER III

EXPERIMENTAL METHODS AND CHARACTERIZATION

3.1 Description

This chapter aims to provide a brief description of the major techniques used in this work. These include Atomic Force Microscopy (AFM), Nanotribometery, Scanning Electron Microscopy (SEM), Transmission Electron Microscopy (TEM), and X-Ray Photon Spectroscopy (XPS).

3.2 Atomic force microscopy (AFM)

Atomic Force Microscopy [148] is a high-resolution scanning probe technique widely employed in the evaluation of topographical and tribological properties of various surfaces at the nano-scale. A schematic diagram of the basic principle of AFM is shown in Figure 13 . AFM consists of a cantilever with a sharp tip typically made of silicon or silicon nitride material. The tip has a nanometer-size radius of curvature and is used to scan a relatively small area of the sample surface. The opposite end of the cantilever is connected to a piezo-scanner which contracts or expands upon the application of an electric field [149]. The piezo-scanner also accommodates the movement of the tip and the sample in the x, y and z directions. The interactions between the tip and the sample result in the movement of the tip which is detected by a four-segment photodiode detector in the form of a laser beam reflected off the back of the tip. Given the spring constant, and the deflection of the tip, forces can be readily calculated using Hooke's law. Typical spring constants range from 0.001 to 100 N/m

resulting in forces on the order of 10^{-11} to 10^{-6} N [150]. Most AFMs are typically operated in two different modes: contact mode and tapping mode. In the contact mode, the tip remains in a constant soft contact with the sample where either the height of the tip is fixed or a constant force is maintained. The ionic repulsion forces which exceed the attractive forces allow for the surface topography to be traced with high atomic resolution [150]. Noise and drift are considered to be drawbacks of this mode of operation, while degradation of the tip can also occur due to repeated contact [151]. In the tapping mode, the tip is oscillated up and down near its resonant frequency, and the oscillation is maintained constant through a feedback loop [152]. The interaction between the tip and the sample cause a change in the amplitude of oscillation as well as vertical adjustment in the piezo-scanner. This vertical adjustment is recorded as height information, allowing for high-resolution topography images to be obtained. One of the advantages of employing this mode of operation is that it reduces the damage of both the tip and the sample [152].

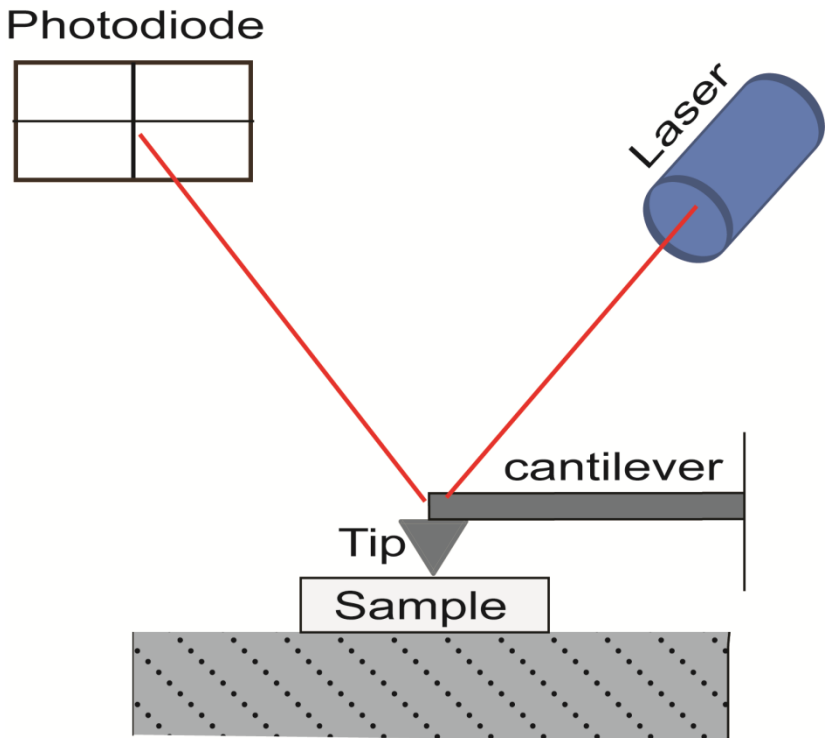

Figure 13. Schematic illustration of the operating principle of an atomic force microscope set up.

A host of information can be obtained with an AFM measuring nano-scale frictional forces resulting from single asperity contacts. AFM can also be used to measure the adhesion forces between the tip and the sample surface. In this work, however, the AFM (Nanoscope IIIa, Veeco Instruments, Santa Barbara, CA) was employed strictly to characterize the topography of various surfaces. Specifically, we aim to quantify the surface structure and develop mathematical correlation between the tribological properties and the surface roughness parameters. One way to mathematically describe the surface structure is to quantify vertical deviations of a real surface from its ideal form. If these deviations are large, the surface is considered to be rough, and smooth if the deviations are small. However, this information is not sufficient to

completely describe the surface structure. As illustrated in Figure 14, although vertical deviations for all three hypothetical structures are the same, the lateral deviations are not. The proper description of the surface structure has to include height parameters, spatial parameters, and hybrid parameters. Thus, we will describe the surfaces in terms of root mean square (rms) height, distance between asperities, number density of asperities, asperity size, and other parameters deemed appropriate. A software analysis package is used to assist in the evaluation of these parameters.

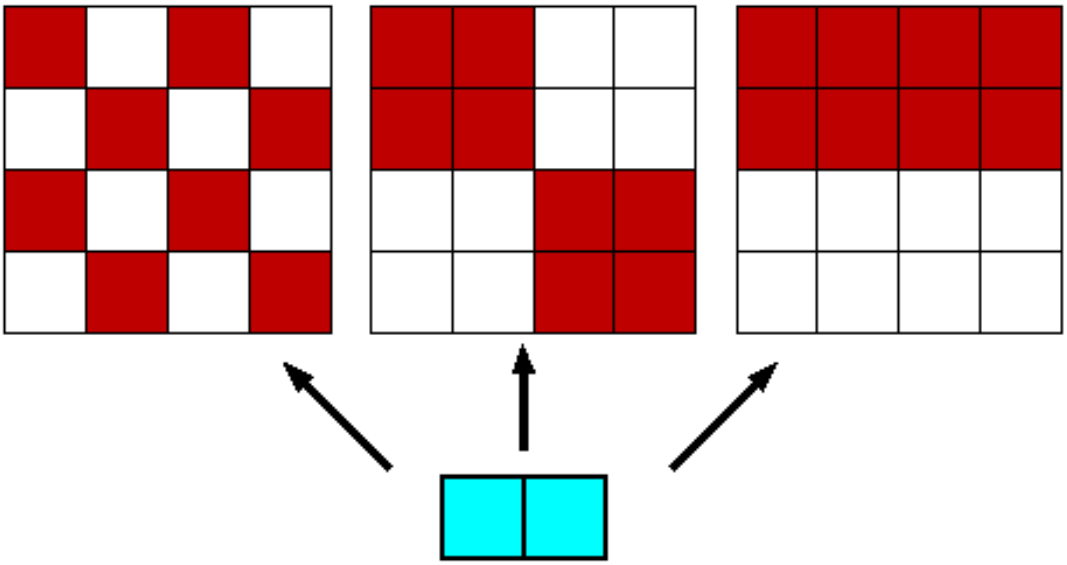

Figure 14. Three hypothetical surfaces having the same vertical deviations from the perfect flatness, but different lateral structures. Their possible interaction with an object (red squares have a finite height, while white ones are mathematically flat.

3.3 Nanotribometry

A nanotribometer is an instrument designed to study the tribological properties between surfaces in contact under dry and lubricated conditions. A large variety of

tribometers exist including pin-on-disk, four-ball, block-on-ring, to name a few. In this work, the primary focus will be on a pin-on-disk tribometer the schematic of which is shown in Figure 15. The tribometer used in this study consists of a linear reciprocating module and a cantilever spring assembly. The cantilever spring assembly consists of a spring with a known spring constant at the tip of which a ball holder is located. In addition to the ball holder, two mirrors are located on top of the spring: one mirror is flush with the spring surface and the other perpendicular to it. Each mirror is faced by an optical sensor to allow the detection of normal and lateral deflections. Given the spring constant, and the deflection of the spring, forces can be obtained using Hooke's law.

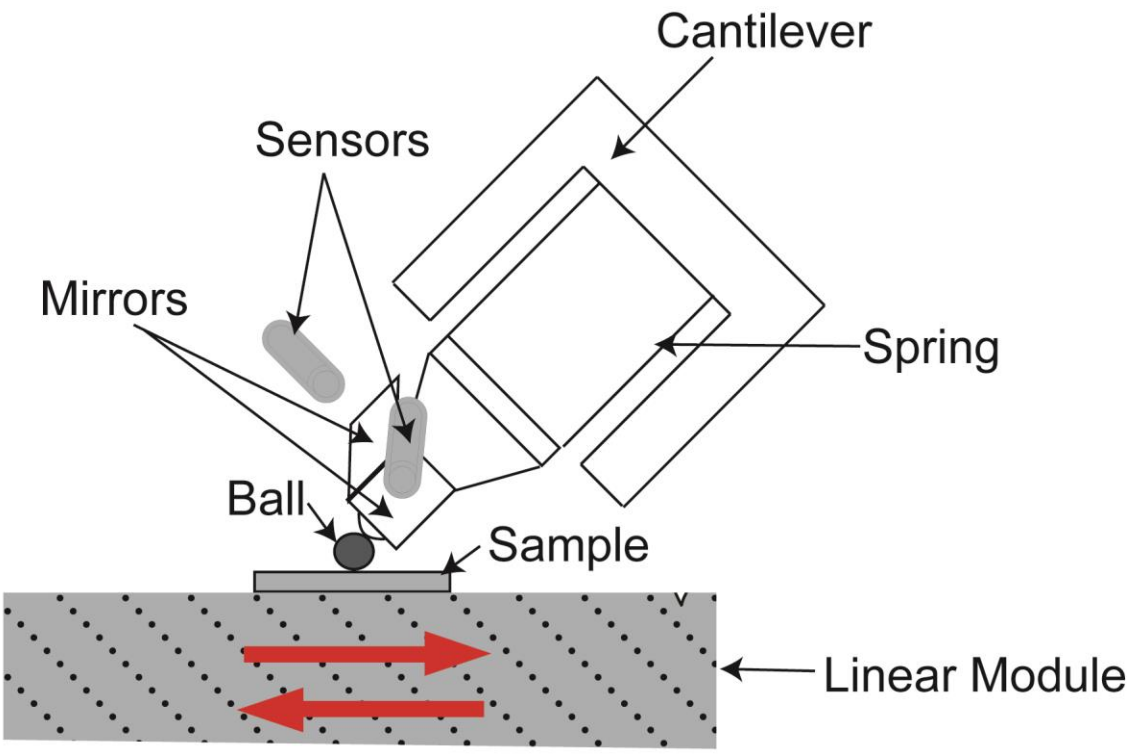

Figure 15. Schematic illustration of the operating principle of a nanotribometer.

In a typical experiment, the cantilever spring assembly is mechanically lowered until the ball (counter body) is in close proximity to the surface (base body). A normal load (the load range depends on the spring stiffness) is then applied and the ball automatically approaches the surface until contact is detected. Once contact is detected, the linear module is set in a linear motion for a pre-determined number of cycles allowing for the shearing process to take place. At the end of a test cycle, the cantilever is automatically retracted to its original position. This procedure is repeated for various normal loads resulting in the recording of their corresponding frictional forces. A plethora of information can also be gained by such experiments, including friction traces, friction coefficient, wear rate, adhesive forces etc. However, in this work plot of the frictional force vs. normal load is typically obtained and the friction coefficient is determined by the slope of the line. In addition, we are interested in the analysis of the friction traces which reveals details about the type of sliding motion (i.e. smooth or stick-slip).

3.4 Scanning electron microscopy (SEM)

SEM is an advanced technique that helps examine the structure and chemical composition of a surface. A schematic illustration of the components of a typical SEM is shown in Figure 16. In contrast to the laser beam used in AFM, an electron beam is employed in SEM. The electron beam originates from a so-called electron gun typically made of tungsten material and is focused on the specimen surface via scanning coils and magnetic lenses under high vacuum conditions. Specimen preparation is a crucial step before microscope examination; That is, the specimen must be fairly conductive (to

avoid the so-called electric charging) for the smooth operation of SEM and for obtaining high quality images. However, if the specimen is not conductive, coating it with a nanometer-thick layer of gold or platinum will not only ensure its conductivity but also protect the specimen from damage by electron bombardment.

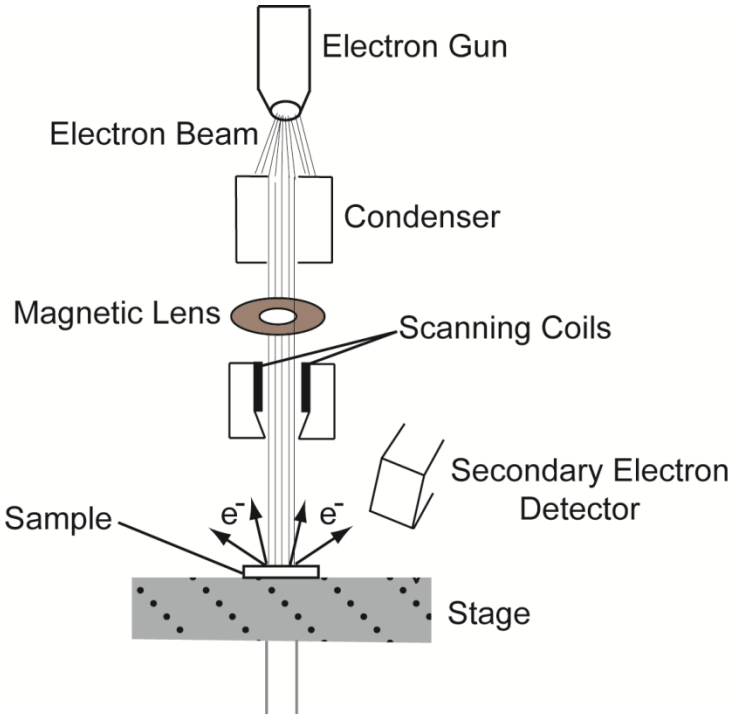

Figure 16. Schematic illustration of a scanning electron microscope.

A typical SEM operates on the following principle: As the specimen is bombarded with electrons, secondary electrons are dislodged in a peculiar pattern and collected by a secondary detector. The signal generated in the secondary detector is used to construct an image consisting of bright and dark spots depending on the number of electrons that reach the detector. Other detectors, such as the backscattered electron detector, are used to collect back scattered electrons to reveal details about the chemical

composition of the scanned area. Elements with high atomic number are represented by bright spots whereas those with lower atomic number appear as dark ones. In this work, SEM was used as a post-characterization tool to examine the topographies of surfaces, specifically wear scars resulting from the shearing of surfaces. The wear scars are analyzed further to obtain information about the extent of damage and quantify the wear volume generated by the shearing mechanism.

3.5 Transmission electron microscopy (TEM)

Transmission electron microscopy is a useful technique for observing the size, shape and structure of functionalized nanoparticles. TEM employs a beam of electrons to create an image of the specimen. Typically, a tungsten filament is placed under a high voltage drop to initiate electron emission. The electron beam enters a vacuum chamber where a series of electromagnetic lenses focuses the beam onto the sample [153]. The interactions between the electron beam and the sample can be detected and interpreted through several modes of TEM operation. The sample must be adequately thin (10-100 nm) to avoid excessive electron scattering and ensure clarity of the image.

Bright field imaging is most straightforward TEM operating mode. This mode discerns between different chemical species within the sample, enabling visualization of object shapes at the nanoscale. The image is formed by detecting the beam of unscattered electrons exiting the sample [153]. Similarly to SEM, high atomic number compounds scatter a greater amount of electrons than low atomic number compounds, and therefore appear dark while low atomic number compounds appear bright. Alternatively, other modes of operation exclude detection of the unscattered beam and

create images from the diffracted electrons. Information about the crystalline structure, phase boundaries, and lattice defects of the sample can be obtained from examination of the diffraction patterns.

Typical sample preparation consists of depositing a small droplet of a diluted solution onto a copper grid/film. After drying at ambient conditions, the sample is placed on a holder inside the vaccum chamber of TEM for characterization. In this work, the TEM (JEOL-2010, Tokyo, Japan) was strictly employed to characterize the size and shape of the nanoparticles.

3.6 X-Ray photon spectroscopy (XPS)

XPS is a powerful technique commonly used in the evaluation of the electronic state and chemical composition of elements present on a sample surface. A schematic illustration of this technique is depicted in Figure 17. The top 1-10 nm layer of the sample surface is typically irradiated by a beam of X-Rays under ultra-high vacuum conditions (10^{-9} Torr). Photoelectrons subsequently escape from the surface and the number of electrons and corresponding kinetic energy are collected in a so-called electron-energy analyzer. The physical principle that lies behind the operation of this technique is based on an energy balance as follows [154]:

$$BE = KE - h\vartheta - \varphi \quad (17)$$

Where BE is the energy required to remove an electron from an atom or molecule and is often referred to in the literature as the binding energy, KE is the kinetic energy of the emitted electron, $h\vartheta$ (h is Plank's constant and ϑ is the frequency of radiation) is the energy of the x-ray source, and φ is the work function of the spectrometer.

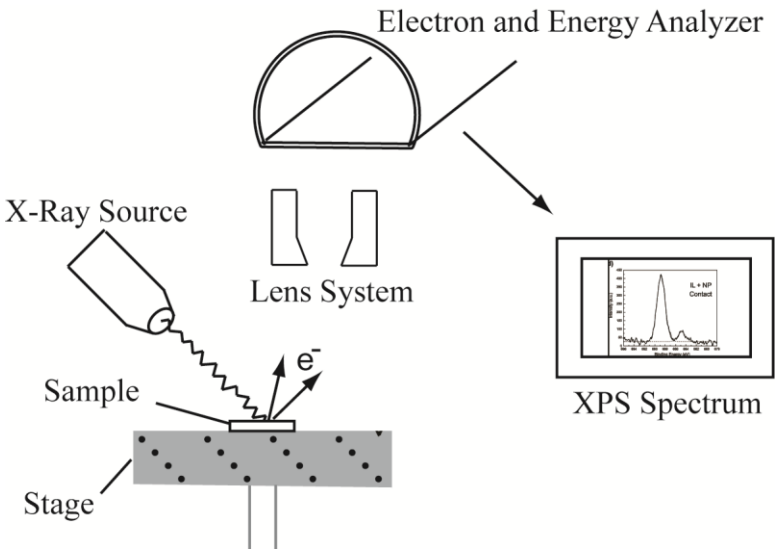

Figure 17. Schematic illustration of X-Ray Photon Spectroscopy (XPS).

Following this principle, an XPS spectrum is generated by plotting the counts per second on the ordinate axis and the binding energies on the x-axis. The spectrum consists of peaks the presence of which indicates the presence of a particular element and its intensity reveals information about the concentration of the element. The area under the peak is usually calculated to gain knowledge about the chemical composition. The chemical state of a species is typically detected by evaluating the so-called chemical shift which is the difference in binding energies between the element in a specific state and the pure form of the element. Generally, XPS peaks are corrected with respect to the binding energy of carbon C_{1s}, which is present on all types of surfaces. Analysis of the peaks involves the comparison of the spectra to well documented database. In our study, a KRATOS Axis Ultra Imaging Instrument (Kratos Analytical, Manchester, UK) was used to analyze the chemical state and composition inside and the outside the shearing area in order to determine the formation of a tribochemical film or lack thereof.

CHAPTER IV

INFLUENCE OF SURFACE TOPOGRAPHY ON FRICTIONAL PROPERTIES OF COPPER SURFACES UNDER DIFFERENT LUBRICATION CONDITIONS:COMPARISON OF DRY, BASE OIL, AND ZINC SULFIDE NANOWIRE-BASED LUBRICATION SYSTEM [*]

4.1 Overview

This chapter deals with the frictional properties of ductile Cu surfaces of varying morphologies under three different lubrication conditions including dry, base oil only, and nanowire + base oil. It was found that the frictional properties of base oil and nanowire-based lubrication system strongly depended on the surface topography while the friction for the dry surfaces was independent of the surface topography.

4.2 Introduction

Recent studies have shown that nanoparticle-based lubrication systems (NBLS) have improved lubrication properties compared to traditional lubricants [44-50, 155, 156]. Because of these promising results, NBLS have received increasing attention in various lubrication applications such as MEMS [51], engines [52-54, 157], turbines[158], and gears[54, 56, 158] with a hope of achieving better tribological efficiency and durability. These applications involve a variety of surface topographies

[*] Reprinted with permission from "Influence of surface topography on frictional properties of Cu surfaces under different lubrication conditions: Comparison of dry, base oil and ZnS nanowire-based lubrication system" by Vinay Narayanunni, Bassem A. Kheireddin, Mustafa Akbulut, 2011. *Tribology International*, 44, 1720-1725, Copyright 2013 by Elsevier.

ranging from molecularly smooth to macroscopically rough surfaces. However, most of the tribological studies on NBLS focus mainly on one type of surface rather than on nanoparticle film friction in relation to surface roughness and structure. Considering that even a 1-2 nm roughness can significantly affect adhesion and friction behavior of unlubricated (dry) surfaces[115, 159], one may hypothesize that roughness and surface structure can strongly influence the friction behavior of nanoparticle-based lubrication systems as well. However, while there are numerous studies on focusing on effect of surface topography on the tribological properties of dry surfaces [13, 160-165] and surfaces between various types of base oil [166-170], comparable investigations on NBLS are lacking.

The main objective of this paper is to determine the relative importance of surface topography on the tribological properties of lubrication systems as a function of lubrication condition (*i.e.* dry, base oil, nanoparticle + base oil). To this end, we utilized a model nanowire-based lubrication system that consists of octadecylamine (ODA) coated zinc sulfide (ZnS) nanowires which are dispersed in dodecane (base oil). ZnS nanowires were chosen as nanoparticle lubricant additives due to their superior tribological and mechanical properties [44, 63, 171-174]. The octadecylamine (ODA) functional groups were applied to ZnS nanowires so that they enable easy dissolution in organic solvents and oils as they reduce interparticle attraction resulting from van der Waals forces [174, 175]. The ZnS nanowire-based lubrication system was sheared between copper (Cu) surfaces of various roughnesses and inox steel ball. Previous tribological studies revealed that the ductility and hardness of the shearing materials are

two opposing properties, which can significantly influence the relations between the surface topography and the contact mechanical and frictional properties [176-184]. In this study, we have focused on the effect of shearing surface topography on the frictional properties of NBLS for the ductile shearing surfaces. Also, we are currently conducting a comparable study for hard brittle surfaces. Cu surfaces were selected in this study because of: (i) their high ductility, which allows greater plastic deformation to occur without particles breaking off *i.e.* the resistance to delamination wear [185]; (ii) their superior tribological properties [186-189]; and (iii) their uses in various tribological applications [190-192]. To the best of our knowledge, this is the first systematic investigation of the effect of surface topography on tribological properties of a nanoparticle-based lubrication system.

4.3 Experimental details

4.3.1 Materials

Cu pellets and Cr rods for thermal evaporation were purchased from Kurt J. Lesker Co. n-dodecane (99+%), was purchased from Alfa Aesar. Atomically smooth muscovite Mica sheets were procured from Axim Mica (NY, USA). The Zinc Sulfide (ZnS) nanowires were prepared by the method described by Pradhan *et al.*[193] and had a surfactant coating of octadecylamine (ODA, $C_{16}H_{35}N$). The ZnS nanowires used for the experiments had a core diameter of ~1 nm, an outer diameter of ~4 nm, and a length of ~110 nm. The ZnS nanowires were dispersed in n-dodecane at a concentration of 0.05 wt. %. TEM micrographs and the corresponding schematic drawings of the nanowires are shown in Figure 18.

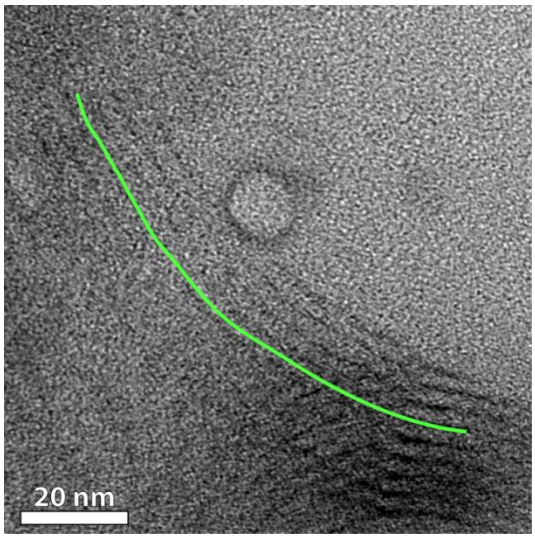

Figure 18. TEM micrographs of the studied ODA-coated ZnS nanowires. The corresponding schematic drawing indicating key dimensions of the nanowires. The mean nanowire length was 109±18 nm; the core diameter was 1.0±0.2 nm; and the total diameter was 4.0±0.4 nm. Nanowires were deposited from dodecane onto a perforated carbon-coated TEM grid.

4.3.2 Surface preparation

To control surface roughness systematically, atomically smooth mica sheets were used as a base substrate for deposition of thin Cu films. All the metal depositions were performed using a thermal evaporator **(**BOC Edwards Auto 306, Wilmington, MA**)**. Initially a 4-5 nm layer of Cr was deposited on the atomically smooth mica sheet to enhance adhesion compatibility between Mica and Cu surfaces. Next, a 100 nm of Cu layer was deposited on top of the Cr layer. The vacuum levels for all depositions were maintained about 10^{-6} mBar. The deposition rate of Cr was kept constant at 0.05 nm/s for all the surfaces. Different topographies were obtained by varying the deposition rate of Cu film (0.1-0.5 nm/s).

4.3.3 Atomic force microscopy

Surfaces topographies were investigated using an AFM (Nanoscope IIIa, Veeco Instruments, Santa Barbara, CA). Standard V-shaped SiN_4 probe with a spring constant of 6 N/m and tip radius of less than 20 nm were used. For all surfaces, surface topography scans were performed at a 0˚ scan angle on a 5-µm×5-µm area at a speed of 10 µm/s. Height and deflection information were obtained and analyzed using a NanoScope analysis software (Veeco, CA).

4.3.4 Friction measurements

Friction response was undertaken by a nano-tribometer (CSM Instruments, Switzerland) in a linear reciprocating mode at a constant sliding speed of 0.5 cm/s and a total distance of 0.05 m. Tests were conducted using a very smooth stainless steel sphere (diameter ~ 1.5 mm) with a roughness of 2.14 ± 0.45 nm along with a medium-load cantilever with normal and tangential stiffnesses of 0.247 mN/µm and 0.128 mN/µm, respectively. For all experiments, the humidity was maintained at <10% using P_2O_5. All tests were conducted with normal loads of 2.5, 5.0, 10, 20, and 40 mN, and each load was applied at three different locations on the sample yielding 15 different measurements for each sample. Each load was applied for 50 cycles of the 'back and forth' motion of the cantilever. Data analysis was performed using TriboX1.06 software (CSM Instrument, Switzerland). All friction data shown here are steady-state kinetic friction data.

4.4 Results and discussion

4.4.1 Surface topographies

Figure 19 shows AFM micrographs of four Cu surfaces obtained by varying deposition rates from 0.1 to 0.5 nm/s, each of which gave rise to visually distinct surface topography. Apart from the visual inspection, a more systematic and quantitative characterization is required to precisely distinguish the surfaces and to be able to derive mathematical correlations between friction and surfaces roughness parameters. To this end, we determined the root-mean-square (*rms*) height, R_q, (amplitude parameter); and the mean island diameter, *d*, and inter-island separation, *b*, (spatial or spacing parameters). The analysis of the AFM micrographs revealed that the mean island size and inter-island separation (spatial parameters) increased with increasing deposition rate (Table 5) while the number density of islands decreased with increasing deposition rate. On the other hand, the *rms* height did not demonstrate any obvious dependence on the deposition rate (Table 5). This trend of varying topographies with varying deposition conditions can be attributed to the fact that growth of thin films is a non-equilibrium process, where the final topography is determined by a complex combination of factors such as the arrival rate of atoms, the initial structure of the substrate, the substrate temperature, the thickness of the film, the diffusion rate of arrival atoms on the surface, and the interaction energies of the atoms involved [194].

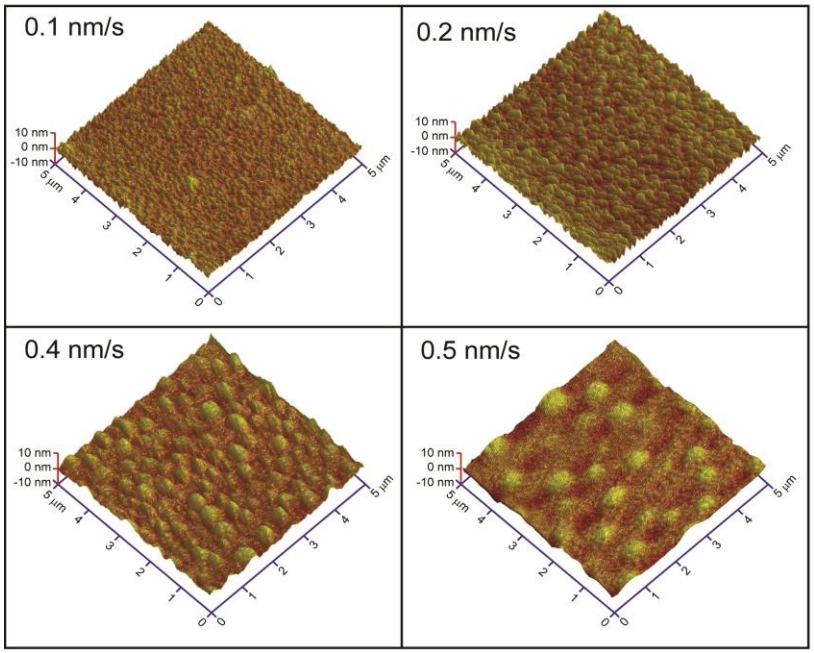

Figure 19. 5 µm × 5 µm AFM images of 100 nm thick Cu films on atomically smooth mica prepared at a deposition rate of 0.1 nm/s, 0.2 nm/s, 0.4 nm/s and 0.5 nm/s.

Table 5. Roughness parameters for surfaces shown in Figure 19.

	***rms* height R_q,(nm)**	**Island diameter *d*, (µm)**	**Number of islands N**	**Inter-island separation *b*, (µm)**
Surface A	1.55 ± 0.26	0.084 ± 0.002	534 ± 47	0.078 ± 0.002
Surface B	4.15 ± 1.01	0.122 ± 0.005	395 ± 34	0.129 ± 0.005
Surface C	1.78 ± 0.25	0.293 ± 0.013	83 ± 7	0.222 ± 0.011
Surface D	0.94 ± 0.03	0.486 ± 0.060	20 ± 2	0.535 ± 0.066

4.4.2 Friction as a function of lubrication conditions

Once the surface topographies were characterized, friction measurements on these surfaces were conducted under three different conditions: (i) dry (unlubricated),

(ii) base oil (dodecane only) lubricated, and (iii) composite (dodecane + nanowire) lubricated conditions for all surfaces (Figures 20-22).

4.4.2.1 Effect of surface topography on friction across dry (unlubricated) surface

As can be seen in Figure 20, under dry condition, the friction followed a linear trend with respect to load in accordance with Amontons' law [12, 33, 195, 196]. In addition, the coefficients of friction, μ, for Cu/steel were roughly the same for all surfaces (μ ≅ 0.26), which is lower than the bulk coefficient of friction values for copper/mild steel pair (0.53-0.54) [197, 198] and for copper/stainless steel pair (0.54) [199]. The lower coefficient of friction value for the thin films can be ascribed to the lowering of mechanical strength (Young's modulus) of the films as compared to the bulk surfaces[200].

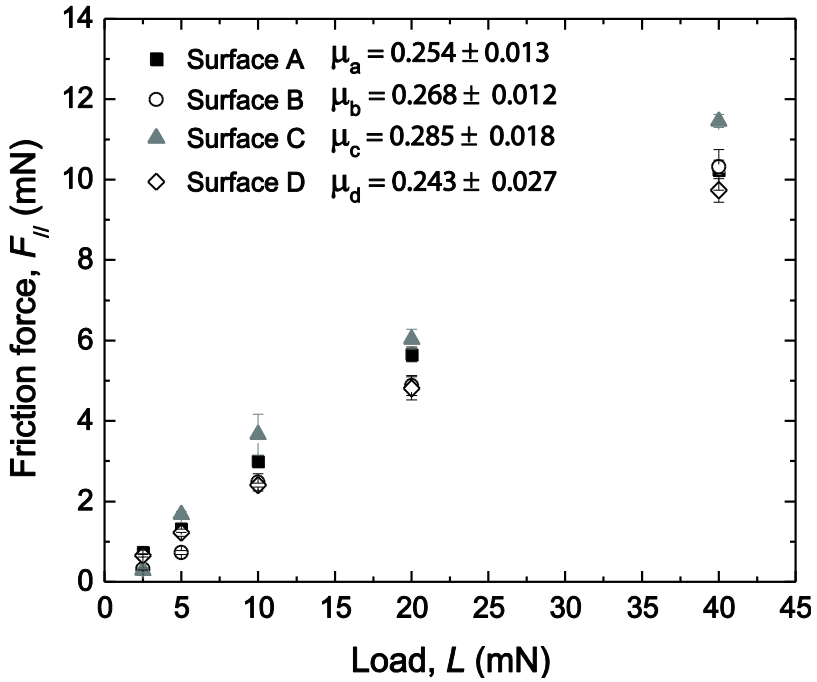

Figure 20. Friction force *versus* load curves for the Cu surfaces shown in Figure 19 under dry conditions.

Plasticity index, which describes whether the surface deforms in a plastic or elastic fashion [201], is an important parameter to consider here to understand possible reasons behind the insensitivity of friction to surface topography for the dry case. The plasticity index, ψ, is mathematically defined as [201]:

$$\psi = \frac{K}{H}\sqrt{\frac{s}{r}} \tag{18}$$

where *K*, *H*, *s* and *r* are the effective elastic modulus of the asperities, hardness, standard deviation of asperity heights and asperity tip radius respectively. Using the effective elastic modulus of the asperities and hardness of Cu thin films reported in Refs. [200, 202, 203] and standard deviation of asperity heights and asperity tip radius values obtained from AFM micrographs, the corresponding plasticity index values were calculated to be 2.86, 3.77, 2.67 and 2.02 for surfaces *A*, *B*, *C*, and *D*, respectively. It is known that elastic contact occurs at ψ <0.6, whereas plastic contact occurs at ψ >1.0, irrespective of the load [204]. The plasticity index values of surfaces *A*-*D* are much larger than the critical value of 1.0. Therefore, all of these four surfaces easily become plastically flattened under the influence of a normal load. Thus, under dry conditions, the differences in the surface topographies quickly disappear upon loading, thereby giving rise to a similar friction behavior for these surfaces.

4.4.2.2 Effect of surface structure on friction across base oil (dodecane) lubricated surfaces

Figure 21 shows the friction force as a function of applied load for surfaces *A*-*D* under dodecane lubrication. The average coefficient of friction for composite lubrication case, μ^0, was 0.145, which was, as expected, smaller than that for the dry surfaces. In

addition, the friction force was linearly dependent upon the applied load for all loads except 40 mN. The possible reason behind the deviation from the linearity is that 40 mN load exceeds the load-carrying capacity of dodecane for our experimental geometry. As shown above, the plasticity indices for the surfaces *A*-*D* were larger than 2. Hence, upon loading, the asperities are expected to deform plastically in the absence of any lubricant. However, the surfaces were lubricated with dodecane, which provides some load-carrying capability [205, 206], and thereby can prevent plastic deformations of asperities for the loads below the load-carrying capacity. Consequently, the friction behavior below (i.e. 2.5-20 mN) and above (i.e. 40 mN) the load-carrying capacity (between 20 mN and 40 mN) are different from one another.

The deviation from the linearity may also be ascribed to the oscillatory forces, which arises when a liquid is confined between two smooth walls and the gap between decreases below several molecular diameters [207-209]. After the oscillatory force appears, as the applied normal load increases or the gap between walls further decreases, liquids confined between two surfaces become progressively more ordered and solid-like [115, 210]. Solid-like behavior is characterized by changes in both the equilibrium and dynamics of interaction forces; the films become structured and are able to sustain both larger normal loads and shear stresses [211, 212]. However, the oscillatory forces can easily disappear in the presence of surface roughness [115]. Thus, the transition of elastic to plastic deformation of Cu is more likely to be responsible non-linear friction behavior at 40 mN load.

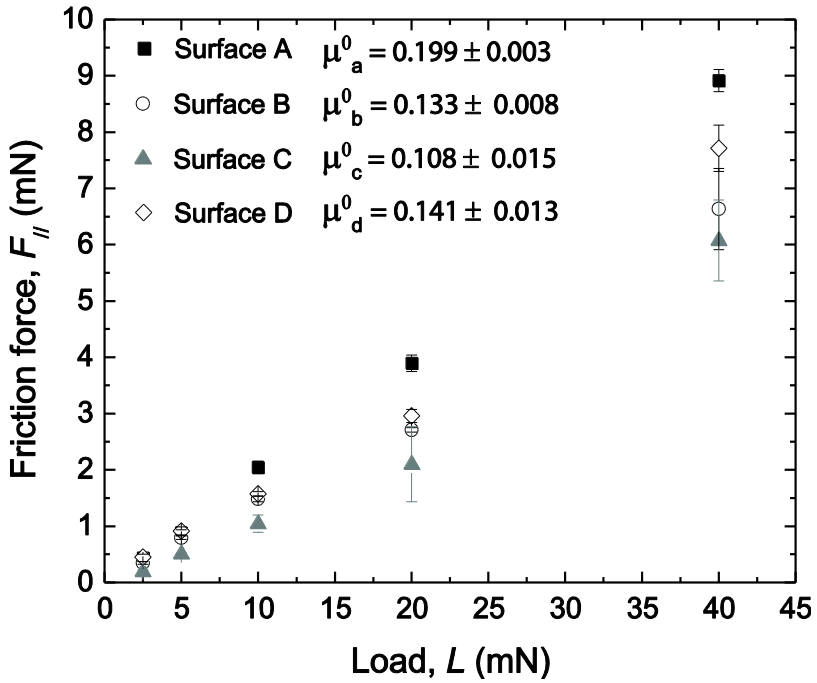

Figure 21 Friction *versus* load curves for Cu surfaces shown in Figure 19 under dodecane lubrication conditions. The coefficient of friction values are calculated using the loads of 2.5 mN to 20 mN.

Comparison of Figure 20 and Figure 21 also revealed that the dodecane lubricated surfaces were more sensitive to the surface topographies than the dry surfaces: The ratio of the largest to smallest coefficient of friction was μ_C/μ_D=1.17 and μ^0_A/μ^0_C=1.84 for dry and dodecane lubrication cases, respectively. Similar trends were previously observed by others as well [166, 213-215], and are typically explained by the cushioning effect of the lubricant which can reduce or prevent the plastic deformation that would have taken place in the absence of the lubricant *i.e.* increase in the longevity of surface topography in the presence of lubricant [213-215].

4.4.2.3 Effect of surface topography on composite lubrication (dodecane + nanowires)

Friction force *versus* load for surfaces *A-D* under composite lubrication conditions is shown in Figure 22. The average coefficient of friction for composite lubrication case, μ*, was 0.094, which is lower than that for the dry (0.263) and dodecane (0.145) lubrication cases. The improved lubricity of ZnS nanoparticles is consistent with the previous tribological studies on ZnS nanoparticles in hydrocarbon oils [63, 171, 172] and our previous studies on ZnS nanoparticles across molecular smooth surfaces [44, 173, 174]. Based on the studies relying on a surface forces apparatus, which is coupled with molecular-resolution interferometry, we have described that a number of reasons is likely to be responsible for enhanced lubrication of ZnS nanowire dispersions[44, 173, 174]. These are: i) Nanoparticle geometry: unlike spherical nanoparticles, nanowires do not easily conform to surface asperities but rather slide or roll over them. ii) Nanoparticle forces: surfactant-coated nanoparticles have a hard interior and a soft exterior, which provides them with a rigid shape but mobile, fluid like surface. This enables them to protect their surfaces (including the shearing surfaces) from becoming damaged and prevents material transfer. iii) Dynamic properties: there are no transient effects or long ‘adaptation times’ in the friction, that is, the friction reaches its steady state value quickly and remains there. iv) nanoparticle chemistry: Zn is a beneficial lubricant additive with a number of chemical functions, including antiwear action, oxidant suppression, and corrosion inhibition [216]. Thus, even if ZnS nanoparticles break down, they will be beneficial to the lubrication system.

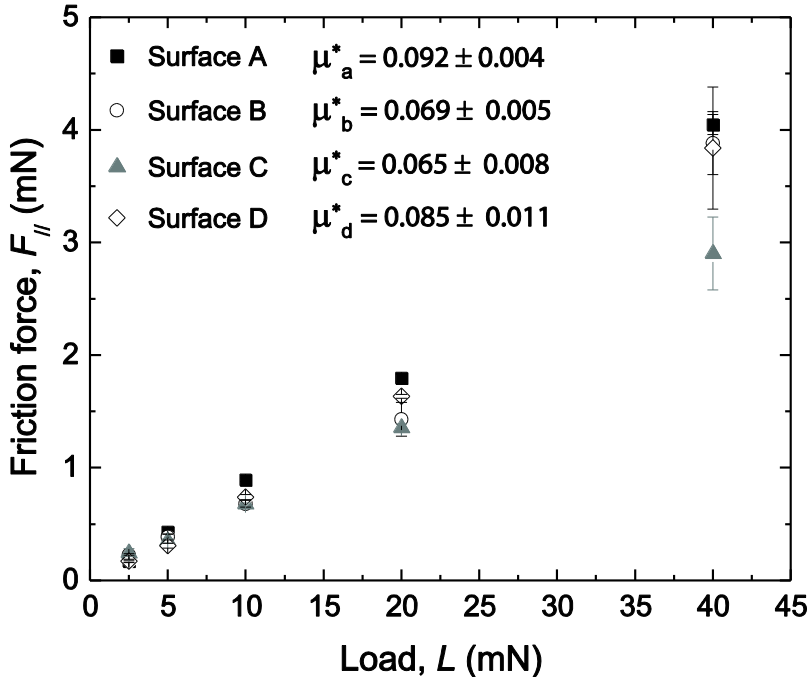

Figure 22. Friction *versus* load for surfaces *A-D* under composite (dodecane + nanowires) lubrication conditions.

The ratio of the largest to the smallest coefficient of friction for the composite lubrication was μ^*_A/μ^*_C=1.41, which lies between that for dry (μ_C/μ_D=1.17) and that for dodecane (μ^0_A/μ^0_C=1.84) lubrication case. This behavior can be explained as follows: ZnS nanowires are less mobile than dodecane and harder than Cu, and can jam up and produce interlocked, non-equilibrium (networks) nanostructures upon loading and shearing [173, 217]. Thus, ZnS nanowires can partially convey stresses from one surface to another and causing deformation of asperities. This means that the longevity of the ductile Cu surface topography is less for the composite lubrication compared to the dodecane lubrication. As such, frictional properties under composite lubrication are less sensitive to variation in the surface topographies compared to the friction properties of dodecane lubricated surfaces. Overall, our tribological studies on NBLS indicated that

the surface topography can be responsible for up to 40% difference in the friction force. Therefore, while designing NBLS for a specific surface, the surface topography needs to be carefully considered.

4.4.2.4 Comparison of friction traces for all lubrication conditions

Figure 23 displays a typical friction trace for 5 mN load under dry, dodecane (base-oil), and nanowire + dodecane lubrication conditions. As observed earlier from Figures 20-22, for a given load, dry surfaces had the highest friction force while nanowire + dodecane lubricated surfaces had the lowest friction. For all lubrication conditions, stick-slip behavior can be seen. For dry friction, the stick-slip is typically explained by distance-dependent model [218, 219]. This model suggests that two rough surfaces adhere through their microscopic asperities of characteristic length D_c. During shearing, each surface must first creep a distance D_c the size of the contacting junctions after which the surfaces continue to slide, but with a lower (kinetic) friction force than the original (static) value [220]. The reason for the decrease in the friction force is that although, on average, new asperity junctions should form as rapidly as the old ones break, the time dependent adhesion and friction of the new ones will be lower than the old ones [218-220]. For the dodecane and composite lubrication case, the stick-slip can be explained by surface topology (roughness) model [219]. This model suggests that as the slider climbs an asperity on the substrate, a resisting force is encountered. Once the peak is reached, the slider will slide down rapidly into the valley, resulting in a slip. The measured friction trace with time will show regular or irregular stick−slip “spikes”

depending on whether the surface corrugations are themselves regular, as for a lattice plane, or irregular, as for a randomly rough surface [115, 220, 221].

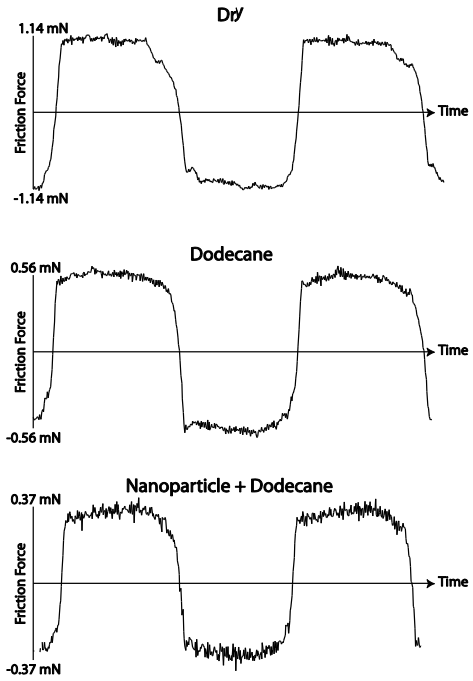

Figure 23. Raw friction force versus time data for 5 mN load under dry, dodecane (base-oil), and nanowire + dodecane lubrication conditions.

4.5 Conclusion

Friction behaviors of ductile Cu surfaces with different topographies were investigated for dry, dodecane, and dodecane+ZnS nanowire lubricated surfaces. It was found that the friction force for the dry surfaces was mostly independent of surface structure, while for the case of lubrication with dodecane and nanowire dodecane dispersion, the friction behavior strongly depended on the surface structure. This discrepancy is primarily due to the fact that dodecane and the nanowire-based lubrication system prevent or reduce asperities of two mating surfaces to come into

direct contact and thereby reduce deformations, *i.e.*, the cushioning effect. This means that the longevity of surface topography increases in the presence of dodecane or a nanowire-based lubrication system compared to the dry case.

In addition, it was found that the nanowire dodecane dispersion on average reduced the surface friction forces by 63% and 34% when compared to the dry and dodecane-lubricated conditions, respectively. The improved lubrication of nanowire dispersion is ascribed to a synergistic combination of nanoparticle geometry, inter-nanoparticle and surface-nanoparticle interactions, and organic-inorganic hybrid nanoparticle composition.

CHAPTER V

INFLUENCE OF SHEARING SURFACE TOPOGRAPHY ON FRICTIONAL PROPERTIES OF ZINC SULFIDE NANOWIRE-BASED LUBRICATION SYSTEM ACROSS DUCTILE SURFACES [*]

5.1 Overview

This chapter deals with the effect of surface roughness parameters on the frictional properties of nanowire-based lubrication systems (NBLS) across Cu surfaces with various topographies. The friction coefficient was discussed in the context of surface roughness parameters including the *rms* height, inter-island separation and a combined roughness parameter related to the pressure experienced by each nanowire. It was concluded that the *rms* height of asperity should not be lower than the radius of nanoparticles for effective lubrication. In addition, when the ratio of inter-island separation is an integer multiple of the nanowire length, nanowires perform as effective lubricants. Furthermore, the friction coefficient increased when the mean pressure experienced by the nanowires increased. The results obtained in this original study offer some interesting insights into the frictional properties of NBLS as a function of surface roughness parameters. This could lead to a great impact on the selection of nanoparticle-based lubricant aimed at reducing wear and energy losses for various applications.

---

[*] Reprinted with permission from "Influence of Shearing Surface Topography on Frictional Properties of ZnS Nanowire-Based Lubrication System across Ductile Surfaces," by Bassem A. Kheireddin, Vinay Narayanunni and Mustafa Akbulut, 2012. *Journal of Tribology*,134, 022001.1-022001.7. Copyright 2013 by ASME.

5.2 Introduction

Surface topography plays a critical role in the frictional behavior of surfaces. This effect was demonstrated by the early work of Kudo [222] who found that lubricants trapped between asperities have a significant effect on friction. Since then, numerous investigations on the effect of surface topography on friction for dry surfaces [13, 160-165, 223, 224] as well as lubricated surfaces [166-170, 225] have rapidly increased. However, it is uncertain what surface roughness parameters are better correlated with friction. For instance, Zappone *et al*. [226] investigated the effect of rms roughness on the friction and adhesion of polymers with various roughnesses, and found that a small change in the nanometer-scale roughness can have a significant effect on the adhesion-controlled part of friction. Moreover, the presence of the nanometer-scale roughness caused the friction coefficient to vary by 45% in the dry case and 80% in the oil lubricated case. Banquy *et al.* [99] explored the effect of surface roughness on the kinetic friction coefficient using polymeric nanoparticles grafted on mica substrates. They concluded that increasing the NP surface coverage increased the *rms* roughness which in turn caused a quasi-exponential increase in the friction coefficient.

While there are numerous studies on the effect of surface topography on the tribological properties of dry surfaces and surfaces between various types of base oil, comparable investigations on nanoparticle-based lubrication systems (NBLS) are lacking. The reason is the complexity of the contact phenomena involved between the surfaces and the nanoparticle based lubricant. However, recent studies have shown that NBLS have improved lubrication properties compared to traditional lubricants, which make them

potential candidates for various applications such as MEMS [51], engines [52-54, 157], turbines [158], and gears [54, 56, 158]. From this standpoint, it becomes important to investigate the correlation between the surface topography and tribological properties of NBLS, thereby obtaining an enhanced tribological understanding of NBLS in general. In a previous work by the authors, it was found that surface topography accounts for up to 40% difference in the friction force in the case of ZnS nanowire lubricant [227] . The aim of this paper is to extend this work and investigate which surface roughness parameters influence the frictional properties of NBLS. In particular, we evaluate the effects of *rms* height, inter-island separation, and island diameter on the coefficient of friction. To these ends, we utilized a model nanowire-based lubrication system that consists of octadecylamine (ODA) coated zinc sulfide (ZnS) nanowires which are dispersed in dodecane (base oil). ZnS nanowires were chosen as nanoparticle lubricant additives due to their superior tribological and mechanical properties [44, 63, 171, 172, 174, 228]. The octadecylamine (ODA) functional groups were applied to ZnS nanowires so that they enable easy dissolution in organic solvents and oils as they reduce interparticle attraction resulting from van der Waals forces [174, 175]. The ZnS nanowire-based lubrication system was sheared between copper (Cu) surfaces of various roughnesses and an inox steel ball. Previous tribological studies revealed that the ductility and hardness of the shearing materials are two opposing properties, which can significantly influence the relations between the surface topography and the contact mechanics and frictional properties [176-184].

In this study, we have focused on the effect of shearing surface topography on the frictional properties of NBLS for the ductile shearing surfaces. Also, we are currently conducting a comparable study for hard brittle surfaces. Cu surfaces were selected in this study because of: (i) their high ductility, which allows greater plastic deformation to occur without particles breaking off *i.e.* the resistance to delamination wear [185], (ii) their superior tribological properties [186-189]; and (iii) their uses in various tribological applications [191, 192, 229]. To the best of our knowledge, this is the first systematic investigation of the effect of surface roughness parameters on tribological properties of a nanoparticle-based lubrication system.

5.3 Experimental details

All the metal depositions were performed using a thermal evaporator (BOC Edwards Auto 306, Wilmington, MA). Surfaces topographies were investigated using an AFM (Nanoscope IIIa, Veeco Instruments, Santa Barbara, CA). Friction response was undertaken by a nano-tribometer (CSM Instruments, Switzerland) in a linear reciprocating mode. Further experimental details may be found in Chapter IV.

5.4 Results and discussion

5.4.1 Surface topographies

Figure 24 shows AFM micrographs of four Cu surfaces obtained by varying deposition rates from 0.1 to 0.5 nm/s, each of which gave rise to visually distinct surface topography. Apart from the visual inspection, a more systematic and quantitative characterization is required to precisely distinguish the surfaces and enable derivation of mathematical correlations between friction and surfaces roughness parameters. To this

end, we determined the root-mean-square (*rms*) height, R_q, (amplitude parameter), the mean island diameter, *d*, and inter-island separation, *b*, (spatial or spacing parameters) (Table 5).

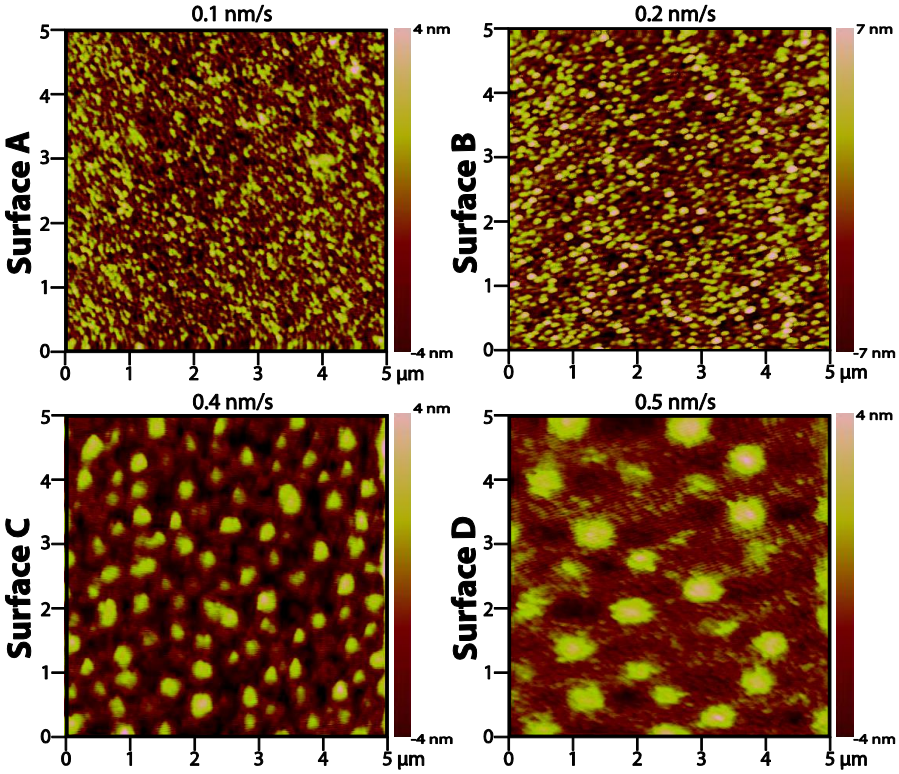

Figure 24. 5 µm × 5 µm AFM images of 100 nm thick Cu films on atomically smooth mica prepared at a deposition rate of 0.1 nm/s, 0.2 nm/s, 0.4 nm/s and 0.5 nm/s.

5.4.2 Frictional properties of NBLS as a function of surface roughness parameters

Our objective was to generate correlations between the surface topography and tribological properties of NBLS. For this purpose, we plotted the friction coefficient versus surface roughness parameters (Figs. 25, 26, and 28), and analyzed the graphs to determine if there is any significant correlation between friction force and surface roughness parameters.

5.4.2.1 Effect of rms height (amplitude roughness parameter)

Figure 25a shows the coefficient of friction (CoF) as a function of *rms* height. While CoF was mostly constant at low rms heights (0.9 nm and 1.6 nm), CoF decreased rapidly at an *rms* height of 1.8 nm and did not change significantly upon a change in *rms* height from 1.8 to 4.2 nm. In other words, there is a transition region between 1.6 and 1.8 nm. This result can be interpreted in several ways. First, it is known that non-adhering nanoparticles act as effective lubricants when they are not squeezed out of contact regions of mating surfaces *i.e.* when they prevent two surfaces from forming cold-welds [156, 230]. If the *rms* height is too low, physical barrier that holds slippery nanoparticles between the asperities is not large enough to keep them in contact zones. Therefore, the nanoparticles can escape from the contact zones and the surfaces can experience high frictional forces upon loading and shearing. To better illustrate this effect, let us consider a cylindrical particle of radius, *r*, near a rectangular barrier with a height, *h* (Figure 25b). The force required to raise the particle over the obstacle can be calculated from the torque balance about the point of contact:

$$F \geq L\sqrt{\frac{2r}{2r-h}-1} \tag{19}$$

where *L* is the normal load applied to the particle, *h* is the height of the obstacle. Thus, for a given particle size (r>h/2), as the height of obstacle increases, the force required to raise the particle over the obstacle also increases. This means at higher *rms* heights, nanowires must have a higher tendency to remain in contact zones, thereby reducing the probability of cold-welding. This simple model seems to be sufficient to explain our observed results described above considering that (i) the total radius of nanowires is

about 1.7-1.9 nm and (ii) a critical change in friction force occurs at an *rms* height of 1.6-1.8 nm.

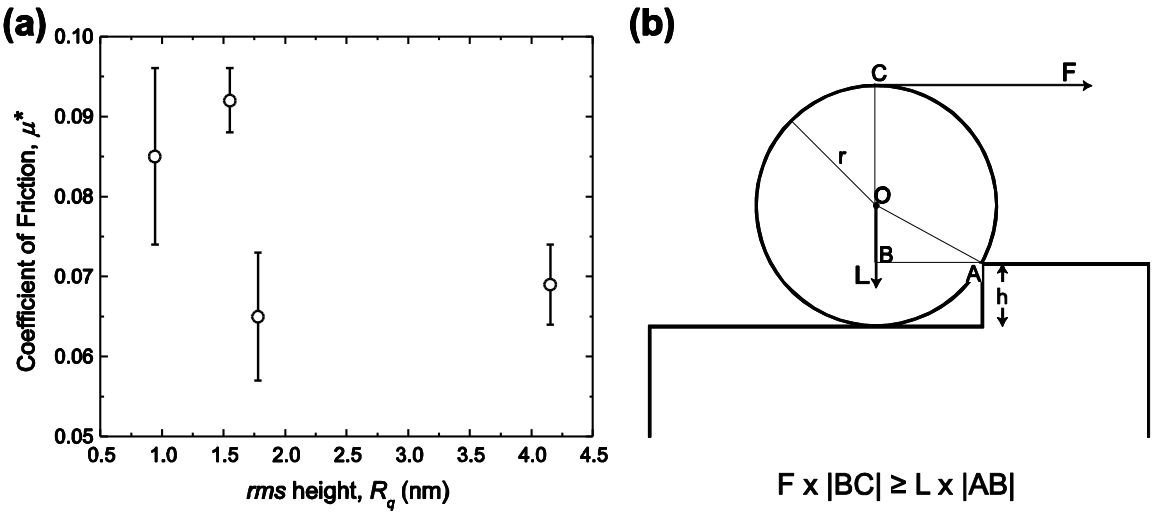

Figure 25. (a) The coefficient of friction *versus rms* height (b) The forces acting on a cylindrical particle that is in contact with a rectangular obstacle.

Second, aside from the reduction of cold-welding, nanoparticles trapped within the valleys can also "*artificially smooth"* the surfaces as they fill voids in the valleys, thereby decreasing frictional forces due to lateral collisions of asperities. Thus, surface topographies that can retain nanowires between asperities can experience a lower friction force due to the reduction in the effective roughness. Otherwise, nanowires are less lubricant-effective.

A third interpretation of Figure 25a is as follows: For surfaces *A-D*, when a roughness parameter changes, other roughness parameters vary as well (Table 5). This could mean that the observed trend is a combined consequence of changes in *rms* height

and other roughness parameters. Thus, we will continue to discuss the effect of *rms* height in conjunction with other roughness parameters in the following paragraphs.

5.4.2.2 Effect of inter-island separation (spatial roughness parameter)

Figure 26a displays the coefficient of friction *versus* inter-island separation, *b*, for the case of composite lubrication. The coefficient of friction was low at inter-island separations of 129 and 222 nm while CoF was high at inter-island separations of 78 and 535 nm. At first glance, there is no obvious explanation for this trend. However, a careful consideration of the data suggests that the lateral distribution and packing of nanowires, which are governed by ratio of inter-island separation to length of nanowires, could well contribute to this behavior: As illustrated in Figure 26b, when the inter-island separation is less than the length of nanowires, the nanowires cannot fit in the space between asperities (islands), and have to align at a non-zero angle, θ ($0<\theta\leq 90°$) with respect to the valleys. On the other hand, when the inter-island separation is equal to the length of nanowires, the nanowires are likely to align horizontally ($\theta=0°$) with respect to the valleys to minimize the interaction energy between the nanowires and surface. In this case, the relative magnitude of *rms* height and the nanowire thickness (diameter) determines whether nanowires will artificially "smooth" the valleys or protrude from the valleys. When the inter-island separation is larger than the length of nanowires, the nanowires have three different configuration options with respect to the surface: (i) all nanowires align at a non-zero angle, (ii) some nanowires align horizontally while others align at a non-zero angle, and (iii) all nanowires align horizontally. While the ordered-state (configuration iii) is a viable option for nanowires only when the inter-island

separation is an integer multiple of the length of nanowires, the nanowires will be in the disordered state (configuration i and ii) for all other inter-island separations. The ratio of inter-island separation to the length of nanowires was 0.7, 1.1, 2.0, and 4.8 for surfaces A, B, C, and D, respectively *i.e*. surfaces B and C have approximately an integer ratio of inter-island separation to the length of nanowires. Various lubrication systems have been shown to display very different frictional properties depending on if they are in ordered or disordered state [115, 231-233]. Thus, considering that surfaces B and C gave rise to low friction while surfaces A and D to high friction, our argument of requirement for an integer ratio of inter-island separation to length of nanowires in order to achieve efficient lubrication seems to be a fairly reasonable one.

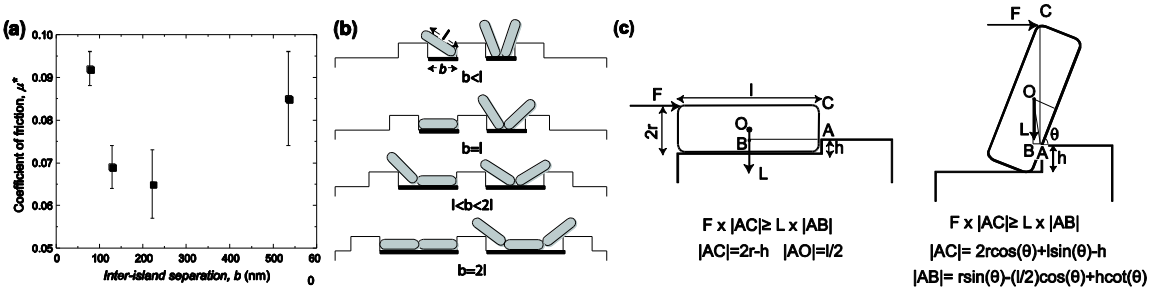

Figure 26. (a) The coefficient of friction *versus* inter-island separation, *b*. (b) Possible effects of variation in the inter-island separation on the organization of nanowires on these surfaces are shown. (c) The forces acting on a cylindrical particle that is in contact with an obstacle of height, *h*.

In addition, for the disordered configurations of nanowires (*i.e.* when they are at a non-zero angle of inclination), the magnitude of the inclination angle could be important in the context of nanowire mobility. To better illustrate this, let us consider the

force, *F*, required to lift an object with angle of inclination θ over an obstacle. Such force can be calculated from the torque balance about the point of contact (Figure 26c):

$$F \geq \frac{L\left[rSin(\theta)-\frac{l}{2}Cos(\theta)+hCot(\theta)\right]}{2rcos(\theta)+lsin(\theta)-h} \quad (20)$$

However, when the object lies parallel to the surface, the required force is:

$$F \geq L\left[\frac{l}{2(r-h)}\right] \quad (21)$$

The geometrical constraints for the nanowires and surface asperities require that Equation 20 be only applicable for $sin^{-1}(h/l)<\theta<90°$ where $h<2r<l$. Otherwise, the nanowires will spontaneously fall into the valley i.e. nanowires are in the ordered state. Comparison of Equations 20 and 21 reveals that when the object (i.e. nanowire) lies parallel to the surface, the force required to overcome the geometrical barrier will always be greater than the case where the object is inclined at an angle θ. This is illustrated in Figure 27 for barrier heights corresponding to the rms heights found in our study (Table 5). Note that when *h* is greater than the nanowire diameter (not shown in Figure 27), as in the case of surface D, an infinite force would be required to overcome the obstacle, which makes it impractical in the context of our argument. Thus, these two equations seem to serve as a supporting tool to further solidify our argument.

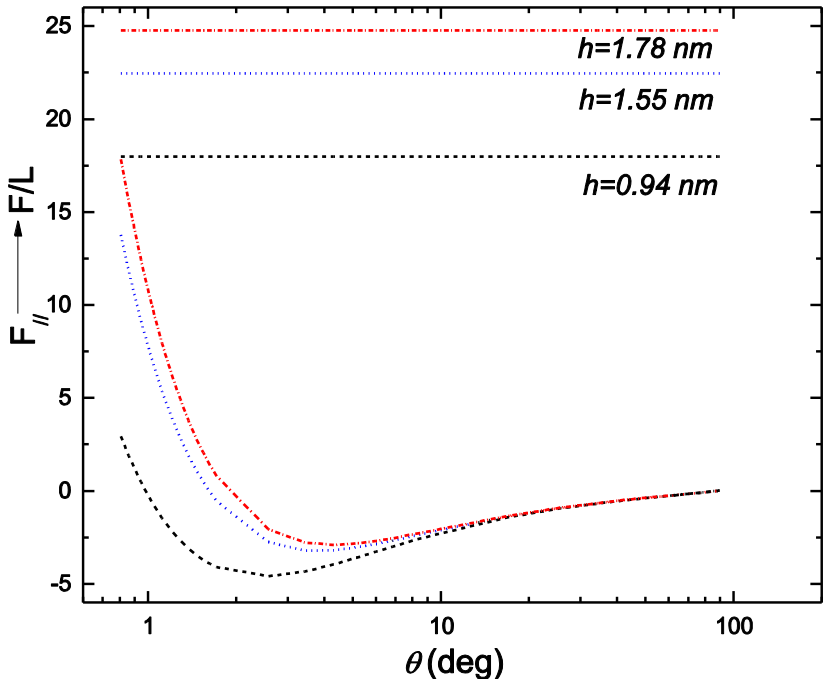

Figure 27. The lateral force required to overcome the barrier normalized by the normal load ($F_{//}$=F/L) versus the angle of inclination θ. Curved lines correspond to the case where the object is at an angle of inclination theta, whereas horizontal lines correspond to the case where the object lies parallel to the surface (h values were selected based upon rms values).

In light of the above discussion and given that the improved lubricity of NBLS is primarily due to their ability to prevent asperities to come together [156, 234], we can claim that when the inter-island separation is an integer multiple of the length of nanowires, the nanowires are less likely to squeeze out of contact, thereby protecting the shearing surfaces. Similarly, when the ratio of inter-island separation to length of nanowire is a non-integer multiple, nanowires resting at a lower angle of inclination to the surfaces are less likely to squeeze out of contact allowing for better protection of the shearing surfaces.

5.4.2.3 Effect of island diameter (spatial roughness parameter)

It is known that for nanoparticles coated (functionalized) with soft surfactants and polymers, the average interparticle separation decreases with increasing pressure, and thereby the degree of interdigitation and steric repulsion increases [173, 228]. Generally, an increase in the degree of interdigitation and entanglement leads to an increase in frictional force [221, 235]. To determine how asperity geometry influences the frictional properties of NBLS in the context of the pressures experienced by nanowires, we considered a model system involving nanowires confined between a smooth plane and a nominally flat surface. We assumed that the smooth plane consists of a number of identical plateaus of similar radius, *R*, and the same height relative to the reference plane. As the surfaces are brought closer together, each plateau carries the same normal load, L_i, so that for N_i islands (plateaus) the total load L will be $N_i \times L_i$ (Figure 28a). Each island is covered with a $N_p=A_i/A_p$ number of nanowires where A_i and A_p are the area of each island and nanowire, respectively. Thus, the load experienced by each particle on the islands is equal to $L_p=L_i \times A_p/A_i$. The mean pressure experienced by each particle can be calculated by dividing the load to the cross sectional area of each particle, $P_p = L_p/A_p = L/(N_iA_i) = L/(\pi N_i R^2)$. To illustrate the combined effect of number and size of islands on the mean pressure experienced by the particles for a given load, we introduced a new parameter, $\xi=(N_iR^2)^{-1}$. We plotted the coefficient of friction *versus* ξ to see if there is any correlation between them, and found that CoF increases linearly with increasing mean pressure experienced by nanoparticles (Figure 28b). The

coefficient of determination, R^2 was 0.97, suggesting a robust correlation between ξ and CoF.

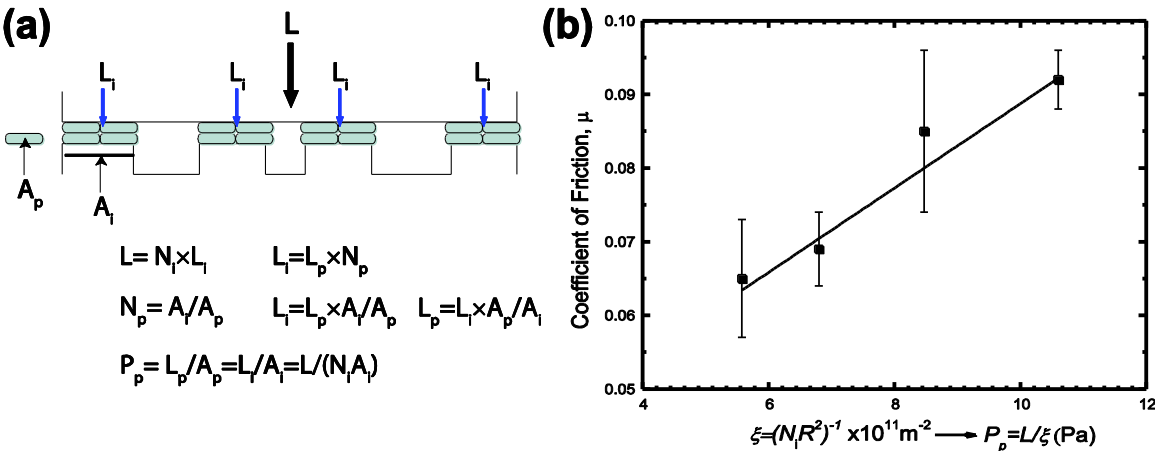

Figure 28. (a) Illustration of a model system involving nanoparticles confined between a smooth plane and a nominally flat surface. (b) The coefficient of friction *versus* ξ, which is an indication of the mean pressure experienced by each nanowire located on top of islands

In addition, the magnitude of the island diameter, *d*, relative to the nanowire size can also be significant in the context of frictional properties of NBLS. For instance, Harnau *et al.* [236] demonstrated that in a corner of a right-angled wedge, for colloidal hard-rods, the excluded-volume overlap is larger than the one on a flat wall leading to an enrichment of rods lying parallel and close to the corner of the wedge using density functional theory. However, if the wedge size (island diameter) is smaller than the length of nanowires, the nanowires cannot properly stack themselves on the wedge (plateaus), and introduce disorder into the packing of nanowires. Namely, the relative magnitude of the length of nanowires and the island diameter can influence the packing and, hence,

frictional properties of nanowire-based lubrication systems. Unfortunately, in our study, because the inter-island separation and island diameter values for the surface topographies prepared are very similar (Table 5), we cannot deconvolute the effect of these two parameters. However, because interlocking of asperities is the main source of friction [237-239], we expect the inter-island separation, governing the packing of nanowires between the asperities, to have a more pronounced effect on the friction of NBLS compared to the island diameter.

Before we draw any overall conclusion on this subject, we would like to elaborate on several limitations of this study. First, we have utilized relatively small number of surface topographies due to the limitations of thermal evaporator used in this study. While these surfaces were useful to identify initial trends in this relatively unexplored area of research, more data points are needed to draw more robust and emphatic conclusions. Second, rms height, island-diameter, and inter-island separation were considered as a single value parameter rather than a distribution. We note that the width of the distribution, which is larger for surfaces A and D, could have an influence on the tribological outcomes observed in this study, especially when we consider the relatively large error bars observed in friction studies involving Surfaces C and D. Third, the roughness parameters are interdependent i.e. when one roughness parameter changes, the other roughness parameters change as well. Therefore, a statistical analysis of the data, which is only feasible when a large number of surfaces with varying surface roughnesses are available, would be necessary to estimate the effective influence of a parameter and eventually of the interaction between more parameters on the tribological

properties of the surfaces. Accordingly, future considerations for a similar study would need to address these limitations.

5.5 Conclusions

Friction behaviors of ductile Cu surfaces with different topographies were investigated for dodecane+ZnS nanowire lubricated surfaces as a function of surface roughness parameters such as *rms* roughness, inter-island separation, and a combined roughness parameter, $\xi=(N_iR^2)^{-1}$, which is directly related to the pressure experienced by the nanoparticles located atop the asperities. Based on our findings, the following heuristics for the design of nanoparticle-based lubrication systems sheared across rough surfaces and coatings can be deduced: (i) for slippery (non-adhering) nanoparticles, the *rms* height should not be lower than the radius of nanoparticle. Otherwise, the nanoparticles can readily squeeze out of the contact region upon loading and shearing, thereby undermining the lubrication properties (ii) when the ratio of inter-island separation to nanowire length is an integer value, nanowires perform more effectively as lubricants, and (iii) the larger the mean pressure experienced by nanowires, the larger the coefficient of friction. These insights would have an impact on the selection of nanoparticle lubricants for surfaces with different topographies encountered in everyday life leading to a reduction in wear and energy loss. Additionally, the data generated in this study provides an opportunity to theoretical groups to investigate the frictional properties of nanoparticle-based lubricants as a function of surface roughness parameters.

CHAPTER VI

EFFECT OF ROUGHNESS ON THE LUBRICATION BEHAVIOR OF ZINC SULFIDE NANOWIRE FILMS ACROSS SILICON OXIDE SURFACES

6.1 Overview

This original study investigates the effect of surface roughness on the lubrication behavior of ZnS nanowires across SiO_2 surfaces with systematically varying roughnesses ranging from 0.14-114 nm. It was found that while the friction coefficient increased with increasing *rms* height at low *rms* values, it became independent of the *rms* height at high *rms* values. In addition, the change in the friction traces from initial-state to steady-state demonstrated an opposite trend for rough and smooth surfaces. These results are important in the context of nanoparticle-based lubricant design, especially when the shearing surfaces involve a range of surface roughnesses.

6.2 Introduction

With the advent of nanotechnology, research into lubricants and additives has experienced a paradigm shift. Instead of traditional materials, new nanomaterials and nanoparticles are currently under investigation as lubricants or lubricant additives because of their unusual and tunable properties [44-50]. Recent advancements in nanoparticle and nanomaterial synthesis routes especially encouraged and facilitated the research on nanoparticle-based lubrication systems [240, 241].

Now, there are a plethora of studies describing the tribological properties of different types of nanoparticles as possible lubricants and lubricant additives in the

literature. For instance, Chhowalla et al. [242] have shown that the presence of thin films of hollow MoS_2 nanoparticles yields a coefficient of friction of 0.006 in ambient as well as humid conditions (i.e. 45% humidity). Filleter et al. [243] , using atomic force microscopy (AFM), showed that the coefficient of friction was very low, and ~0.01 and ~0.03 for bilayer and single-layer graphene, respectively. Nanoparticles of WS_2 with a closed cage structure (fullerene-like) were demonstrated to decrease the friction coefficient up to 50% under mixed lubrication regime when such nanoparticles were added in the base oils[61]. A recent investigation demonstrated that SiO_2 nanoparticles can also be dispersed in ionic liquids and significantly improve the tribological properties of ionic liquids as well [244].

However, most of these studies focus on the nanoparticle film friction on one type of surface rather than on nanoparticle film friction in relation to surface roughness and structure. By contrast, previous studies have shown that the roughness of shearing surfaces has a significant effect on the mechanical properties of the surface including adhesion, friction and wear as well as failure mechanisms [245]. For instance, previous studies show that even a difference on the order of few nanometers in root-mean-square (*rms*) roughness can have a significant impact on adhesion energy as well as friction behavior [226, 246]. Specifically, they investigated the effect of *rms* roughness on the friction and adhesion of polymers with various roughnesses, and found that a small change in the nanometer-scale roughness can have a significant effect on the adhesion-controlled part of friction. Moreover, the presence of the nanometer-scale roughness caused the friction coefficient to vary by 45% in the dry case and 80% in the oil

lubricated case. Banquy et al. [99] explored the effect of surface roughness on the kinetic friction coefficient using polymeric nanoparticles grafted on mica substrates. They concluded that increasing the NP surface coverage increased the *rms* roughness which in turn caused a quasi-exponential increase in the friction coefficient.

Thus, one may hypothesize that roughness and surface structure influence the friction behavior of lubrication systems involving nanoparticles as well. In fact, a recent work by the authors has shown that surface topography accounts for up to 40% difference in the friction force in the case of ductile Cu surfaces with very low *rms* values less than 5 nm when the surfaces were lubricated with ZnS nanowires in dodecane [227]. However, to date, there is still no systematic study for the interactions of hard and *brittle* surfaces displaying a broad variation in surface roughness across nanoparticle films to confirm this hypothesis. This article is aimed at addressing this gap in literature.

6.3 Experimental details

6.3.1 Materials

Reagent grade Potassium Hydroxide (KOH) flakes were purchased from The Science Company (Denver, CO). N-dodecane (99+%), hydrogen peroxide (27% w/w aqueous solution), and sulfuric acid (ACS grade, 95-98%) were purchased from Alfa Aesar (Ward Hill, MA). Silicon wafers (100) were purchased from Addison Engineering (San Jose, CA). All materials were used as received. Zinc Sulfide (ZnS) straight nanowires were synthesized following the method developed by Pradhan et al [247]. Briefly, a solution of zinc ethylxanthate was dissolved in molten octadecylamine (ODA).

The ODA-ZnS nanowires were collected after washing and centrifuging with methanol and then redispersed in dodecane.

6.3.2 Surface preparation

All silicon substrates were cleaned with a Piranha solution (3:1 concentrated sulfuric acid to hydrogen peroxide) prior to tribological measurements. The substrates were subsequently rinsed with deionized (DI) water and blown dry with compressed nitrogen gas. Test samples were then immersed in a 10% KOH solution for etching purposes. Temperature and etching times were varied in order to obtain the desired *rms* roughnesses. A temperature range from 23 ˚C to 60˚C was used in this study, and etching times were varied from 0 to 15 min depending on the temperature.

6.3.3 Atomic force microscopy

Surface topographies were characterized by AFM in contact mode (Nanoscope IIIa, Veeco Instruments, Santa Barbara, CA). Standard V-shaped Si_3N_4 probe from Veeco with a spring constant of 6 N/m and tip radius of less than 20 nm were used. Surface topography scans were performed at a 0˚ scan angle on a 5-μm area at a speed of 10 μm/s. Height and deflection information were obtained and analyzed using a Gwyddion analysis software.

6.3.4 Friction measurements

Friction response was undertaken by a nano-tribometer (CSM Instruments, Switzerland) at a constant sliding speed of 0.0005 m/s and a total distance of 0.05 m. Tests were conducted using a very smooth stainless steel sphere (diameter ~ 1.5 mm) with *rms* roughness of 2.14 ± 0.45 nm along with a medium-load cantilever with normal

and tangential stiffnesses of 246.6 N/m and 127.9 N/m, respectively. All tests were conducted with normal loads of 2.5, 5.0, 10.0, 20.0, and 40.0 mN, and each load was applied at least in three different locations. This procedure was repeated three times for statistical analysis. In this study, three different types of lubrication conditions were investigated: dry (bare silicon), simple lubrication (silicon surfaces across dodecane), and composite lubrication (silicon surfaces across ZnS nanowires that are dispersed in dodecane). Throughout this study, the humidity was maintained between 45-55%.

6.4 Results and discussion

6.4.1 Prepared surfaces

Figure 29 shows 3-D AFM micrographs of the different surface topographies obtained by varying the temperature and the etching time until enough root-mean-square (*rms)* roughnesses were obtained. Although the roughness of a surface can be characterized by various parameters, for this study, we chose the *rms* roughness to label the surfaces. The *rms* roughnesses ranged from 0.14 nm to 114.1 nm and are tabulated in Table **6** with respect to each surface. The untreated silicon surface had the lowest *rms* roughness and did not exhibit any noticeable features. As the temperature and etching duration increased, rougher samples were obtained and facet-like structures became apparent. These trends were consistent with prior studies on anisotropic etching of Si (100) using alkaline solutions (KOH) [248] and the findings showing that the etching process is strongly dependent on temperature, crystallographic orientation, etching duration and concentration [249].

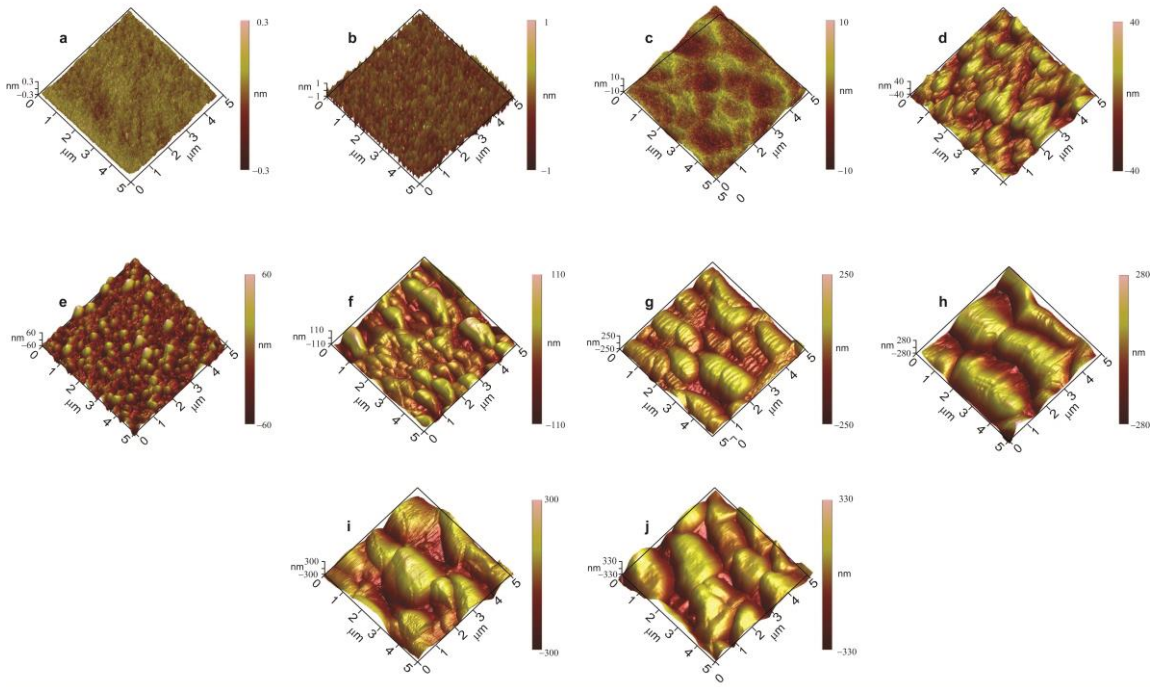

Figure 29**.** 3-D AFM micrographs of ten different silicon/silica surfaces obtained by using different KOH etching times and temperatures.

Table 6. Roughness parameters of surfaces a-j

Surface	**RMS Height (nm)**
a	0.14 ± 0.02
b	0.77 ± 0.02
c	2.64 ± 0.32
d	8.92 ± 0.62
e	12.27± 0.76
f	28.30±0. 67
g	65.90 ±0.50
h	86.13±5.80
i	102.29 ± 3.87
j	114.10 ± 2.38

6.4.2 Effect of lubrication type on friction

Three different lubrication conditions were investigated in this study: dry (no lubricant i.e. bare surfaces), simple lubrication (dodecane lubrication), and composite lubrication (nanowire + dodecane lubrication). Figure 30 displays a friction force versus normal load plot for the different lubrication cases. The friction force was a linear function of the load for all three cases, a behavior also observed for other surfaces having different surface structures and roughnesses. This linear behavior is in accordance with Amontons' first law, which states that the friction coefficient for a given surface is independent of the load applied [8]. As expected, the friction force was highest for dry conditions owing to the absence of the lubricant which causes the asperities to be in direct contact. However, the addition of the ZnS nanowires to dodecane reduced the friction coefficient by approximately 80% compared to the dry case and 55% compared to the simply lubricated case.

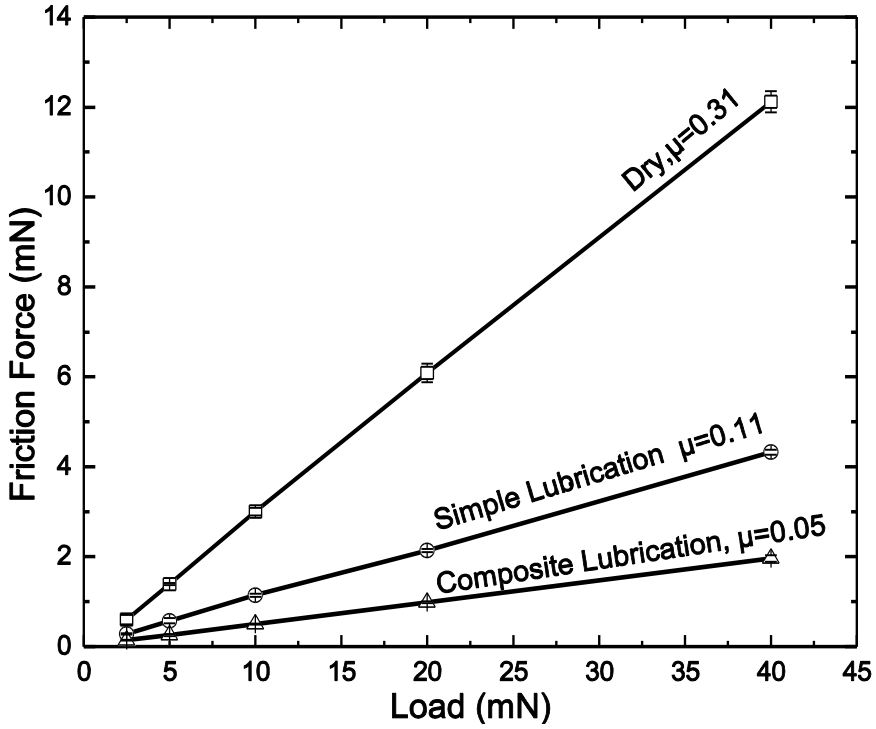

Figure 30. The friction force for *surface c* (shown in Figure 29) as a function of load for dry, simply and compositely lubricated conditions. A linear behavior is observed for all conditions and the coefficient of friction for the dry case about six times that of the composite lubrication case.

The improved lubricity of ZnS nanoparticles is consistent with previous tribological studies on ZnS nanoparticles in hydrocarbon oils [63, 113, 172] and our previous studies on ZnS nanoparticles across molecularly smooth surfaces [44, 173, 174] and rough Cu surfaces [227]. Based on these studies, a number of reasons have been detailed for enhanced lubrication of ZnS nanowire dispersions [44, 173, 174]. These include: i) Nanoparticle geometry ii) Nanoparticle forces iii) Dynamic properties: and iv) Nanoparticle chemistry.

6.4.3 Wear behavior for all lubrication cases

Figure 31 shows SEM images of surface c after shearing under dry, simply, and compositely lubricated conditions. The images show that there are some grooves, wear scars, and debris on the sheared surfaces which indicates that the surfaces have been worn to a certain extent. The length of the wear tracks for all lubrication cases is consistent with the stroke length used for shearing the surfaces (i.e. ~0.25 mm). For the dry case, the depth and width of the groove are a clear indication of the significant damage that occurred which is expected due to the absence of the lubricant. Moreover, it can be seen that for the simple lubrication case, although wear is significantly reduced compared to the dry case, wear tracks are still visible on the surface which indicates that the stand-alone lubricant is not enough to prevent intimate contact between the tribopair. On the other hand, the addition of the ZnS nanowires to the base lubricant displayed the best anti-wear properties as evidence of the near wear-less contact region. A possible explanation for this excellent anti-wear behavior can be attributed to the increase in load carrying capacity of the lubricant, which in turn reduces the asperity-asperity contact between the moving surfaces.

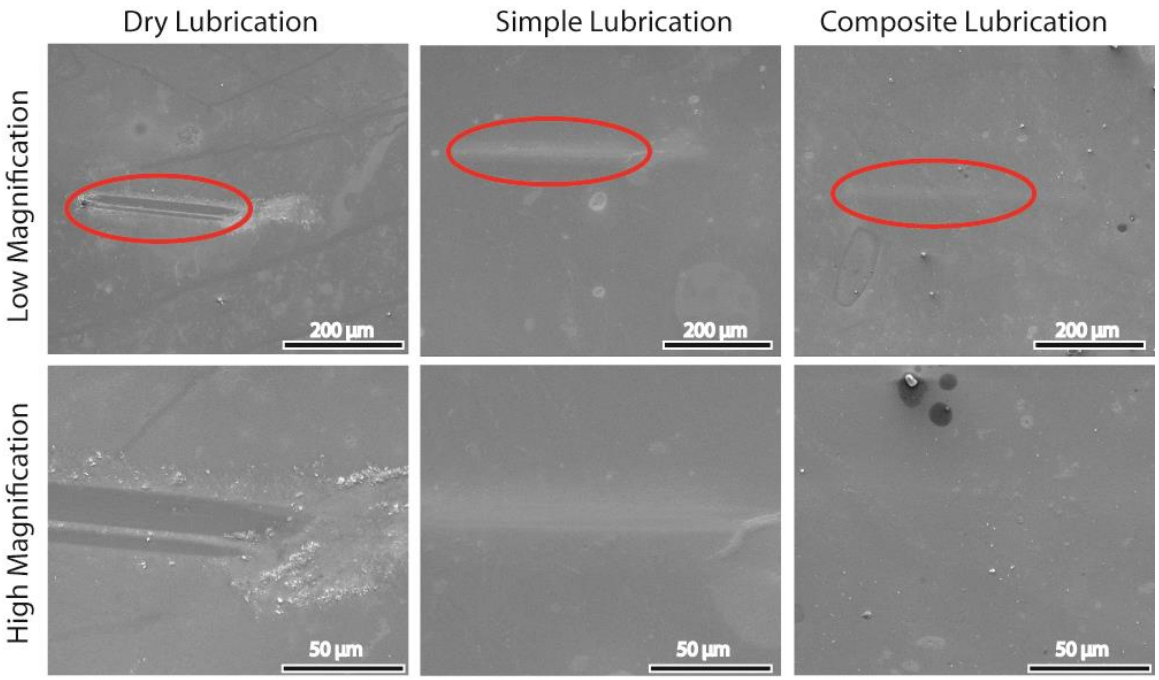

Figure 31. Wear tracks resulting from shearing surface *c* under various lubrication conditions.

6.4.4 Effect of rms roughness on friction

Figure 32 shows the coefficient of friction (CoF) as a function of *rms* roughness. While the CoF increased with increasing *rms* roughness values between 0.14 nm and 8.92 nm, it did not change significantly upon a change in *rms* height from 8.92 to 114.1 nm. In other words, there exist two different regimes in which the CoF exhibits two different behaviors.

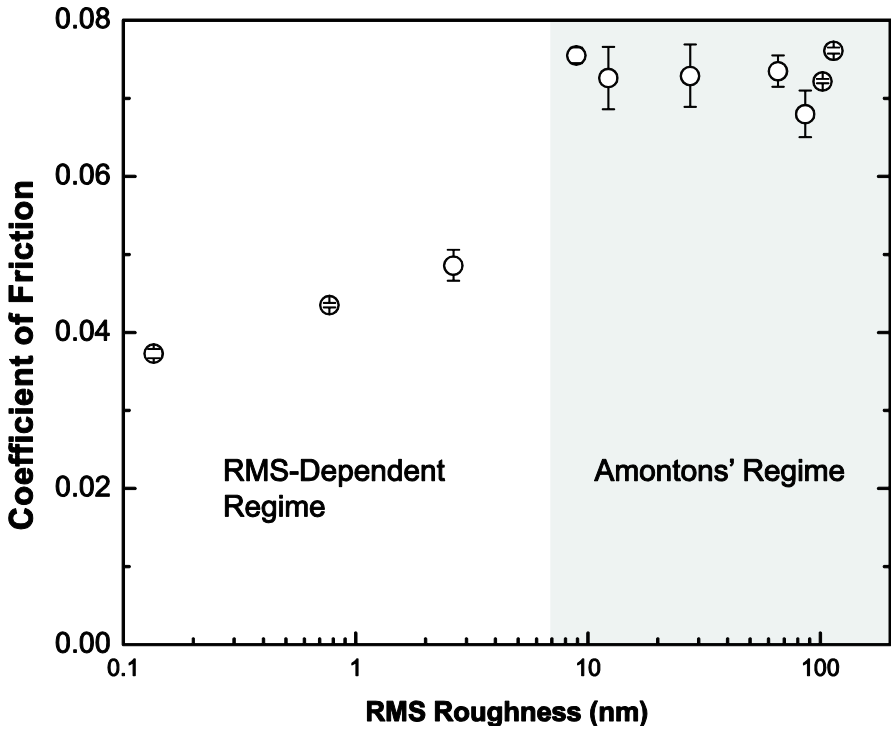

Figure 32**.** Friction coefficient vs *rms* roughness for the composite lubrication case.

The first regime reveals an increase in the friction coefficient with increasing *rms* roughness. This result can be interpreted by carefully considering the geometry of the nanowires as follows: it is known that non-adhering nanoparticles act as effective lubricants when they are not squeezed out of contact regions of mating surfaces *i.e.* when they prevent two surfaces from forming cold-welds [156, 230]. If the *rms* height is too low, physical barrier that holds slippery nanoparticles between the asperities is not large enough to keep them in contact zones. In our case, the diameter of the nanowire is about 4 nm, which indicates that at *rms* values comparable or lower than the nanowire diameter, the nanowires are likely to be squeezed out of the contact area, causing the surfaces to experience high frictional forces upon loading and shearing. However, at *rms* heights significantly higher than the nanowire diameter, the asperities will act as a

barrier and are likely to help retain the nanowires in the contact area. Therefore, nanowires that are trapped in the valleys between the asperities will artificially smooth the surface, thereby not only decreasing the lateral frictional forces due to lateral collisions of asperities but also reducing the effective *rms* roughness. Since the *rms* roughnesses at which the friction coefficient remains virtually unchanged are significantly higher in magnitude than the diameter of the nanowire, we think that our argument seems to be reasonable, especially considering a recent publication describing forces required to displace a nanowire over a physical barrier [250].

The above arguments cannot be substantiated unless detailed imaging of the sheared surfaces is provided. For this reason we obtained SEM images (Figure 33) of a "smooth" (i.e. surface *c*) and "rough" (i.e. surface *h*) surface after shearing under composite lubrication condition. The SEM images of the contact area reveal that no nanowires are found on the "smooth" surface (Figure 33A), which could only imply that they were squeezed out of the contact region. By contrast, it can be clearly seen from the contact area of the "rough" surface that the nanowires were concentrated in the valleys between the asperities. For comparison purposes, SEM images were obtained for the region outside the contact area (Figure 33C), and the results show only a few nanowires which were spontaneously adsorbed on the surface. These results indicate that the trapping of concentrated nanowires in the contact area is due to the loading and shearing of the surfaces as well as the presence of obstacles in the form of asperities with high *rms* heights.

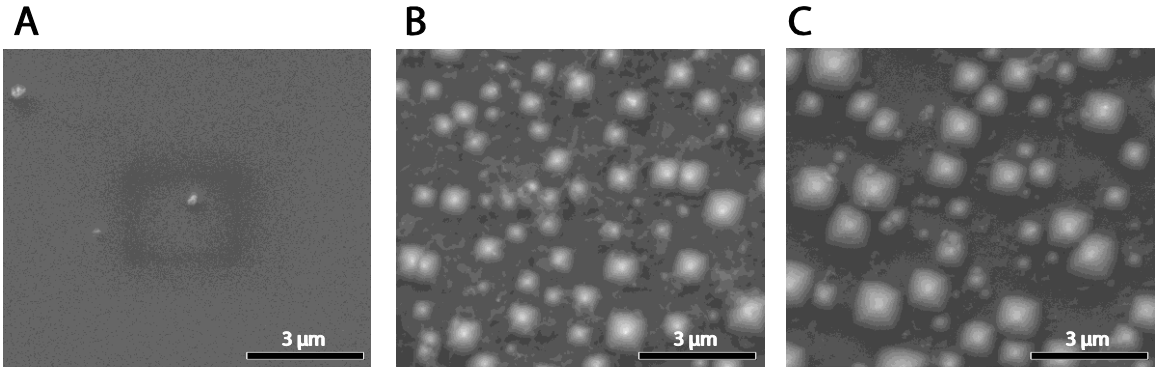

Figure 33. SEM images obtained after shearing under compositely lubricated conditions of A) contact area of smooth surface B) Contact area of rough surface and C) outside contact area of a rough surface.

The initial increase in friction coefficient with increasing *rms* roughness has been observed in many previous studies [99, 251, 252]. Most of these models attribute this behavior to a ploughing action by the harder asperities on the softer ones [20]. Another possible mechanism for this behavior may be due to the interlocking of the asperities as proposed by Tabor [253]. On the other hand, the friction coefficient becomes independent of the *rms* roughness at large *rms* values in accordance with Amontons' law [8, 226] and previous studies [254, 255]. However, one may still wonder why Amontons' law only applies to roughness beyond a certain threshold height? A possible answer to this dilemma is that at high roughnesses the real area of contact is significantly smaller than the apparent area, whereas at very low roughnesses it is very close to the apparent area where Amontons' law fails [256].

6.4.5 Friction traces

Friction traces can provide useful information about the behavior of surfaces undergoing a shearing process. For example, the underlying cause of damage occurred

on the surfaces can be understood by analyzing the friction traces for initial and steady state sliding (Figure 34). As clearly seen, the initial and steady-state sliding under dry conditions are characterized by a stick-slip behavior illustrated by spikes the amplitudes of which increase upon transition from initial to steady state. According to Yoshizawa and Israelachvili [257], the spikes have a significant tribological implication and could well be indicative of the damage and wear of moving surfaces. Various models have been developed in attempts to explain the origin of the stick slip behavior: Rough surfaces model, velocity-dependent friction model and phase transition models. The second model is not of much concern here since the sliding velocity was maintained constant throughout our study. However, the rough surfaces model is more suitable to describe the friction traces obtained where the slip occurs when asperities go over one another. This model has been detailed elsewhere and the more adventurous reader is urged to consult refs [218-220]. We think that the friction traces for the dry case can be interpreted in a similar manner.

Figure 34 also sheds the light on the friction traces for a "rough" surface (i.e. surface *h*) compared to a "smooth" (i.e. surface *b*) one in an attempt to explain the friction coefficient behavior as a function of the *rms* height. The results reveal that under simple lubrication conditions the rough surface exhibits smooth initial behavior followed by a progressive stick-slip motion characterized by the appearance of spikes the amplitude of which increased upon transitioning from initial to steady-state. This behavior can be explained in a similar fashion to that of the dry case. However, for the smooth surface, a smooth continuous motion was observed initially and maintained

throughout the shearing process. It is believed that the smooth sliding is a consequence of the low *rms* height.

The smooth surface for the composite lubrication case exhibits a similar behavior to that of the simple lubrication. That is, a smooth continuous motion is obtained with no effect on the magnitude of the friction force upon transition from initial to steady state. This behavior implies that the nanoparticles do not play a significant role in the shearing process of this surface. In other words, the nanoparticles may not present in the contact area at the time they are required. This explanation seems to be consistent with the friction coefficient behavior at low roughnesses. However, in the rough surface case, the nanoparticles play an essential role in that the initial stick-slip motion is transformed into a smooth and continuous one and that the magnitude of the friction force at steady state is reduced in comparison to its initial value. A possible explanation for this behavior is that at the beginning of the sliding motion the nanoparticles have not had enough time to reorganize themselves in the valleys and consequently a stick slip motion is observed due to a combination of relatively high effective roughness and jamming of the nanowires. However, as time progresses, the nanoparticles become more organized under the shearing as they fill the valleys, thereby reducing the effective *rms* roughness and resulting in a smoother behavior at steady state.

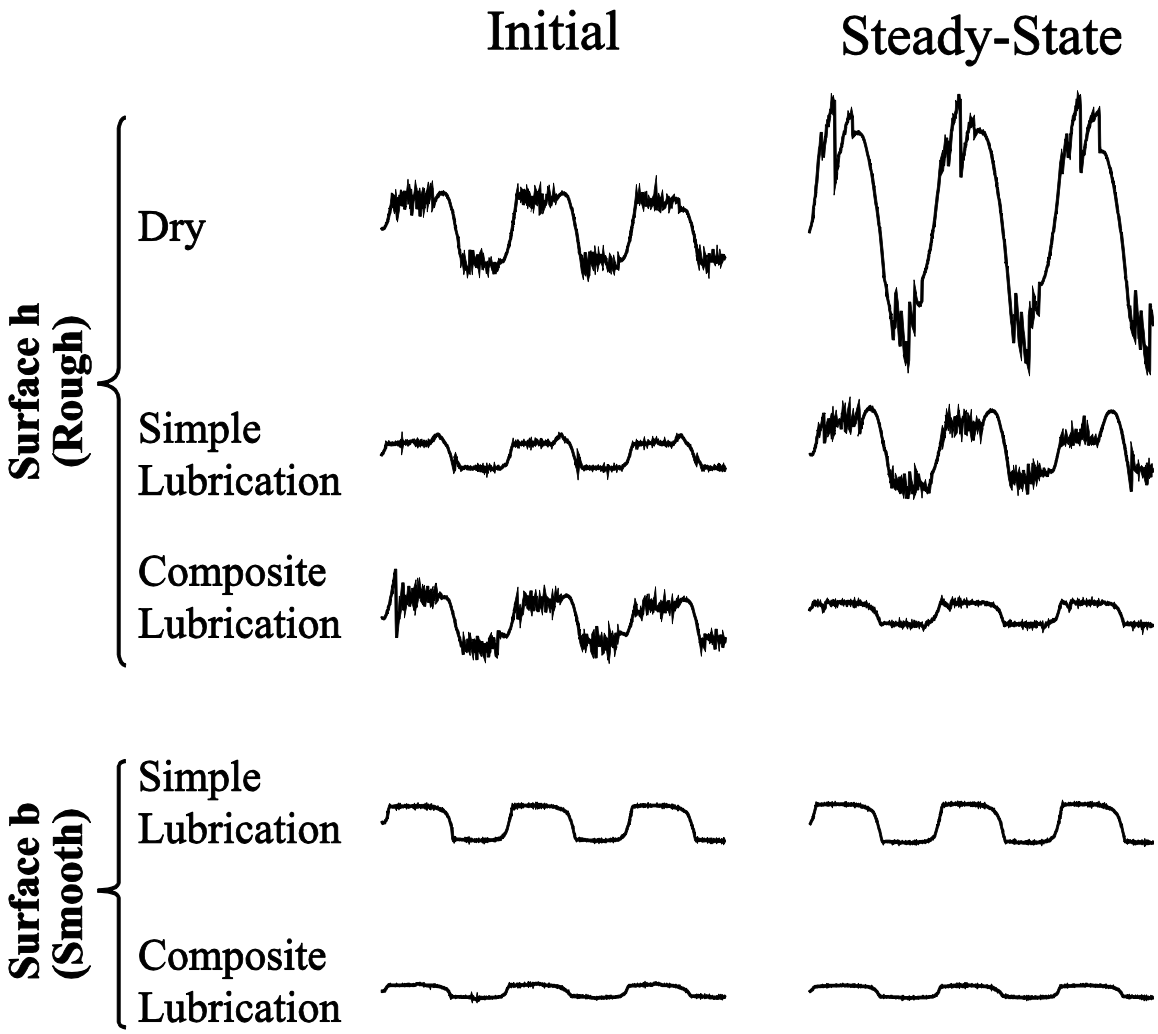

Figure 34. Initial and steady-state friction traces for surfaces *b* and *h* under various lubrication conditions.

6.5 Conclusion

Friction behaviors of brittle SiO_2 surfaces with different topographies were investigated for dodecane+ZnS nanowire lubricated surfaces as a function of surface roughness parameters such as *rms* roughness. Based on the findings of this original study, the friction coefficient initially increases with increasing *rms* roughness and then reaches a virtually constant value beyond a threshold roughness. This behavior was

explained in the context of two different regimes depending on whether or not nanowires fill the valleys. SEM images and friction traces provided supporting evidence of the observed behavior which was mainly attributed to asperities acting as barriers that helped keep the nanowires in the contact region. Based on our findings, it appears that the friction coefficient for real engineering surfaces where the roughness is significantly higher than the diameter of nanowires will not be affected by the surface topography. The insights provided in this article help shed the light on nanoparticle based lubricants in relation to surface roughness in efforts to reduce friction, wear and energy losses. Additionally, the trends observed in this study open up the opportunity for similar investigations.

CHAPTER VII

INORGANIC NANOPARTICLE-BASED IONIC LIQUID LUBRICANTS [*]

7.1 Overview

This chapter deals with the tribological properties of recently described mixtures of nanoparticles (NPs) and ionic liquids (ILs), specifically mixtures of SiO_2 (silica) nanoparticles and 1-butyl-3-methylimidazolium (trifluoromethysulfony)imide. Friction force profiles, kinetic friction coefficients, friction traces, rheological properties, and wear behavior of these mixtures were compared with that of the pristine ionic liquids at various concentrations of nanoparticles for a tribo-pair of stainless steel ball and a steel surface. It was shown that NP concentration significantly influences the tribological properties of the NP-IL mixtures: the friction coefficient for the optimum NP concentration (0.05 wt.%) was ~ 35% less than that for high NP concentrations (> 3 wt.%) and 25% less than that for low NP concentrations (< 0.01 wt.%). At the optimum NP concentration, while the friction force was slightly lower for NP-IL mixture at low loads, the friction force was about 28% lower for NP-IL mixture at high loads, compared to the pristine ionic liquid. In addition, the wear volume was found to decrease by 24% upon the addition of the optimum amount of nanoparticles into ionic liquid. Overall, this study concludes that promising tribological properties of ionic liquids can be further enhanced by incorporating nanoparticles into ionic liquid.

---

[*] Reprinted with permission from "Inorganic nanoparticle-based ionic liquid lubricant" by Bassem A. Kheireddin, Wei Lu, I-Cheng Chen, Mustafa Akbulut, 2013. *Wear*, 303, 185-190. Copyright 2013 by Elsevier.

7.2 Introduction

Ionic Liquids (ILs) are a relatively new class of materials that consist entirely of ionic species with a melting point lower than 375.15 K. Owing to their relatively low vapor pressure, they have been of considerable interest to chemists and green chemistry since they cannot emit volatile organic compounds [258]. Other interesting properties of ILs include non-flammability, high-thermal and chemical stability, low melting point, and wide ranges of viscosity to name a few [259, 260]. These properties have enabled them to be potential candidates in various applications such as solvents for synthesis, catalysis, analytical chemistry, space and electronics applications [261-263]. In addition, the aforementioned properties of ILs are highly desired in the field of tribology [264]. While the very first attempt to use ionic liquid as lubricant was described in 1961[265], it was not until almost forty years later that ILs were broadly recognized as potential lubricants [266]. Since then, tens of articles were published in various journals on the evaluation of the tribological properties of ionic liquids [266-278].

Past decades have witnessed an explosive growth in studies focusing on the tribology of inorganic nanoparticles that are dispersed in base oils such as paraffin oil and polyalphaolefins [44, 61, 62, 113, 227, 279-288]. These studies have shown that they deposit on the rubbing surface and improve the tribological properties of the base oil, displaying superior friction and wear reduction characteristics. Considering the promising results of nanoparticles in improving lubrication properties of base oil, we hypothesize that the dispersion of inorganic nanoparticles in ionic liquids can improve the tribological properties of ionic liquids. To test this hypothesis, we investigate the

tribological properties of spherical SiO_2 (silica) nanoparticles dispersed in the ionic liquid 1-butyl-3-methylimidazolium (trifluoromethysulfony)imide (BMIM TFSI) in comparison to the pristine ionic liquid for steel/steel contact under ambient conditions.

7.3 Experimental details

7.3.1 Materials

All materials were used as received. The ionic liquid 1-butyl-3-methylimidazolium (trifluoromethysulfony) imide (BASF quality, ≥ 98%) was purchased from Sigma Aldrich. Silicon dioxide nanopowder (10-20 nm in size) was also purchased from purchased from Sigma Aldrich. Stainless steel sheets with a mirror polish were purchased from Metals Depot (Winchester, KY).

7.3.2 Surface preparation

The steel sheets were cut in the shape of a 2 cm x 2 cm square to form the substrate. Prior to testing, the substrate is cleaned with acetone and blown dry with nitrogen. After testing and shearing the surfaces, the lubricant is removed by rinsing the substrate with acetone, and the substrate is stored for post-shearing characterization.

7.3.3 Friction measurements

Friction response was undertaken by a nano-tribometer (CSM Instruments, Switzerland) at a constant sliding speed of 0.0005 m/s and a total distance of 0.05 m. Tests were conducted using a very smooth stainless steel sphere (diameter ~ 2 mm) with *rms* roughness of 2.14 ± 0.45 nm along with a medium-load cantilever with normal and tangential stiffnesses of 150 N/m and 128 N/m, respectively. All tests were conducted with normal loads of 2.5, 5.0, 10.0, 15.0, 20.0, and 40.0 mN, and each load was applied

at least three different times at various locations on the sample until a standard deviation (based on the average of the measurements) of less than 10% is obtained. In this study, two different types of lubrication conditions were investigated: simple lubrication (steel surfaces across IL), and composite lubrication (steel surfaces across silica nanoparticles dispersed in IL). For the composite lubrication case, various concentrations of silica nanoparticles were used in an effort to understand the effect of concentration on the lubricating behavior. Throughout this study, the humidity was maintained between 45-50%.

7.3.4 Rheological measurements

Rheological measurements were performed with an Anton Paar Rheometer Physica MCR 301(Ashland, VA). The shear rate was increased from 1 s^{-1} to 1000 s^{-1} within 10 min allowing for the recording of several data points for the viscosity. The experiments were conducted using Neat IL, and 3 different nanoparticle concentrations (0.05%, 1%, and 5%) dispersed in IL at 22ºC. Each of these conditions was repeated three times for statistical analysis.

7.3.5 X-Ray photoelectron spectroscopy (XPS)

Tribochemical changed were characterized using KRATOS Axis Ultra Imaging Instrument (Kratos Analytical, Manchester, UK). Photoelectrons were excited using an incident monochromated X-Ray beam emanating from the Al target (1486.71eV, 8mA). The beam was focused on a 300 μm × 700 μm area of the sample surface with high resolution scans (40 eV pass energy) for all surface elements. The spectra were reported as an average of three measurements for each condition. XPS characterization was

performed on different samples, specifically the contact and non-contact areas of steel surfaces that are sheared with IL and IL + SiO_2 NPs.

7.4 Results and discussion

7.4.1 Effect of nanoparticles on friction

Figure 35. displays a friction force versus normal load plot for the ionic liquid with and without NPs. It was found that at normal loads less than 15 mN, the frictional forces for the composite lubrication condition are slightly lower than those of the simple lubrication condition. However, the effect of incorporating 0.05 wt.% silica nanoparticles into the ionic liquid on the frictional forces becomes more pronounced at loads above 15 mN . Furthermore, it was observed that, for the simple lubrication case, the friction force was a linear function of the normal load, which is in accordance with the well-known Amontons' law [8]. On the other hand, for the composite lubrication case, a deviation from linearity is observed at high loads.

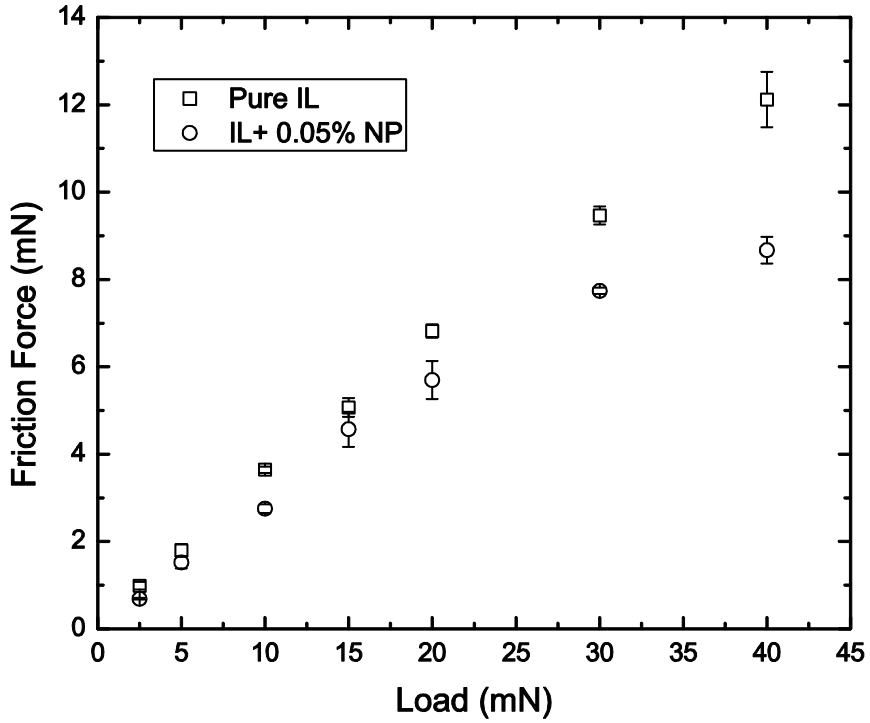

Figure 35. The friction force as a function of load for simply and compositely lubricated conditions.

One possible explanation for these behaviors is related to the formation of particulate network by the silica nanoparticles. It is known that bare nanoparticles dispersed in ILs adhere to each other and form aggregates leading to the formation of particulate network and subsequently the gelation of the ionic liquid [289, 290]. This network, which confers a higher viscosity to the ionic liquid, presumably leads to an enhancement of the mechanical properties (i.e. load carrying capacity) of the composite lubricant [289]. At low loads, the particulate network may be maintained for the duration of the shearing test due to insufficient loading force (i.e. low normal load). During this period the nanoparticulate network may not fully penetrate the interface or fill the valleys (due to the large network size). Therefore, the slight reduction in frictional forces

at load loads may be attributed to the increased load carrying capacity of the lubricant. However, at high loads there is a high possibility that the particulate network is disrupted more rapidly as shown in Figure 36, leading to high fluidity under shear [289] and allowing the nanoparticles to smooth out the valleys, thereby providing better lubrication. This explanation agrees well with previous studies on non-adhering nanoparticles that act as effective lubricants when they are not squeezed out of contact regions of mating surfaces *i.e.* when they prevent two surfaces from forming cold-welds [156, 227, 230, 282].

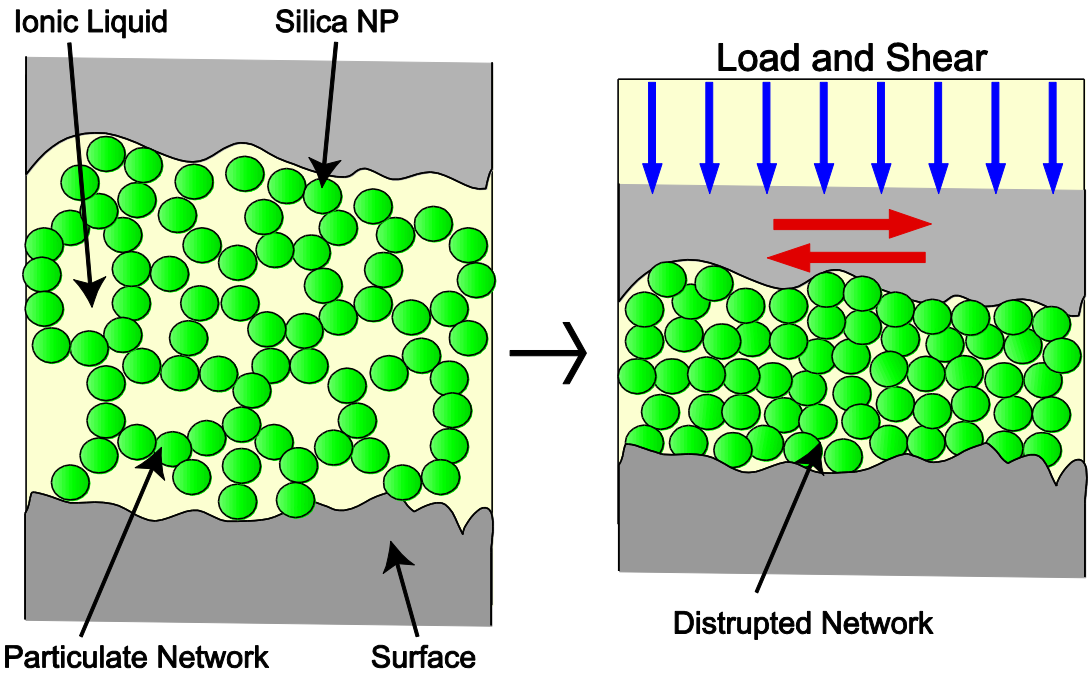

Figure 36. Schematic of the network formation of silica nanoparticles and its disruption upon loading and shearing.

7.4.2 Effect of nanoparticle concentration

Eight different concentrations ranging from 0.01 wt.% to 5% were used in this study in order to cover three different concentration regimes: dilute, intermediate and concentrated solutions. As can be seen in Figure 37, the friction coefficient decreases with increasing nanoparticle concentration and then increases gradually as the nanoparticle concentration rises above 0.05 wt. %. Therefore, 0.05 wt. % is considered to be the optimal concentration of silica nanoparticles in the ionic liquid.

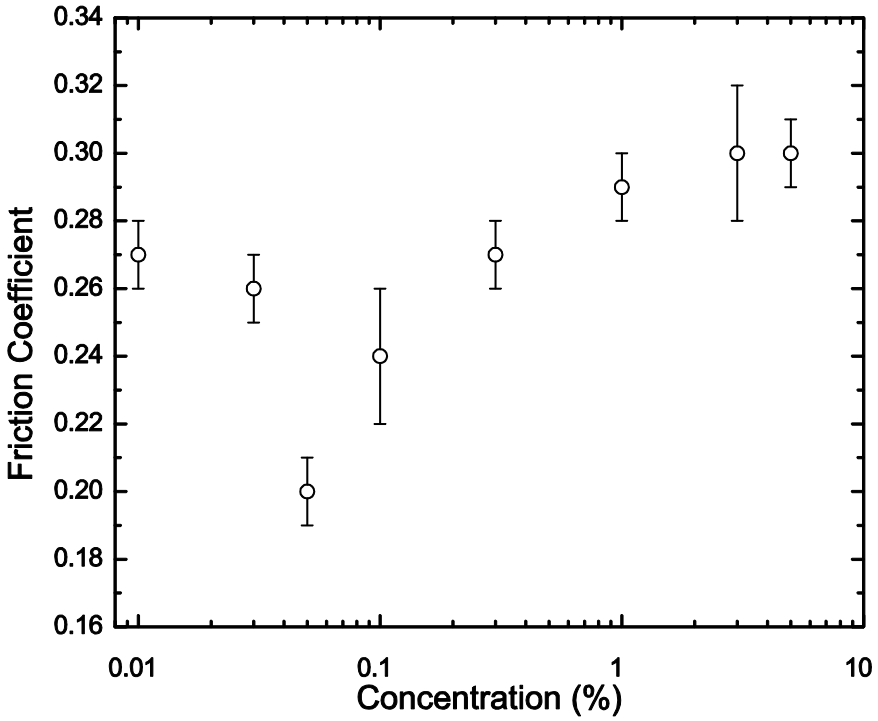

Figure 37. Effect of nanoparticle concentration on the friction coefficient.

These results can be explained as follows: at very low concentrations, the nanoparticle coverage is low and therefore there are not enough nanoparticles to form a

protective film or to prevent contact between asperities, causing the friction coefficient to be relatively high. On the other hand, at high concentrations the nanoparticles tend to form large aggregates and cannot properly fill the valleys between the asperities [45, 291]. Instead, they may behave similar to the debris particles that are known to scratch and wear shearing surfaces under loading and sliding. All of these factors combined suggest that high nanoparticle concentration can have a detrimental effect on the lubrication of shearing surfaces, illustrated by an increase in the friction coefficient [292]. Therefore, it can be concluded that the optimal concentration of 0.05 wt.% provides enough nanoparticle coverage so that a protective film can be formed without the agglomeration of the nanoparticles.

7.4.3 Rheological properties

The rheological characterization for various concentrations of SiO_2 dispersions were performed and compared to that of the neat IL in efforts to quantify the viscosity and evaluate the stability of the nanoparticle suspension. Figure 38 shows that viscosity increases with increasing concentration, a result that is consistent with that reported in previous studies dealing with similar systems [293-295]. This result is not surprising since increasing the NP concentration will increase the possibility of nanoparticle agglomeration and eventually the gelation of the ionic liquid. The magnitudes of the viscosities obtained in this study also agree well with those reported elsewhere [296]. Moreover, for the neat IL and 0.05 wt.% (very dilute regime) NP dispersion, a Newtonian fluid behavior is obtained whereby the viscosity is mostly constant and independent of the shear rate. However, at higher concentrations, departure from the

Newtonian behavior is observed whereby the viscosity becomes dependent on the shear rate. This behavior is consistent with previous studies and indicates that at higher concentrations agglomerates and networks tend to form especially at lower shear rates followed by the destruction of the network at higher shear rates [294]. Therefore, at concentrations above 0.05%, which was the optimal concentration from a tribological standpoint, the nanoparticle suspension is considered to be unstable.

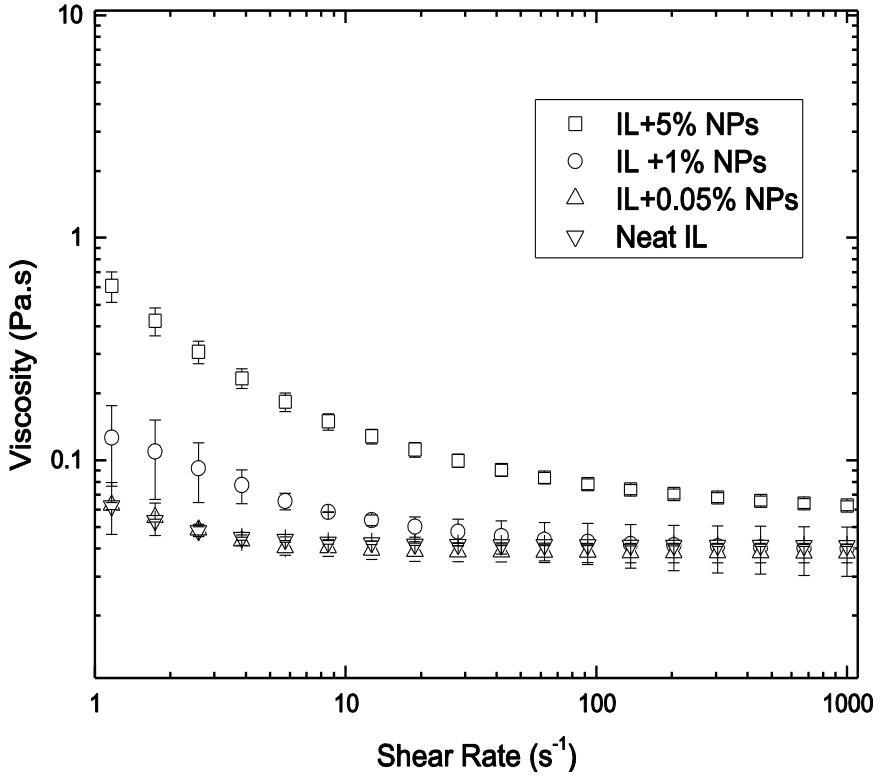

Figure 38. Viscosity versus shear rate for the neat IL and various concentrations of SiO_2 NPs + IL.

7.4.4 Wear behavior of surfaces

The morphology of the worn surfaces was examined using a scanning electron microscope (SEM). Figure 39 shows SEM images of surfaces after shearing under

simply, and compositely lubricated conditions (0.05 wt. % and 5 wt.%). Specific attention is paid for the middle and edge parts of the wear tracks in order to elucidate the amount of debris resulting from the damage. The images show that there are some grooves, wear scars, and debris on the sheared surfaces which indicates that the surfaces have been worn to a certain extent. In order to quantitatively evaluate the extent of wear on the surfaces, the wear volumes were calculated by analyzing the surface profile (data not shown) generated with a stylus profilometer and are shown in Table 7.

Table 7. Wear volumes for steel/steel contact under various lubrication conditions at 20 mN load

Lubrication Condition	**Wear Volume (x 10^{-4} μm^3)**
Pristine IL	9.7 ± 1.0
5 wt. % NP + IL	11.4 ± 0.8
0.05 wt. % NP + IL	7.4 ± 1.0

Under a 20 mN load, the wear volume for the 0.05 wt. % NP + IL lubrication case was found to decrease by 24% compared to the pristine IL. The reason for this decreasing wear can be attributed to the presence of the protective nanoparticles in the contact zone. This result is consistent with the SEM images and the frictional measurements as it was established that at the optimum concentration the nanoparticles can fill the valleys and prevent asperity contact, thereby reducing the wear volume. Interestingly, the addition of 5 wt. % NPs to the ionic liquid caused an increase in the wear volume by approximately 18%. This result agrees well with the SEM images (Figure 39c) as illustrated by the multiple scratches found on the wear track corresponding to the 5 wt. % NP + IL case. The reason for this increase can be explained

as follows: at high NP concentration, the nanoparticles tend to collide and aggregate, and consequently form large clusters which act as abrasive bodies that can have a detrimental effect on the wear behavior of surfaces [297]. Therefore, it can be concluded that the 0.05 wt. % NP concentration is also optimal in terms of providing excellent antiwear behavior as shown in Figure 39b.

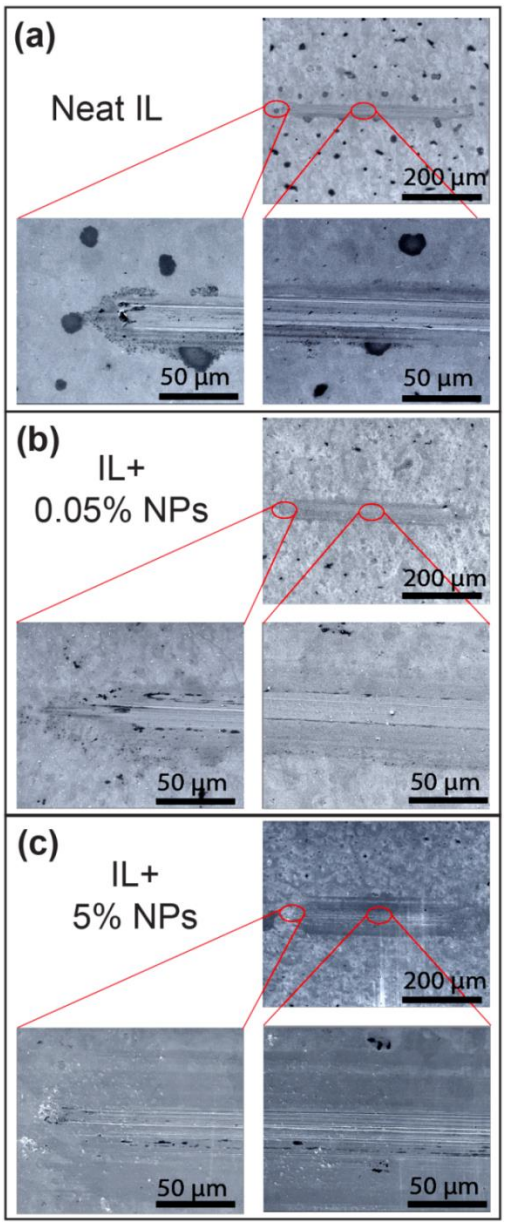

Figure 39. SEM morphologies of steel surfaces after shearing under three lubrication conditions: (a) neat IL (b) IL+ 0.05 wt.% NP, and (c) IL + 5 wt.% NP. Low and high magnifications of the middle and edge parts of the wear track are shown.

7.4.5 XPS analysis

XPS measurements were conducted to examine the chemical changes on the surfaces due to the shearing process in the presence of ionic liquid or ionic liquid and

nanoparticles. The XPS high-resolution spectra of F_{1s} are shown in Figure 40, with binding energies corrected by using the C_{1s} peak at 285.0 eV as a reference. Figure 40 shows the presence of a peak at 688.8 eV [298, 299] which corresponds to the fluorine (F_{1s}) in the TFSI anion, and appears in the no-shear and shear conditions. However, upon shearing the appearance of a new peak at 684.8 eV is evidence of the transformation of fluorine (F_{1s}) to an iron fluoride compound in the form of FeF_2 or FeF_3 [299, 300].

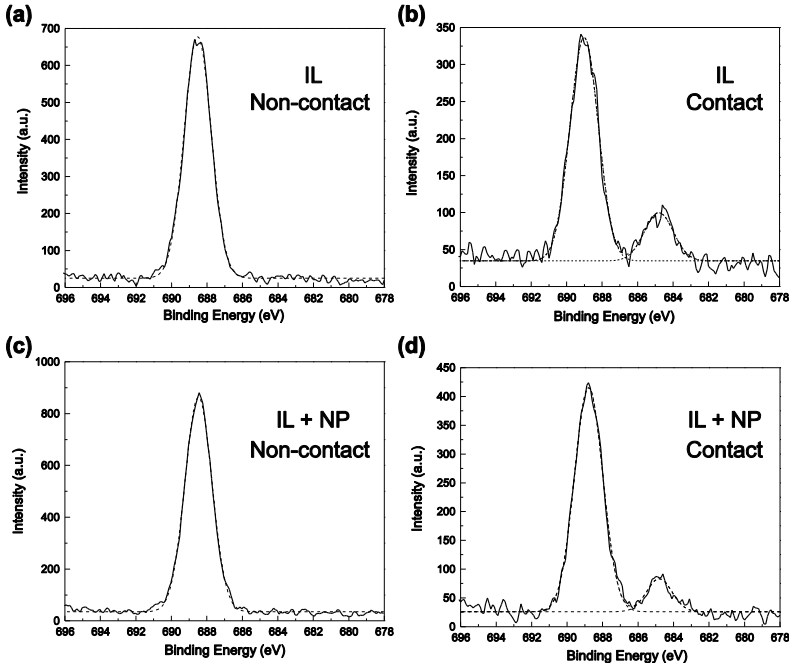

Figure 40. XPS spectra of F_{1s} for (a) IL non-contact area (b) IL contact area (c) IL + NP non-contact area and (d) IL + NP contact area.

These results agree well with previous studies whose results show the formation of a tribochemical film between the substrate and the anion moiety of the ionic liquid [271, 299, 301, 302]. The formation of the iron fluoride compounds on the sheared surfaces serve as protective films that help to improve the tribological properties. The

XPS results confirm the friction-reduction and anti-wear properties through tribochemistry and prove that the presence of the SiO_2 nanoparticles does not hinder the formation of such films.

7.4.6 Friction traces

Analysis of friction traces can provide detailed information about dynamics of lubricant under load and shearing. Figure 41 shows the friction traces for the initial and steady state sliding across the neat ionic liquid and ionic liquid + 0.05 wt. % silica nanoparticles. For the case of simple lubrication, while the sliding was initially smooth (i.e. relatively small stick-slip spikes in comparison to the friction force), there was an increase in the amplitude of the spikes under steady-state condition. Furthermore, the initial friction force was smaller than the steady-state one.

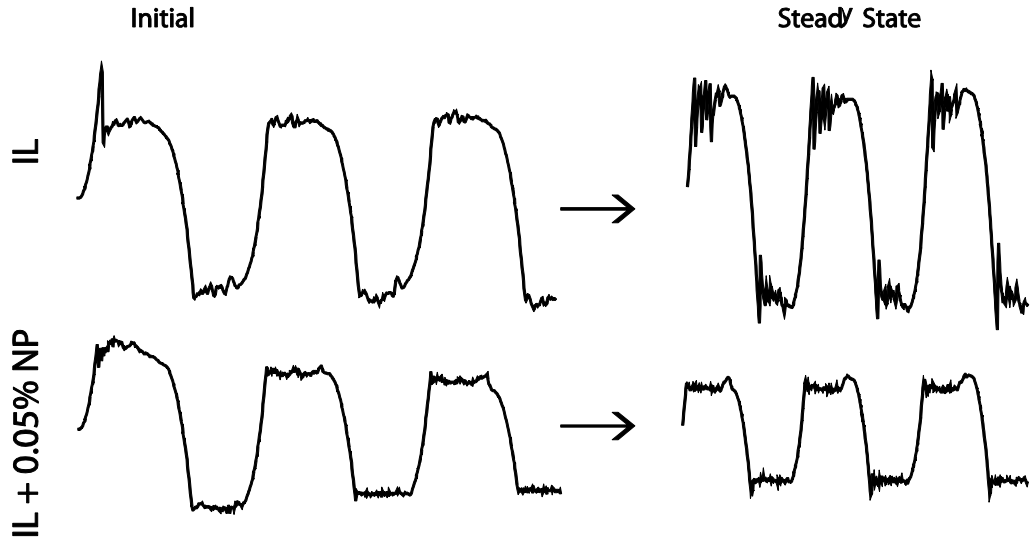

Figure 41. Initial and steady-state friction traces for both pristine IL and IL + 0.05 wt.% NP. Drawn to scale.

According to some researchers [257, 303-305], the stick-slip motion has significant tribological implications and could well be indicative of the damage and wear of moving surfaces. This result agrees well with the SEM images of the worn surfaces, where a significant damage occurs under the simply lubricated condition. Moreover, the amplitude of the friction forces increases upon transition from initial to steady sliding. Studies have shown that this increase in frictional force may be due to the increase in wear volume with sliding distance, which increases the contact area owing to the destruction of the asperities [306]. Another possible reason for the stick-slip motion is the shear induced ordering transition. However, the idea of the surface-fluid interaction inducing the ionic liquid molecules to solidify is not plausible due to the amorphous structure of the substrate [229]. Therefore, we mainly attribute the stick slip motion observed in the neat ionic liquid case to the surface damage.

On the other hand, for the case of composite lubrication, the amplitude of stick-slip spikes was almost unchanged for initial and steady-state cases, and significantly lower than that of the pristine ionic liquid case. However, there was a reduction in frictional forces upon transitioning from initial to steady state. The steady-state was reached in 10 cycles of shearing for the composite lubrication case, in comparison to the 18 cycles required for the simple lubrication. After careful dissection of these results, it is believed that this difference in spike amplitude supports the analysis of the damage occurred in both cases, where high amplitudes are associated with severe damage and low amplitude with minimal damage. Moreover, steady-state in the composite lubrication case was reached relatively quickly possibly due to the rapid destruction of

the particulate network allowing the nanoparticles to swiftly and properly fill out the valleys and prevent surface damage, a behavior which ultimately leads to a reduction in the frictional forces. This was not the case for the pristine IL as the progressive damage occurred on the surface extended the number of cycles required to reach steady-state.

7.5 Conclusion

The tribological properties of the ionic liquid 1-butyl-3-methylimidazolium (trifluoromethy-sulfony) imide and various concentrations of silica nanoparticles were investigated. The results indicate that at certain concentrations the silica nanoparticles dispersed in the ionic liquid can outperform the neat ionic liquid. In particular, it was found that a concentration of 0.05 wt. % was optimal in terms of providing the best friction-reduction as well as antiwear properties for steel/steel contact. This improvement in the tribological properties was attributed to: i) the increased loading capacity of ionic liquids in the presence of silica nanoparticles; (ii) the ability of nanoparticles to fill out valleys between asperities, thereby effectively smoothing out the shearing surfaces. In essence, this study has shown that the addition of silica nanoparticles to ionic liquids can improve the lubrication behavior of ionic liquid lubricants and encourages more investigations on using nanoparticle additives with green solvents such as ionic liquids in order to protect the environment as well as prolong the lifetime of machinery.

CHAPTER VIII

SUMMARY

This dissertation is a compilation of seven chapters pertaining to the tribological properties of nanoparticle-based lubrication systems (NBLS). In chapter I, a brief review is presented on the importance of tribology and related phenomena such as friction, wear and lubrication and their impact on our everyday lives and the life of machinery. In chapter II, a comprehensive review is presented and details the important considerations that must be taken into account when designing NBLS. These considerations into 3 categories: physicochemical, mechanical and geometrical, each of which encompasses various parameters that has direct implications on the tribological performance of such systems. Chapter II also offers a review on previous tribological studies involving nanoparticle additives to a base oil across various surfaces and their important findings as well the as lubrication mechanisms involved.

In chapter III I review the experimental techniques employed to characterize the surfaces and nanoparticles used in this work. These include atomic force microscopy (AFM), nanotribometry, scanning electron microscopy (SEM), transmission electron microscopy (TEM), and x-ray photon spectroscopy.

In chapter IV, I detail the effects of shearing surface topography on the friction behavior of ZnS nanowire films deposited on copper surfaces prepared using a metal evaporation method. I found that the friction behavior of the nanowire dispersion strongly depends on the surface roughness parameters. On the other hand, the friction

force for the surfaces under dry conditions was independent of changes in the surface roughness parameters. In addition, the nanowire dispersion on average reduced the surface friction forces by 38% and 47% when compared to the dry and base-oil lubricated surface conditions, respectively. This was attributed to the ability of the nanowires to shear, slide and roll on the surface and of the nanowire surfactant to aid smooth motion.

Chapter V is an extension of chapter IV and details the effect of surface roughness parameters on the frictional properties of nanowire-based lubrication systems across ductile surfaces. I found that the nanowires performed as effective lubricants when a) the *rms* height of asperity is greater than the nanowire radius and b) the inter-island separation is an integer-multiple of the nanowire length. In addition, I found that the friction coefficient was linearly dependent on the mean pressure experienced by the nanoparticles.

Chapter VI details the study of effects of root-mean-square (*rms*) roughness on the friction behavior of ZnS nanowire films. It was observed that a plot of the friction coefficient as a function of *rms* roughness yields two different regimes: i) At *rms* roughnesses comparable or slightly higher than the nanowire diameter the friction coefficient increases with increasing *rms* roughness ii) At roughnesses significantly higher than the nanowire diameter the friction coefficient is insensitive to increasing *rms* roughness in accordance with the infamous Amontons' law. SEM images and friction traces were obtained and helped provide supporting evidence to the observed behavior.

Chapter VII investigates the tribological properties of various silica nanoparticle concentrations in ionic liquid for steel/steel contact. We found that an optimal nanoparticle concentration exists and yields the best frictional and anti-wear properties. This improved behavior was attributed to a) the formation of a protective film, b) the ability of the nanoparticles to penetrate the interface and c) the disruption of particulate network by shearing. In addition, we anticipate that our findings are valuable and encourage further investigations on energy-efficient lubricants based on nanoparticle additives in ionic liquids.

Although significant strides were made in laying the groundwork for designing of tribological surfaces that are sheared across nanoparticle dispersions, future work is recommended in order to gain a complete knowledge of the tribological properties of NBLS. As such, I recommend experiments involving a systematic preparation of surfaces whereby only one roughness parameter is changed in order to deconvolute its effect on the tribological properties. Moreover, it would be ideal if molecular dynamic simulations are conducted along with the experimental work. This will not only confirm the observed results but will yield insights on the organization of nanoparticles and their interaction with the shearing surfaces.

With regards to the ionic liquid study, it would be interesting to conduct comparable studies on functionalized SiO_2 nanoparticles in order to determine if the tribological properties of ionic liquids can be further improved. Moreover, it would also be of interest to investigate various kinds of nanoparticle additives in green solvents such as ionic liquids.

REFERENCES

1. Rabinowicz, E., *Friction and wear of materials*. New York:Wiley, 2005.
2. Stachowiak, G.W. and Batchelor, A.W., *Engineering tribology*. Oxford: Elsevier,2005.
3. Braun, O.M. and Naumovets , A.G., *Nanotribology: microscopic mechanisms of friction.* Surface Science Reports, 2006. **60**(6-7): p. 79-158.
4. Gao, J., et al., *Frictional forces and Amontons' law: from the molecular to the macroscopic scale.* The Journal of Physical Chemistry B, 2004. **108**(11): p. 3410-3425.
5. Blau, P.J., *Friction science and technology : from concepts to applications*. Boca Raton: CRC Press, 2009.
6. Bowden, F. and D. Tabor, *The area of contact between stationary and between moving surfaces.* Proceedings of the Royal Society of London Series A-Mathematical and Physical Sciences, 1939. **169**(938): p. 391-413.
7. Johnson, K., K. Kendall, and A. Roberts, *Surface energy and the contact of elastic solids.* Proceedings of the Royal Society of London Series A-Mathematical and Physical Sciences, 1971. **324**(1558): p. 301-313.
8. Gao, J., et al., *Frictional forces and Amontons' law: from the molecular to the macroscopic scale.* The Journal of Physical Chemistry B, 2004. **108**(11): p. 3410-3425.

9. Johnson, K.L., *Adhesion and friction between a smooth elastic spherical asperity and a plane surface.* Proceedings of the Royal Society of London Series A-Mathematical Physical and Engineering Sciences, 1997. **453**(1956): p. 163-179.

10. Tas, N., et al., *Stiction in surface micromachining.* Journal of Micromechanics and Microengineering, 1996. **6**(4): p. 385-397.

11. Johnson, K.L., *Contact mechanics*. Cambridge: Cambirdge University Press, 1987.

12. Gao, J., et al., *Frictional forces and Amontons' law:From the molecular to the macroscopic scale.* The Journal of Physical Chemistry B, 2004. **108**(11): p. 3410-3425.

13. Persson, B.N.J., *Contact mechanics for randomly rough surfaces.* Surface Science Reports, 2006. **61**(4): p. 201-227.

14. Persson, B.N.J., et al., *On the nature of surface roughness with application to contact mechanics, sealing, rubber friction and adhesion.* Journal of Physics-Condensed Matter, 2005. **17**(1): p. R1-R62.

15. Luan, B.Q. and Robbins, M.O., *The breakdown of continuum models for mechanical contacts.* Nature, 2005. **435**: p. 929-932.

16. Luan, B.Q. and Robbins , M.O., *Contact of single asperities with varying adhesion: comparing continuum mechanics to atomistic simulations.* Physical Review E, 2006. **74**(2).

17. Luan, B.Q. and Robbins , M.O., *Hybrid atomistic/continuum study of contact and friction between rough solids.* Tribology Letters, 2009. **36**(1): p. 1-16.

18. Gao, J.P., Luedtke , W.D., and Landman , U., *Layering transitions and dynamics of confined liquid films.* Physical Review Letters, 1997. **79**(4): p. 705-708.

19. Landman, U., Luedtke , W.D., and Gao , J.P., *Atomic-scale issues in tribology: Interfacial junctions and nano-elastohydrodynamics.* Langmuir, 1996. **12**(19): p. 4514-4528.

20. Holmberg, K. and Matthews , A., *Coatings tribology : properties, mechanisms, techniques and applications in surface engineering*. Amsterdam: Elsevier Science, 2009.

21. Burwell Jr, J.T., *Survey of possible wear mechanisms.* Wear, 1957. **1**(2): p. 119-141.

22. P. Suh, N., *The delamination theory of wear.* Wear, 1973. **25**(1): p. 111-124.

23. Celis, J.-P., P. Ponthiaux, and F. Wenger, *Tribo-corrosion of materials: interplay between chemical, electrochemical, and mechanical reactivity of surfaces.* Wear, 2006. **261**(9): p. 939-946.

24. Archard, J., *Wear theory and mechanisms.* Wear Control Handbook, 1980: p. 35-80.

25. Dowson, D., *History of tribology*. New York: Longman, 1979.

26. Jacobson, B., *The Stribeck memorial lecture.* Tribology International, 2003. **36**(11): p. 781-789.

27. Hamrock, B.J., Schmid , S.R., and Jacobson , B.O., *Fundamentals of fluid film lubrication*. New York: Marcel Dekker, 2004.

28. Höglund, E., *Influence of lubricant properties on elastohydrodynamic lubrication.* Wear, 1999. **232**(2): p. 176-184.

29. Stachowiak, G.W. and Batchelor , A.W., *Engineering tribology*. 2000, Boston: Elsevier, 2000.

30. Esfahanian, M. and B.J. Hamrock, *Fluid-film lubrication regimes revisited.* Tribology Transactions, 1991. **34**(4): p. 628-632.

31. Booser, E.R., et al., *Tribology data handbook*. Boca Raton.: CRC Press, 1997.

32. Guangteng, G. and H.A. Spikes, *Behaviour of lubricants in the mixed elastohydrodynamic regime*, in *Tribology Series*, C.M.T.T.H.C.C. D. Dowson and G. Dalmaz, Editors. 1995, Elsevier. p. 479-485.

33. Rabinowicz, E., *Friction and Wear of Materials*. New York: Wiley, 1995.

34. Spikes, H.A., *Thin films in elastohydrodynamic lubrication: the contribution of experiment.* Proceedings of the Institution of Mechanical Engineers Part J-Journal of Engineering Tribology, 1999. **213**(J5): p. 335-352.

35. Kleiman, G.G. and Landman , U., *Theory of physisorption - He on metals.* Physical Review B, 1973. **8**(12): p. 5484-5495.

36. Hironaka, S., *Friction properties of C18-fatty acids.* Sekiyu Gakkai Shi, 1988. **31**(3): p. 216-220.

37. Jahanmir, S., *Chain length effects in boundary lubrication.* Wear, 1985. **102**(4): p. 331-349.

38. Hironaka, S., *Boundary lubrication, tribology of mechanical systems: a guide to present and future technologies*, 2004: p. 41-51.

39. Bhushan, B. and Gupta, B.K., *Handbook of tribology : materials, coatings, and surface treatments*. Malabar:Krieger, 1997.

40. Maboudian,R., Ashurst W.R., and Carraro C., *Tribological challenges in micromechanical systems.* Tribology letters, 2002. **12**(2): p. 95-100.

41. Prasad, S. and Asthana R., *Aluminum metal-matrix composites for automotive applications: tribological considerations.* Tribology Letters, 2004. **17**(3): p. 445-453.

42. Khurshudov, A. and Waltman , R.J., *Tribology challenges of modern magnetic hard disk drives.* Wear, 2001. **251**(1): p. 1124-1132.

43. Terrell, E.J., Needelman, W.M., and Kyle, J.P., *Tribological challenges to the system.* Wind Systems Magazine, 2010: p. 25-30.

44. Akbulut, M., et al., *Frictional Properties of Confined Nanorods.* Advanced Materials, 2006. **18**(19): p. 2589-2592.

45. Rapoport, L., Fleischer, N., and Tenne, R., *Fullerene-like WS_2 nanoparticles: superior lubricants for harsh conditions.* Advanced Materials, 2003. **15**(7-8): p. 651-655.

46. Dickrell, P.L., et al., *Tunable friction behavior of oriented carbon nanotube films.* Tribology Letters, 2006. **24**(1): p. 85-90.

47. Enomoto, K., et al., *Frictional properties of carbon nanofiber reinforced polymer matrix composites.* New Diamond and Frontier Carbon Technology, 2004. **14**(1): p. 11-20.

48. Chen, W.X., et al., *Tribological application of carbon nanotubes in a metal-based composite coating and composites.* Carbon, 2003. **41**(2): p. 215-222.

49. Cumings, J. and Zettl, A. Zettl, *Low-friction nanoscale linear bearing realized from multiwall carbon nanotubes.* Science, 2000. **289**(5479): p. 602-604.

50. Falvo, M.R., et al., *Nanometre-scale rolling and sliding of carbon nanotubes.* Nature, 1999. **397**(6716): p. 236-238.

51. Steven, T.P., et al., *Bimetallic nanoparticles for surface modification and lubrication of MEMS switch contacts.* Nanotechnology, 2008. **19**(40): p. 405705.

52. Wu, Y.Y., Tsui ,W.C., and Liu ,T.C., *Experimental analysis of tribological properties of lubricating oils with nanoparticle additives.* Wear, 2007. **262**(7-8): p. 819-825.

53. Gullac, B. and Akalin ,O., *Frictional characteristics of IF-WS_2 nanoparticles in simulated engine conditions.* ASME Conference Proceedings, **2009**(48951): p. 261-263.

54. Wornyoh, E.Y.A., et al., *A review of dry particulate lubrication: powder and granular materials.* Journal of Tribology, 2007. **129**(2): p. 438-449.

55. Rapoport, L., Fleischer ,N., and Tenne, R., *Applications of WS_2 (MoS_2) inorganic nanotubes and fullerene-like nanoparticles for solid lubrication and for structural nanocomposites.* Journal of Materials Chemistry, 2005. **15**(18): p. 1782-1788.

56. Lee, C.-G., et al., *A study on the tribological characteristics of graphite nano lubricants.* International Journal of Precision Engineering and Manufacturing, 2009. **10**(1): p. 85-90.

57. Martin, J.M. and Ohmae, N., *Nanolubricants*. Chichester:Wiley, 2008.

58. Pawlak, Z., *Tribochemistry of lubricating oils*. London: Elsevier, 2003.

59. Minfray, C., et al., *A multi-technique approach of tribofilm characterisation.* Thin Solid Films, 2004. **447**: p. 272-277.

60. Morina, A., et al., *ZDDP and MoDTC interactions and their effect on tribological performance–tribofilm characteristics and its evolution.* Tribology Letters, 2006. **24**(3): p. 243-256.

61. Rapoport, L., et al., *Tribological properties of WS_2 nanoparticles under mixed lubrication.* Wear, 2003. **255**(7–12): p. 785-793.

62. Chen, S., Liu ,W., and Yu, L., *Preparation of DDP-coated PbS nanoparticles and investigation of the antiwear ability of the prepared nanoparticles as additive in liquid paraffin.* Wear, 1998. **218**(2): p. 153-158.

63. Liu, W. and Chen, S., *An investigation of the tribological behaviour of surface-modified ZnS nanoparticles in liquid paraffin.* Wear, 2000. **238**(2): p. 120-124.

64. Sunqing, Q., Junxiu,D., and Guoxu, C., *Tribological properties of CeF_3 nanoparticles as additives in lubricating oils.* Wear, 1999. **230**(1): p. 35-38.

65. Bakunin, V., et al., *Synthesis and application of inorganic nanoparticles as lubricant components–a review.* Journal of Nanoparticle Research, 2004. **6**(2): p. 273-284.

66. Tenne, R., *Advances in the synthesis of inorganic nanotubes and fullerene-like nanoparticles.* Angewandte Chemie International Edition, 2003. **42**(42): p. 5124-5132.

67. Liu, W. and Wang , X., *Nanolubricants made of Metals*, in *nanolubricants*. New York: Wiley, 2008.

68. Ma, J., Y. Mo, and M. Bai, *Effect of Ag nanoparticles additive on the tribological behavior of multialkylated cyclopentanes (MACs).* Wear, 2009. **266**(7): p. 627-631.

69. Zhou, J., et al., *Tribological behavior and lubricating mechanism of Cu nanoparticles in oil.* Tribology Letters, 2000. **8**(4): p. 213-218.

70. Yu, H.-L., et al., *Tribological properties and lubricating mechanisms of Cu nanoparticles in lubricant.* Transactions of Nonferrous Metals Society of China, 2008. **18**(3): p. 636-641.

71. Kolodziejczyk, L., et al., *Surface-modified Pd nanoparticles as a superior additive for lubrication.* Journal of Nanoparticle Research, 2007. **9**(4): p. 639-645.

72. Sun, L., et al., *Synthesis and characterization of DDP coated Ag nanoparticles.* Materials Science and Engineering: A, 2004. **379**(1): p. 378-383.

73. Rohr, O., *Bismuth–the new ecologically green metal for modern lubricating engineering.* Industrial Lubrication and Tribology, 2002. **54**(4): p. 153-164.

74. Zhang, L., et al., *WS_2 nanorods prepared by self-transformation process and their tribological properties as additive in base oil.* Materials Science and Engineering: A, 2007. **454**: p. 487-491.

75. Joly-Pottuz, L., et al., *Tribological properties of Mo–S–I nanowires as additive in oil.* Tribology Letters, 2005. **18**(3): p. 385-393.

76. Hu, K., et al., *Tribological properties of molybdenum disulfide nanosheets by monolayer restacking process as additive in liquid paraffin.* Tribology International, 2009. **42**(1): p. 33-39.

77. Cizaire, L., et al., *Mechanisms of ultra-low friction by hollow inorganic fullerene-like MoS_2 nanoparticles.* Surface and Coatings Technology, 2002. **160**(2): p. 282-287.

78. Joly-Pottuz, L. and F. Dassenoy, *Nanoparticles made of metal dichalcogenides,* in *nanolubricants*. New York: Wiley, 2008.

79. Erdemir, A., *Boron-based solid nanolubricants and lubrication additives*, in *nanolubricants*. New York: Wiley, 2008.

80. Hu, Z.S., et al., *Preparation and tribological properties of nanometer magnesium borate as lubricating oil additive.* Wear, 2002. **252**(5): p. 370-374.

81. Hu, Z. and J. Dong, *Study on antiwear and reducing friction additive of nanometer titanium borate.* Wear, 1998. **216**(1): p. 87-91.

82. Dong, J. and Z. Hu, *A study of the anti-wear and friction-reducing properties of the lubricant additive, nanometer zinc borate.* Tribology International, 1998. **31**(5): p. 219-223.

83. Zhang, M., et al., *Performance and anti-wear mechanism of $CaCO_3$ nanoparticles as a green additive in poly-alpha-olefin.* Tribology International, 2009. **42**(7): p. 1029-1039.

84. Gu, C., et al., *Study on application of CeO_2 and $CaCO_3$ nanoparticles in lubricating oils.* Journal of Rare Earths, 2008. **26**(2): p. 163-167.

85. Zhou, J., et al., *Study on an antiwear and extreme pressure additive of surface coated LaF_3 nanoparticles in liquid paraffin.* Wear, 2001. **249**(5): p. 333-337.

86. Qiu, S., et al., *Preparation of Ni nanoparticles and evaluation of their tribological performance as potential additives in oils.* Journal of Tribology, 2001. **123**: p. 441.

87. Zhang, Z., Liu , W., and Xue , Q., *Study on lubricating mechanisms of La $(OH)_3$ nanocluster modified by compound containing nitrogen in liquid paraffin.* Wear, 1998. **218**(2): p. 139-144.

88. Hernández Battez, A., et al., *CuO, ZrO_2 and ZnO nanoparticles as antiwear additive in oil lubricants.* Wear, 2008. **265**(3): p. 422-428.

89. Hu, Z., Dong, J., and Chen, G., *Study on antiwear and reducing friction additive of nanometer ferric oxide.* Tribology International, 1998. **31**(7): p. 355-360.

90. Li, X., et al., *Surface-modification in situ of nano-SiO_2 and its structure and tribological properties.* Applied Surface Science, 2006. **252**(22): p. 7856-7861.

91. Xue, Q., Liu, W., and Zhang, Z., *Friction and wear properties of a surface-modified TiO_2 nanoparticle as an additive in liquid paraffin.* Wear, 1997. **213**(1): p. 29-32.

92. Gao, Y., et al., *Study on tribological properties of oleic acid-modified TiO_2 nanoparticle in water.* Wear, 2002. **252**(5): p. 454-458.

93. Kang, X., et al., *Synthesis and tribological property study of oleic acid-modified copper sulfide nanoparticles.* Wear, 2008. **265**(1): p. 150-154.

94. Joly-Pottuz, L. and Ohmae, N., *Carbon-based nanolubricants*, in *nanolubricants*. New York: Wiley, 2008.

95. Tao, X., Jiazheng, Z., and Kang, X., *The ball-bearing effect of diamond nanoparticles as an oil additive*. Journal of Physics D: Applied Physics, 1996. **29**(11): p. 2932.

96. Peng, Y., Y. Hu, and H. Wang, *Tribological behaviors of surfactant-functionalized carbon nanotubes as lubricant additive in water.* Tribology Letters, 2007. **25**(3): p. 247-253.

97. Zhang, Z., Xue , Q., and Zhang , J., *Synthesis, structure and lubricating properties of dialkyldithiophosphate-modified MoS_2 compound nanoclusters.* Wear, 1997. **209**(1): p. 8-12.

98. Rosentsveig, R., et al., *Fullerene-like MoS_2 nanoparticles and their tribological behavior.* Tribology Letters, 2009. **36**(2): p. 175-182.

99. Banquy, X., Zhu , X.X., and Giasson, S., *Mechanical and frictional properties of nanoparticle monolayers grafted on functionalized mica substrates.* The Journal of Physical Chemistry B, 2008. **112**(39): p. 12208-12216.

100. Colonne, M., et al., *Binding of streptavidin with biotinylated thermosensitive nanospheres based on poly(N,N-diethylacrylamide-co-2-hydroxyethyl methacrylate).* Bioconjugate Chemistry, 2007. **18**(3): p. 999-1003.

101. Rong, M.Z., et al., *Graft polymerization onto inorganic nanoparticles and its effect on tribological performance improvement of polymer composites.* Tribology International, 2003. **36**(9): p. 697-707.

102. Pei, X.W., et al., *Polyelectrolyte-grafted carbon nanotubes: synthesis, reversible phase-transition behavior, and tribological properties as lubricant additives.* Journal of Polymer Science Part a-Polymer Chemistry, 2008. **46**(21): p. 7225-7237.

103. Droppo, I.G., *Flocculation in natural and engineered environmental systems*. Boca Raton: CRC Press, 2005.

104. Min, Y.J., et al., *The role of interparticle and external forces in nanoparticle assembly*. Nature Materials, 2008. **7**(7): p. 527-538.

105. Bakunin, V.N., et al., *Synthesis and application of inorganic nanoparticles as lubricant components - a review*. Journal of Nanoparticle Research, 2004. **6**(2-3): p. 273-284.

106. Bishop, K.J.M., et al., *Nanoscale Forces and Their Uses in Self-Assembly*. Small, 2009. **5**(14): p. 1600-1630.

107. Hertel, T., Walkup, R.E., and Avouris , P., *Deformation of carbon nanotubes by surface van der Waals forces.* Physical Review B, 1998. **58**(20): p. 13870-13873.

108. Jiang, A.Q., et al., *Theoretical study of the thermal behavior of free and alumina-supported Fe-C nanoparticles.* Physical Review B, 2007. **75**(20).

109. Sun, J. and Simon, S.L., *The melting behavior of aluminum nanoparticles.* Thermochimica Acta, 2007. **463**(1-2): p. 32-40.

110. Lai, S.L., et al., *Size-dependent melting properties of small tin particles: nanocalorimetric measurements.* Physical Review Letters, 1996. **77**(1): p. 99-102.

111. Goldstein, A.N., Echer, C.M., and Alivisatos, A.P., *Melting in semiconductor nanocrystals.* Science, 1992. **256**(5062): p. 1425-1427.

112. Xiong, X., et al., *Preparation and evaluation of tribological properties of Cu nanoparticles surface modified by tetradecyl hydroxamic acid.* Tribology Letters, 2012. **46**(3): p. 211-220.

113. Qiu, S., et al., *Preparation of Ni nanoparticles and evaluation of their tribological performance as potential additives in oils.* Journal of Tribology, 2001. **123**(3): p. 441-443.

114. Quon, R., Ulman ,A., and Vanderlick , T., *Impact of humidity on adhesion between rough surfaces.* Langmuir, 2000. **16**(23): p. 8912-8916.

115. Israelachvili, J., et al., *Effects of sub-angstrom (pico-scale) structure of surfaces on adhesion, friction, and bulk mechanical properties.* Journal of Materials Research, 2005. **20**(8): p. 1952-1972.

116. Godfrey Alig, A., et al., *Forces between surfactant-coated ZnS nanoparticles in dodecane: effect of water.* Advanced Functional Materials, 2006. **16**(16): p. 2127-2134.

117. Savage, R.H., *Graphite Lubrication.* Journal of Applied Physics, 1948. **19**(1): p. 1-10.

118. Chhowalla, M. and Amaratunga , G.A., *Thin films of fullerene-like MoS_2 nanoparticles with ultra-low friction and wear.* Nature, 2000. **407**(6801): p. 164-167.

119. Rapoport, L., et al., *Friction and wear of fullerene-like WS_2 under severe contact conditions: friction of ceramic materials.* Tribology Letters, 2005. **19**(2): p. 143-149.

120. Rapoport, L., et al., *Hollow nanoparticles of WS_2 as potential solid-state lubricants.* Nature, 1997. **387**(6635): p. 791-793.

121. Tannous, J., et al., *Understanding the tribochemical mechanisms of IF-MoS_2 nanoparticles under boundary lubrication.* Tribology Letters, 2011. **41**(1): p. 55-64.

122. Hu, Z.S., et al., *Preparation and tribological properties of nanoparticle lanthanum borate.* Wear, 2000. **243**(1–2): p. 43-47.

123. Costantini, G., et al., *Tuning surface reactivity by in situ surface nanostructuring.* Journal of Chemical Physics, 2000. **112**(15): p. 6840-6843.

124. Akbulut, M., Alig ,A.R.G., and Israelachvili , J., *Friction and tribochemical reactions occurring at shearing interfaces of nanothin silver films on various substrates.* Journal of Chemical Physics, 2006. **124**(17).

125. Schiotz, J. and Jacobsen , K.W., *A maximum in the strength of nanocrystalline copper.* Science, 2003. **301**(5638): p. 1357-1359.

126. Weertman, J.R., *Hall-Petch strengthening in nanocrystalline metals.* Materials Science and Engineering a-Structural Materials Properties Microstructure and Processing, 1993. **166**(1-2): p. 161-167.

127. Yamakov, V., et al., *Deformation-mechanism map for nanocrystalline metals by molecular-dynamics simulation.* Nature Materials, 2004. **3**(1): p. 43-47.

128. Hahn, H., Mondal, P., and Padmanabhan , K.A., *Plastic deformation of nanocrystalline materials.* Nanostructured Materials, 1997. **9**(1-8): p. 603-606.

129. Fan, G.J., et al., *A model for the inverse Hall-Petch relation of nanocrystalline materials.* Materials Science and Engineering a-Structural Materials Properties Microstructure and Processing, 2005. **409**(1-2): p. 243-248.

130. Jhi, S.H., et al., *Vacancy hardening and softening in transition metal carbides and nitrides.* Physical Review Letters, 2001. **86**(15): p. 3348-3351.

131. Morris, D.G., Joye , J.C., and Leboeuf , M., *Hardening and strain-aging by vacancies and their aggregates in feal.* Philosophical Magazine a-Physics of Condensed Matter Structure Defects and Mechanical Properties, 1994. **69**(5): p. 961-980.

132. Pugno, N.M., *Young's modulus reduction of defective nanotubes.* Applied Physics Letters, 2007. **90**(4).

133. Bernholc, J., et al., *Mechanical and electrical properties of nanotubes.* Annual Review of Materials Research, 2002. **32**(1): p. 347-375.

134. Hisakado, T., Tsukizoe,T., and Yoshikawa, H., *Lubrication mechanism of solid lubricants in oils.* Journal of Lubrication Technology, 1983. **105**(2): p. 245-252.

135. Chiñas-Castillo, F. and Spikes,H., *Behaviour of colloidally-dispersed solid particles in very thin film lubricated contacts.* Tribology Series, 2000. **38**: p. 719-731.

136. Peng, D.-X., et al., *Size effects of SiO_2 nanoparticles as oil additives on tribology of lubricant.* Industrial Lubrication and Tribology, 2010. **62**(2): p. 111-120.

137. Min, Y.J., et al., *Normal and shear forces generated during the ordering (directed assembly) of confined straight and curved nanowires.* Nano Letters, 2008. **8**(1): p. 246-252.

138. Zhao, Q.Q., Boxman , A., and Chowdhry, U., *Nanotechnology in the chemical industry–opportunities and challenges.* Journal of Nanoparticle Research, 2003. **5**(5-6): p. 567-572.

139. Park, J., et al., *Ultra-large-scale syntheses of monodisperse nanocrystals.* Nature materials, 2004. **3**(12): p. 891-895.

140. Gavi, E., Marchisio , D.L., and Barresi , A.A., *CFD modelling and scale-up of confined impinging jet reactors.* Chemical Engineering Science, 2007. **62**(8): p. 2228-2241.

141. Wegner, K. and Pratsinis, S.E., *Scale-up of nanoparticle synthesis in diffusion flame reactors.* Chemical Engineering Science, 2003. **58**(20): p. 4581-4589.

142. Jang, H.D. and Kim , S.-K., *Controlled synthesis of titanium dioxide nanoparticles in a modified diffusion flame reactor.* Materials Research Bulletin, 2001. **36**(3): p. 627-637.

143. Tsutsumi, A., et al., *A nano-coating process by the rapid expansion of supercritical suspensions in impinging-stream reactors.* Powder Technology, 2003. **138**(2): p. 211-215.

144. Nowack, B. and Bucheli ,T.D., *Occurrence, behavior and effects of nanoparticles in the environment.* Environmental Pollution, 2007. **150**(1): p. 5-22.

145. Mueller, N.C. and Nowack , B., *Exposure modeling of engineered nanoparticles in the environment.* Environmental Science & Technology, 2008. **42**(12): p. 4447-4453.

146. Gottschalk, F. and Nowack , B., *The release of engineered nanomaterials to the environment.* Journal of Environmental Monitoring, 2011. **13**(5): p. 1145-1155.

147. Gottschalk, F., et al., *Modeled environmental concentrations of engineered nanomaterials (TiO2, ZnO, Ag, CNT, fullerenes) for different regions.* Environmental Science & Technology, 2009. **43**(24): p. 9216-9222.

148. Binnig, G., Quate , C.F., and Gerber , C., *Atomic force microscope.* Physical Review Letters, 1986. **56**(9): p. 930-933.

149. Christman, J.A., et al., *Piezoelectric measurements with atomic force microscopy.* Applied Physics Letters, 1998. **73**(26): p. 3851-3853.

150. Meyer, E., *Atomic force microscopy.* Progress in Surface Science, 1992. **41**(1): p. 3-49.

151. Moreno-Herrero, F., et al., *Atomic force microscopy contact, tapping, and jumping modes for imaging biological samples in liquids.* Physical Review E, 2004. **69**(3): p. 031915.

152. Magonov, S.N., V. Elings, and M.H. Whangbo, *Phase imaging and stiffness in tapping-mode atomic force microscopy*. Surface Science, 1997. **375**(2–3): p. L385-L391.

153. Thomas, J.M. and Ducati , C., *Transmission electron microscopy*. New York:Wiley, 1979.

154. Vickerman, J.C. and Gilmore , I.S., *Surface analysis : the principal techniques*. Chichester: Wiley, 2009.

155. Voevodin, A.A., et al., *Nanoparticle-wetted surfaces for relays and energy transmission contacts.* Small, 2007. **3**(11): p. 1957-1963.

156. Hsu, S.M., *Nano-lubrication: concept and design.* Tribology International, 2004. **37**(7): p. 537-545.

157. Yu, L.G., et al., *Study of silane-based antiwear additives: Wear and chemistry.* Tribology International, 2011. **44**(6): p. 692-701.

158. Rapoport, L., Fleischer ,N., and Tenne, R., *Applications of WS_2 (MoS_2) inorganic nanotubes and fullerene-like nanoparticles for solid lubrication and for*

structural nanocomposites. Journal of Materials Chemistry, 2005. **15**(18): p. 1782-1788.

159. Benz, M., et al., *The deformation and adhesion of randomly rough and patterned surfaces.* Journal of Physical Chemistry B, 2006. **110**(24): p. 11884-11893.

160. Komvopoulos, K., *Surface engineering and microtribology for microelectromechanical systems.* Wear, 1996. **200**(1-2): p. 305-327.

161. Chang, W.-R., *The effect of surface roughness and contaminant on the dynamic friction of porcelain tile.* Applied Ergonomics, 2001. **32**(2): p. 173-184.

162. Burton, Z. and Bhushan , B., *Surface characterization and adhesion and friction properties of hydrophobic leaf surfaces.* Ultramicroscopy, 2006. **106**(8-9): p. 709-719.

163. Davis, R.H., et al., *Solid-solid contacts due to surface roughness and their effects on suspension behaviour.* Philosophical Transactions of the Royal Society of London. Series A- Mathematical, Physical and Engineering Sciences, 2003. **361**(1806): p. 871-894.

164. Holmberg, K., et al., *Friction and wear of coated surfaces -- scales, modelling and simulation of tribomechanisms.* Surface and Coatings Technology, 2007. **202**(4-7): p. 1034-1049.

165. Carpick, R.W. and Salmeron, M., *Scratching the surface: fundamental investigations of tribology with atomic force microscopy.* Chemical Reviews, 1997. **97**(4): p. 1163-1194.

166. Rasp, W. and Wichern, C.M., *Effects of surface-topography directionality and lubrication condition on frictional behaviour during plastic deformation.* Journal of Materials Processing Technology, 2002. **125-126**: p. 379-386.

167. Zum Gahr, K.H., Wahl , R., and Wauthier , K., *Experimental study of the effect of microtexturing on oil lubricated ceramic/steel friction pairs.* Wear, 2009. **267**(5-8): p. 1241-1251.

168. Sedlacek, M., Podgornik , B., and Vizintin, J., *Influence of surface preparation on roughness parameters, friction and wear.* Wear, 2009. **266**(3-4): p. 482-487.

169. Bhuyan, S., et al., *Effect of crosslinking on the friction and wear behavior of soybean oil-based polymeric materials.* Wear, 2007. **263**(7-12): p. 965-973.

170. Kovalchenko, A., et al., *The effect of laser surface texturing on transitions in lubrication regimes during unidirectional sliding contact.* Tribology International, 2005. **38**(3): p. 219-225.

171. Chen, S. and Liu, W., *Characterization and antiwear ability of non-coated ZnS nanoparticles and DDP-coated ZnS nanoparticles.* Materials Research Bulletin, 2001. **36**(1-2): p. 137-143.

172. Chen, S. and Liu , W., *Preparation and characterization of surface-coated ZnS nanoparticles.* Langmuir, 1999. **15**(23): p. 8100-8104.

173. Akbulut, M., et al., *Forces between surfaces across nanoparticle Solutions: role of size, shape, and concentration.* Langmuir, 2007. **23**(7): p. 3961-3969.

174. Min, Y., et al., *Frictional properties of surfactant-coated rod-shaped nanoparticles in dry and humid dodecane.* The Journal of Physical Chemistry B, 2008. **112**(46): p. 14395-14401.

175. Chen, Y.L., Xu , Z., and Israelachvili , J., *Structure and interactions of surfactant-covered surfaces in nonaqueous (oil-surfactant-water) media.* Langmuir, 1992. **8**(12): p. 2966-2975.

176. Kato, K., *Wear in relation to friction -- a review.* Wear, 2000. **241**(2): p. 151-157.

177. Schey, J.A. and Nautiyal , P.C., *Effects of surface roughness on friction and metal transfer in lubricated sliding of aluminium alloys against steel surfaces.* Wear, 1991. **146**(1): p. 37-51.

178. Persson, B.N.J. , et al., *On the nature of surface roughness with application to contact mechanics, sealing, rubber friction and adhesion.* Journal of Physics: Condensed Matter, 2005. **17**(1): p. R1.

179. Jeong, J.-H., Bae , H.-T., and Lim , D.-S., *The effect of iron catalysts on the microstructure and tribological properties of carbide-derived carbon.* Carbon, 2010. **48**(12): p. 3628-3634.

180. Berke, P.,El Houdaigui, F., and Massart , T.J., *Coupled friction and roughness surface effects in shallow spherical nanoindentation.* Wear, 2010. **268**(1-2): p. 223-232.

181. Sahin, M., Çetinarslan , C.S., and Akata , H.E., *Effect of surface roughness on friction coefficients during upsetting processes for different materials.* Materials & Design, 2007. **28**(2): p. 633-640.

182. Menezes, P.L., Kishore, and Kailas , S.V., *Effect of surface topography on friction and transfer layer during sliding.* Tribology Online, 2008. **3**(1): p. 25-30.

183. Ajayi, O.O., et al., *Frictional anisotropy under boundary lubrication: effect of surface texture.* Wear, 2009. **267**(5-8): p. 1214-1219.

184. Keller, J., et al., *Surface topography and tribology of cast iron in boundary lubrication.* Tribology International, 2009. **42**(6): p. 1011-1018.

185. Suh, N.P., *The delamination theory of wear.* Wear, 1973. **25**(1): p. 111-124.

186. Sadykov, F.A., Barykin , N.P., and Aslanyan, I.R., *Wear of copper and its alloys with submicrocrystalline structure.* Wear, 1999. **225-229**(Part 1): p. 649-655.

187. Zhang, Y.S., et al., *Friction and wear behaviors of nanocrystalline surface layer of pure copper.* Wear, 2006. **260**(9-10): p. 942-948.

188. Liang, H. and Helen Xu ,G., *Lubricating behavior in chemical-mechanical polishing of copper.* Scripta Materialia, 2002. **46**(5): p. 343-347.

189. Fang, T.H., et al., *Revealing extraordinary intrinsic tensile plasticity in gradient nano-grained Copper.* Science, 2011.

190. Hu, C.K., et al., *Copper interconnection integration and reliability.* Thin Solid Films, 1995. **262**(1-2): p. 84-92.

191. Lakshminarayanan, S., et al., *Contact and via structures with copper interconnects fabricated using dual Damascene technology.* Electron Device Letters, IEEE, 1994. **15**(8): p. 307-309.

192. Liang, H., et al., *Wear phenomena in chemical mechanical polishing.* Wear, 1997. **211**(2): p. 271-279.

193. Pradhan, N., B. Katz, and S. Efrima, *Synthesis of high-quality metal sulfide nanoparticles from alkyl xanthate single precursors in alkylamine solvents.* The Journal of Physical Chemistry B, 2003. **107**(50): p. 13843-13854.

194. Das, D. and Singh , R.N., *A review of nucleation, growth and low temperature synthesis of diamond thin films.* International Materials Reviews, 2007. **52**: p. 29-64.

195. Amontons, G., M'emoires de l' Acad'emie Royale A, 1699: p. 257-282.

196. Persson, B.N.J., Tosatti, E., *Physics of sliding friction*. Dordrecht: Kluwer Academic, 1996.

197. Bhushan, B., *Tribology: Friction, Wear and Lubrication*. Boca Raton: CRC Press, 2000.

198. Rabinowicz, E., *The nature of the static and kinetic coefficients of friction.* Journal of Applied Physics, 1951. **22**(11): p. 1373-1379.

199. Bouchoucha, A., Chekroud , S., and Paulmier , D., *Influence of the electrical sliding speed on friction and wear processes in an electrical contact copper-stainless steel.* Applied Surface Science, 2004. **223**(4): p. 330-342.

200. Yu, D.Y.W. and Spaepen, F., *The yield strength of thin copper films on Kapton.* Journal of Applied Physics, 2004. **95**(6): p. 2991-2997.

201. Greenwood, J.A. and Williamson, J.B.P., *Contact of nominally flat surfaces.* Proceedings of the Royal Society of London-Series A, Mathematical and Physical Sciences, 1966. **295**(1442): p. 300-319.

202. Haibo, H. and Spaepen , F., *Tensile testing of free-standing Cu, Ag and Al thin films and Ag/Cu multilayers.* Acta Materialia, 2000. **48**(12): p. 3261-3269.

203. Tabor, D., *The hardness of metals*. Oxford: Clarendon Press, 1951.

204. Kadin, Y., Kligerman , Y., and Etsion , I., *Unloading an elastic-plastic contact of rough surfaces.* Journal of the Mechanics and Physics of Solids, 2006. **54**(12): p. 2652-2674.

205. Stolarski, T.A., *Tribology of polyetheretherketone.* Wear, 1992. **158**(1-2): p. 71-78.

206. Appeldoorn, J.K. and Tao , F.F., *The lubricity characteristics of heavy aromatics.* Wear, 1968. **12**(2): p. 117-130.

207. Snook, I.K. and van Megen , W., *Solvation forces in simple dense fluids. I.* The Journal of Chemical Physics, 1980. **72**(5): p. 2907-2913.

208. Christenson, H.K., *Experimental measurements of solvation forces in nonpolar liquids.* The Journal of Chemical Physics, 1983. **78**(11): p. 6906-6913.

209. Israelachvili, J., *Solvation forces and liquid structure, as probed by direct force measurements.* Accounts of Chemical Research, 1987. **20**(11): p. 415-421.

210. Dhinojwala, A., *Nanorheology of confined fluids.* Materials Science and Technology, 2003. **19**: p. 1170-1174.

211. Jabbarzadeh, A., Harrowell , P., and Tanner , R.I., *The structural origin of the complex rheology in thin dodecane films: Three routes to low friction.* Tribology International. **40**(10-12): p. 1574-1586.

212. Stevens, M.J., et al., *Comparison of shear flow of hexadecane in a confined geometry and in bulk.* The Journal of Chemical Physics, 1997. **106**(17): p. 7303-7314.

213. Blencoe, K.A. and Williams , J.A., *The contact of rough surfaces carrying pressure sensitive boundary layers*. Tribology and Interface Engineering Series, 2000, p. 45-56.

214. Rabinowicz, E., *Metal transfer during static loading and impacting.* Proceedings of the Physical Society. Section B, 1952. **65**(8): p. 630.

215. Schwartz, C.J. and Bahadur , S., *Development and testing of a novel joint wear simulator and investigation of the viability of an elastomeric polyurethane for total-joint arthroplasty devices.* Wear, 2007. **262**(3-4): p. 331-339.

216. *ASM Handbook.* Materials Park:ASM International,1992.

217. Godfrey Alig, A.R., et al., *Forces between surfactant-coated ZnS nanoparticles in dodecane: effect of water.* Advanced Functional Materials, 2006. **16**(16): p. 2127-2134.

218. Rabinowicz, E., *The intrinsic variables affecting the stick-slip process.* Proceedings of the Physical Society, 1958. **71**(4): p. 668.

219. Rabinowicz, E., *Friction and wear of materials*. New York: Wiley, 1995.

220. Berman, A.D., Ducker ,W.A., and Israelachvili , J.N., *Origin and characterization of different stick–slip friction mechanisms.* Langmuir, 1996. **12**(19): p. 4559-4563.

221. Yoshizawa, H., McGuiggan , P., and Israelachvili , J., *Identification of a second dynamic state during stick-slip motion.* Science, 1993. **259**(5099): p. 1305-1308.

222. Kudo, H., *A note on the role of microscopically trapped lubricant at the tool-work interface.* International Journal of Mechanical Sciences, 1965. **7**(5): p. 383-388.

223. Kusy, R.P. and Whitley, J.Q., *Effects of surface roughness on the coefficients of friction in model orthodontic systems.* Journal of Biomechanics, 1990. **23**(9): p. 913-925.

224. Zum Gahr, K.H., Bundschuh , W., and Zimmerlin , B., *Effect of grain size on friction and sliding wear of oxide ceramics.* Wear, 1993. **162-164** (Part 1): p. 269-279.

225. Wakuda, M., et al., *Effect of surface texturing on friction reduction between ceramic and steel materials under lubricated sliding contact.* Wear, 2003. **254**(3-4): p. 356-363.

226. Zappone, B., Rosenberg , K., and Israelachvili , J., *Role of nanometer roughness on the adhesion and friction of a rough polymer surface and a molecularly smooth mica surface.* Tribology Letters, 2007. **26**(3): p. 191-201.

227. Narayanunni, V., Kheireddin . B.A., and Akbulut , M., *Influence of surface topography on frictional properties of Cu surfaces under different lubrication conditions: comparison of dry, base oil, and ZnS nanowire-based lubrication system.* Tribology International, 2011. **44**(12): p. 1720-1725.

228. Min, Y., et al., *Normal and shear forces generated during the ordering (directed assembly) of confined straight and curved nanowires.* Nano Letters, 2007. **8**(1): p. 246-252.

229. Bhushan, B., Israelachvili , J.N., and Landman , U., *Nanotribology: friction, wear and lubrication at the atomic scale.* Nature, 1995. **374**(6523): p. 607-616.

230. Savan, A., et al., *Modern solid lubrication: recent developments and applications of MoS_2.* Lubrication Science, 2000. **12**(2): p. 185-203.

231. Gosvami, N.N., Egberts , P., and Bennewitz , R., *Molecular order and disorder in the frictional response of alkanethiol self-assembled monolayers.* The Journal of Physical Chemistry A, 2011. **115**: p. 6942-6947.

232. Jorge, G.A., et al., *A specific heat anomaly in multiwall carbon nanotubes as a possible sign of orientational order-disorder transition.* Carbon, 2010. **48**(2): p. 525-530.

233. Chremos, A., Margaritis , K., and Panagiotopoulos, A.Z., *Ultra thin films of diblock copolymers under shear.* Soft Matter, 2010. **6**(15): p. 3588-3595.

234. Rudnick, L.R., *Lubricant additives : chemistry and applications*. Boca Raton: CRC Press, 2009.

235. Wijmans, C.M., Zhulina , E.B., and Fleer , G.J., *Effect of free polymer on the structure of a polymer brush and interaction between two polymer brushes.* Macromolecules, 1994. **27**(12): p. 3238-3248.

236. Harnau, L., Penna , F., and Dietrich , S., *Colloidal hard-rod fluids near geometrically structured substrates.* Physical Review E, 2004. **70**(2): p. 021505.

237. Al-Bender, F. and Swevers, J., *Characterization of friction force dynamics.* Control Systems, IEEE Control Systems, 2008. **28**(6): p. 64-81.

238. Al-Bender, F., Lampaert , V., and Swevers, J., *A novel generic model at asperity level for dry friction force dynamics.* Tribology Letters, 2004. **16**(1): p. 81-93.

239. Muser, M.H., Wenning , L., and Robbins , M.O., *Simple microscopic theory of Amontons's laws for static friction.* Physical Review Letters, 2001. **86**(7): p. 1295.

240. Masala, O. and Seshadri , R., *Synthesis routes for large volumes of nanoparticles.* Annual Review of Materials Research, 2004. **34**: p. 41-81.

241. Cushing, B.L., Kolesnichenko , V.L., and O'Connor , C.J., *Recent advances in the liquid-phase syntheses of inorganic nanoparticles.* Chemical Reviews, 2004. **104**(9): p. 3893-3946.

242. Chhowalla, M. and Amaratunga , G.A.J., *Thin films of fullerene-like MoS_2 nanoparticles with ultra-low friction and wear.* Nature, 2000. **407**(6801): p. 164-167.

243. Filleter, T., et al., *Friction and dissipation in epitaxial graphene films.* Physical Review Letters, 2009. **102**(8).

244. Kheireddin, B., et al., *Inorganic nanoparticle-based ionic liquid lubricants.* Wear, 2013. **185** (1-2): p. 185-190.

245. Renger, A., Johnson, K. L., *Contact Mechanics.* Cambridge, Cambridge University Press, 1985.

246. Israelachvili J., Rosenburg , M.N., Akbulut M., , *Effects of sub-angstrom (pico-scale) structure of surfaces on adhesion, friction, and bulk mechanical properties.* Journal of Materials, 2005: p. 1952-1972.

247. Pradhan, N. and Efrima , S., *Supercrystals of uniform nanorods and nanowires, and the nanorod-to-nanowire oriented transition.* The Journal of Physical Chemistry B, 2004. **108**(32): p. 11964-11970.

248. Seidel, H., et al., *Anisotropic etching of crystalline silicon in alkaline-solutions 2: influence of dopants.* Journal of the Electrochemical Society, 1990. **137**(11): p. 3626-3632.

249. H. Seidel, L.C., Heuberger , A., Baumgartel , H., *Anisotropic etching of crystalline silicone in alkaline solutions.* Electrochemistry, 1990. **137**(11): p. 3612-3626.

250. Kheireddin, B.A., Narayanunni , V., and Akbulut , M., *Influence of shearing surface topography on frictional properties of ZnS nanowire-based lubrication system across ductile surfaces.* Journal of Tribology, 2012. **134**(2): p. 022001-7.

251. Ho-Chieh, W., Umehara , N., and Kato , K., *The effect of surface roughness on friction of ceramics sliding in water.* Wear, 1998. **218**(2): p. 237-243.

252. Hayward, I.P., Singer , I.L., and Seitzman , L.E., *Effect of roughness on the friction of diamond on Cvd diamond coatings.* Wear, 1992. **157**(2): p. 215-227.

253. Tabor, D. and Field , J., *The properties of diamond.* London: Academic Press, 1979.

254. Menezes, P.L., Kishore, and Kailas , S.V., *Effect of surface roughness parameters and surface texture on friction and transfer layer formation in tin–steel tribo-system.* Journal of Materials Processing Technology, 2008. **208**(1–3): p. 372-382.

255. Furey, M.J., *Surface roughness effects on metallic contact and friction.* ASLE Transactions, 1963. **6**(1): p. 49-59.

256. Robbins, M.O., *Jamming, friction and unsteady rheology, in jamming and rheology*. London: Taylor and Francis, 2000.

257. Yoshizawa, H. and J. Israelachvili, *Fundamental mechanisms of interfacial friction. 2. Stick-slip friction of spherical and chain molecules.* The Journal of Physical Chemistry, 1993. **97**(43): p. 11300-11313.

258. Earle Martyn, J. and Seddon Kenneth, R., *Ionic liquids: green solvents for the future* in *clean solvents*. 2002, American Chemical Society. p. 10-25.

259. Min, Y., et al., *Measurement of forces across room temperature ionic liquids between mica surfaces.* The Journal of Physical Chemistry C, 2009. **113**(37): p. 16445-16449.

260. Perkin, S., *Ionic liquids in confined geometries.* Physical Chemistry Chemical Physics, 2012. **14**(15): p. 5052-5062.

261. Pandey, S., *Analytical applications of room-temperature ionic liquids: a review of recent efforts.* Analytica Chimica Acta, 2006. **556**(1): p. 38-45.

262. Nakashima, T. and Kawai ,T., *Quantum dots-ionic liquid hybrids: efficient extraction of cationic CdTe nanocrystals into an ionic liquid.* Chemical Communications, 2005 (12): p. 1643-1645.

263. Welton, T., *Room-temperature ionic liquids. solvents for synthesis and catalysis.* Chemical Reviews, 1999. **99**(8): p. 2071-2084.

264. Zhou, F., Liang , Y., and Liu ,W., *Ionic liquid lubricants: designed chemistry for engineering applications.* Chemical Society Reviews, 2009. **38**(9): p. 2590-2599.

265. Smith, P.G., *High-temperature molten-salt lubricated hydrodynamic journal bearings.* ASLE Transactions, 1961. **4**(2): p. 263-274.

266. Ye, C., et al., *Room-temperature ionic liquids: a novel versatile lubricant.* Chemical Communications, 2001 (21): p. 2244-2245.

267. Zhu, M., et al., *Effect of the anion on the tribological properties of ionic liquid nano-films on surface-modified silicon wafers.* Tribology Letters, 2008. **29**(3): p. 177-183.

268. Wang, H., et al., *Friction and wear behaviors of ionic liquid of alkylimidazolium hexafluorophosphates as lubricants for steel/steel contact.* Wear, 2004. **256**(1–2): p. 44-48.

269. Jiménez, A.-E. and Bermúdez , M.-D., *Imidazolium ionic liquids as additives of the synthetic ester propylene glycol dioleate in aluminium–steel lubrication.* Wear, 2008. **265**(5–6): p. 787-798.

270. Jiménez, A.-E. and Bermúdez , M.-D., *Ionic liquids as lubricants for steel–aluminum contacts at low and elevated temperatures.* Tribology Letters, 2007. **26**(1): p. 53-60.

271. Minami, I., *Ionic liquids in tribology*. Molecules, 2009. **14**(6): p. 2286-2305.

272. Qu, J., et al., *Ionic liquids with ammonium cations as lubricants or additives.* Tribology Letters, 2006. **22**(3): p. 207-214.

273. Jiménez, A.E., et al., *Room temperature ionic liquids as lubricant additives in steel–aluminium contacts: Influence of sliding velocity, normal load and temperature*. Wear, 2006. **261**(3–4): p. 347-359.

274. Battez, A.H., et al., *Tribological behaviour of two imidazolium ionic liquids as lubricant additives for steel/steel contacts.* Wear, 2009. **266**(11–12): p. 1224-1228.

275. Qu, J., et al., *Tribological characteristics of aluminum alloys sliding against steel lubricated by ammonium and imidazolium ionic liquids.* Wear, 2009. **267**(5–8): p. 1226-1231.

276. Liu, X., et al., *Tribological performance of phosphonium based ionic liquids for an aluminum-on-steel system and opinions on lubrication mechanism.* Wear, 2006. **261**(10): p. 1174-1179.

277. Liu, W., et al., *Tribological performance of room-temperature ionic liquids as lubricant*. Tribology Letters, 2002. **13**(2): p. 81-85.

278. Bermúdez, M.-D., et al., *Ionic liquids as advanced lubricant fluids.* Molecules, 2009. **14**(8): p. 2888-2908.

279. Peng, D.X., et al., *Tribological properties of diamond and SiO_2 nanoparticles added in paraffin.* Tribology International, 2009. **42**(6): p. 911-917.

280. Li, X., et al., *Surface-modification in situ of nano-SiO_2 and its structure and tribological properties.* Applied Surface Science, 2006. **252**(22): p. 7856-7861.

281. Hernández Battez, A., et al., *CuO, ZrO_2 and ZnO nanoparticles as antiwear additive in oil lubricants.* Wear, 2008. **265**(3-4): p. 422-428.

282. Kheireddin, B.A., Narayanunni ,V., and Akbulut, M., *Influence of shearing surface topography on frictional properties of ZnS nanowire-based lubrication system across ductile surfaces.* Journal of Tribology-Transactions of the ASME, 2012. **134** (2): p. 022001-1-7.

283. Huang, H.D., et al., *Friction and wear properties of IF-MoS_2 as additive in paraffin oil.* Tribology Letters, 2005. **20**(3-4): p. 247-250.

284. Ye, W., et al., *Preparation and tribological properties of tetrafluorobenzoic acid-modified TiO_2 nanoparticles as lubricant additives.* Materials Science and Engineering: A, 2003. **359**(1–2): p. 82-85.

285. Bakunin, V.N., et al., *Synthesis and application of inorganic nanoparticles as lubricant components - a review.* Journal of Nanoparticle Research, 2004. **6**(2): p. 273-284.

286. Li, B., et al., *Tribochemistry and antiwear mechanism of organic-inorganic nanoparticles as lubricant additives.* Tribology Letters, 2006. **22**(1): p. 79-84.

287. Kim, D. and L.A. Archer, *Nanoscale organic−inorganic hybrid lubricants.* Langmuir, 2011. **27**(6): p. 3083-3094.

288. Jiao, D., et al., *The tribology properties of alumina/silica composite nanoparticles as lubricant additives.* Applied Surface Science, 2011. **257**(13): p. 5720-5725.

289. Ueno, K. and M. Watanabe, *From colloidal stability in ionic liquids to advanced soft materials using unique media.* Langmuir, 2011. **27**(15): p. 9105-9115.

290. Wang, P., et al., *Gelation of ionic liquid-based electrolytes with silica nanoparticles for quasi-solid-state dye-sensitized solar cells.* Journal of the American Chemical Society, 2003. **125**(5): p. 1166-1167.

291. Moshkovith, A., et al., *Friction of fullerene-like WS_2 nanoparticles: effect of agglomeration.* Tribology Letters, 2006. **24**(3): p. 225-228.

292. Bartz, W.J., *Solid lubricant additives—effect of concentration and other additives on anti-wear performance.* Wear, 1971. **17**(5–6): p. 421-432.

293. Ueno, K., et al., *Colloidal interaction in ionic liquids: effects of ionic structures and surface chemistry on rheology of silica colloidal dispersions.* Langmuir, 2008. **25**(2): p. 825-831.

294. Wittmar, A., Ruiz-Abad ,D., and Ulbricht ,M., *Dispersions of silica nanoparticles in ionic liquids investigated with advanced rheology*. Journal of Nanoparticle Research, 2012. **14**(2).

295. Wang, B., et al., *Rheological and tribological properties of ionic liquid-based nanofluids containing functionalized multi-walled carbon nanotubes.* The Journal of Physical Chemistry C, 2010. **114**(19): p. 8749-8754.

296. Chen, H., et al., *Rheological and heat transfer behaviour of the ionic liquid, [C4mim][NTf2]*. International Journal of Heat and Fluid Flow, 2008. **29**(1): p. 149-155.

297. Hernandez Battez, A., et al., *The tribological behaviour of ZnO nanoparticles as an additive to PAO6.* Wear, 2006. **261**(3–4): p. 256-263.

298. Beamson, G. and Briggs , D., *High resolution XPS of organic polymers : the scienta ESCA300 database*. New York: Wiley, 1992.

299. Kamimura, H., et al., *Effect and mechanism of additives for ionic liquids as new lubricants.* Tribology International, 2007. **40**(4): p. 620-625.

300. Kasrai, M. and Urch ,D.S., *Electronic structure of iron(II) and (III) fluorides using X-ray emission and X-ray photoelectron spectroscopies.* Journal of the Chemical Society, Faraday Transactions 2: Molecular and Chemical Physics, 1979. **75**(0): p. 1522-1531.

301. Ye, C.F., et al., *Room-temperature ionic liquids: a novel versatile lubricant.* Chemical Communications, 2001 (21): p. 2244-2245.

302. Zhou, F., Y.M. Liang, and W.M. Liu, *Ionic liquid lubricants: designed chemistry for engineering applications.* Chemical Society Reviews, 2009. **38**(9): p. 2590-2599.

303. Bowden, F.P. and D. Tabor, *The friction and lubrication of solids*. The International series of monographs on physics. Oxford: Clarendon Press, 1986.

304. Mulliah, D., Kenny ,S.D., and R. Smith, *Modeling of stick-slip phenomena using molecular dynamics.* Physical Review B, 2004. **69**(20): p. 205407.

305. Bhushan, B., *Principles and applications of tribology*. New York:Wiley, 1999.

306. Archard, J.F., *Contact and rubbing of flat surfaces.* Journal of Applied Physics, 1953. **24**(8): p. 981-988.